AD-A219 136

DTIC FILE COPY ARO 21125.3-EL

(2)

NONRECIPROCAL COMPONENTS IN THE 140 & 220 GHZ BANDS UTILIZING MAGNETOPLASMONS ON SEMICONDUCTING SUBSTRATES

FINAL REPORT

DTIC ELECTE MAR 07 1990 S D D

D. M. BOLLE
D. R. DECKER

JANUARY 9, 1990

U. S. ARMY RESEARCH OFFICE

CONTRACT / GRANT NUMBER
DAAG29-85-K-0081

INSTITUTION

LEHIGH UNIVERSITY
BETHLEHEM, PA 18015

APPROVED FOR PUBLIC RELEASE;
DISTRIBUTION UNLIMITED.

90 03 06 049

THE VIEW, OPINIONS, AND/OR FINDINGS CONTAINED IN THIS REPORT ARE THOSE OF THE AUTHOR(S) AND SHOULD NOT BE CONSTRUED AS AN OFFICIAL DEPARTMENT OF THE ARMY POSITION, POLICY, OR DECISION, UNLESS SO DESIGNATED BY OTHER DOCUMENTATION.

UNCLASSIFIED
SECURITY CLASSIFICATION OF THIS PAGE

MASTER COPY - FOR REPRODUCTION PURPOSES

REPORT DOCUMENTATION PAGE

1a. REPORT SECURITY CLASSIFICATION: Unclassified	1b. RESTRICTIVE MARKINGS
2a. SECURITY CLASSIFICATION AUTHORITY	3. DISTRIBUTION / AVAILABILITY OF REPORT: Approved for public release; distribution unlimited.
2b. DECLASSIFICATION / DOWNGRADING SCHEDULE	
4. PERFORMING ORGANIZATION REPORT NUMBER(S)	5. MONITORING ORGANIZATION REPORT NUMBER(S): ARO 21125.3-EL
6a. NAME OF PERFORMING ORGANIZATION: Lehigh University; 6b. OFFICE SYMBOL (If applicable)	7a. NAME OF MONITORING ORGANIZATION: U. S. Army Research Office
6c. ADDRESS (City, State, and ZIP Code): CSEE Department, Lehigh University, Bethlehem, PA 18015	7b. ADDRESS (City, State, and ZIP Code): P. O. Box 12211, Research Triangle Park, NC 27709-2211
8a. NAME OF FUNDING / SPONSORING ORGANIZATION: U. S. Army Research Office; 8b. OFFICE SYMBOL (If applicable)	9. PROCUREMENT INSTRUMENT IDENTIFICATION NUMBER: DAAG29-85-K-0081
8c. ADDRESS (City, State, and ZIP Code): P. O. Box 12211, Research Triangle Park, NC 27709-2211	10. SOURCE OF FUNDING NUMBERS: PROGRAM ELEMENT NO. / PROJECT NO. / TASK NO. / WORK UNIT ACCESSION NO.

11. TITLE (Include Security Classification): Nonreciprocal Components in the 140 & 220 GHZ Bands Utilizing Magnetoplasmons on Semiconducting Substrates

12. PERSONAL AUTHOR(S): D. M. Bolle and D. R. Decker

13a. TYPE OF REPORT	13b. TIME COVERED	14. DATE OF REPORT (Year, Month, Day)	15. PAGE COUNT
Final	FROM 6-1-85 TO 9-30-89	9 Jan 1990	163

16. SUPPLEMENTARY NOTATION: The view, opinions and/or findings contained in this report are those of the author(s) and should not be construed as an official Department of the Army position, policy, or decision, unless so designated by other documentation.

17. COSATI CODES		
FIELD	GROUP	SUB-GROUP

18. SUBJECT TERMS (Continue on reverse if necessary and identify by block number): Nonreciprocal components, millimeter and sub-millimeter waves, magnetoplasmons, surface waves, semiconductors.

19. ABSTRACT (Continue on reverse if necessary and identify by block number)

This report presents the progress made during the period of June 1985 to June 1988 on experimental and theoretical investigations of waveguiding structures utilizing surface waves on high quality semiconducting substrates. When exposed to a d.c. biasing magnetic field, these structures display nonreciprocal behavior which can be used to design nonreciprocal devices such as circulators, isolators, and phase shifters in the millimeter and submillimeter wave frequency ranges. Reasonable losses can be achieved for device purposes when operated at cryogenic temperatures.

20. DISTRIBUTION / AVAILABILITY OF ABSTRACT: ☐ UNCLASSIFIED/UNLIMITED ☒ SAME AS RPT. ☐ DTIC USERS	21. ABSTRACT SECURITY CLASSIFICATION: Unclassified
22a. NAME OF RESPONSIBLE INDIVIDUAL: Dr. Michael Stroscio	22b. TELEPHONE (Include Area Code) / 22c. OFFICE SYMBOL

DD FORM 1473, 84 MAR — 83 APR edition may be used until exhausted. All other editions are obsolete.

SECURITY CLASSIFICATION OF THIS PAGE
UNCLASSIFIED

OUTLINE OF REPORT

1- Title page

2- Table of contents

3- Summary

4- Publication #1 (1985)

5- Publication #2 (1987)

6- Progress reports and materials not covered by other sections. (theoretical work)

7- Experimental work by Tom Hwang

8- New results presently being prepared for publication

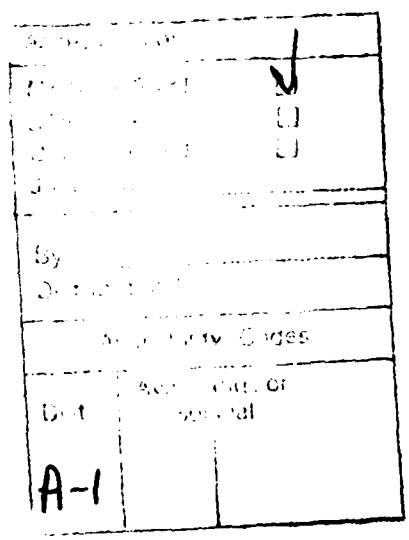

NONRECIPROCAL COMPONENTS IN THE 140 & 220 GHZ BANDS UTILIZING MAGNETOPLASMONS ON SEMICONDUCTING SUBSTRATES

Nader Mohsenian*, Dong-Hyun Hwang•

Terry J. Delph†, and D.M. Bolle‡

Final Report

month/1988

prepared for

Army Research Office

This research was supported by the Army Research Office under contract No. DAAG29-85-K-0081.

---

*Department of Computer Science and Electrical Engineering, Lehigh University, Packard Laboratory #19, Bethlehem, Pa. 18015.

•Dong-Hyun Hwang received his MSEE degree from Lehigh University and has returned to Korea to fulfill his military obligations.

†Department of Mechanical Engineering and Mechanics, Lehigh University, Packard Laboratory #19, Bethlehem, Pa. 18015.

‡D.M.Bolle was with CSEE Department of Lehigh University until August 1,1988. He is presently at New York Polytechnic Institute.

TABLE OF CONTENTS

	Page
I. OVERVIEW	3
II. ACCOMPLISHMENTS	5
III. ANALYSIS OF RECTANGULAR WAVEGUIDING STRUCTURES BY THE FINITE-ELEMENT METHOD	7
IV. EXPERIMENTAL EXCITATION OF SURFACE PLASMONS ON n-TYPE GaAs SUBSTRATES IN THE 110-160 GHz FREQUENCY BAND*	27
V. FUTURE PLANS	69
VI. APPENDIX A, "FINITE-ELEMENT ANALYSIS APPLIED TO GYROELECTRICALLY LOADED WAVEGUIDING STRUCTURES"	71
VII. APPENDIX B, "ANALYSIS OF WAVEGUIDING STRUCTURES EMPLOYING SURFACE MAGNETOPLASMONS BY THE FINITE-ELEMENT METHOD"	84
VIII. APPENDIX C, "TWO-DIMENSIONAL FINITE-ELEMENT ANALYSIS OF RECTANGULAR WAVEGUIDES WITH ISOTROPIC n-TYPE SEMICONDUCTOR MATERIAL"	101

* Excerpted from Master's thesis of Dong-Hyun Hwang.

I. OVERVIEW

This report presents the progress made during the period of June 1985 to June 1988 on experimental and theoretical investigations of waveguiding structures utilizing surface waves on high quality semiconducting substrates. When exposed to a d.c. biasing magnetic field, these structures display nonreciprocal behavior which can be used to design nonreciprocal devices such as circulators, isolators, and phase shifters in the millimeter and submillimeter wave frequency ranges. Reasonable losses can be achieved for device purposes when operated at cryogenic temperatures.

Various experimental techniques were explored to achieve surface plasmon excitation on n-type semiconducting materials in the near-millimeter wave ranges. Although some limited studies have been carried out on this topic in the optical frequency range, very little work is available on experimental derivation of propagation characteristics of surface plasmon on III-V semiconductor compounds. For our purposes, most of the theory was deduced from optics with numerous experiments conducted to obtain a reasonable interpretation for the quasi-optical theory applied to the millimeter wave range.

The quasi-optical method employed both the prism coupling and grating coupling techniques to generate surface plasmon on highly doped semiconductor materials in the frequency range of 110-160 GHz. Preliminary measurements were carried out for the two experimental approaches with results compared against the theoretical predictions of an air-GaAs single interface. The prism coupling method utilizing a Kretschmann configuration emerged as the most convenient technique to analyze the propagation characteristics of semiconducting materials employing surface plasmons.

The verification of surface plasmon generation in the near-millimeter frequency range has encouraged us to apply our experimental technique to two-dimensional structures consisting of n-type semiconducting materials in contact with different dielectric media. Such models could prove to be essential in development of planar integrated quasi-optical devices in the millimeter

and submillimeter wave ranges. However, since no rigorous theoretical solutions exist for these structures, we are in need of a powerful numerical technique that can provide accurate solutions to be compared against the experimental results. Finite-element method, a versatile and efficient technique, can handle waveguiding structures with arbitrary shaped cross sections and arbitrary electrical properties. We developed a finite-element formulation in terms of the transverse components of the magnetic field to carry out theoretical investigations of rectangular waveguides. The use of magnetic field components as dependent variables became possible, since the permeability is a constant for all regions of the guides described here and consequently components h_x, h_y, and h_z are all continuous along interfaces. Eight-noded isoparametric quadrilateral elements were employed in our numerical model to obtain dispersive behavior and complete modal field distributions of various dielectric and semiconductor waveguides applicable to optical and quasi-optical component design.

II. ACCOMPLISHMENTS

Our experimental efforts focused on both prism coupling and grating coupling techniques to excite surface plasmon polaritons on highly doped n-type GaAs wafers in the frequency range of 110-160 GHz. Reflection intensity measurements were conducted for this frequency range and the preliminary results of the prism coupler showed better match between theory and experiment than the data obtained using periodic structures. Although surface plasmon was generated at $2mm$ of grating distance, the height, shape, and periodic length of the gratings greatly influenced the end coupling detection procedure of the surface wave. Furthermore the presence of the scattered waves contributed to a high level of noise. On the contrary, prism couplers provided a non-destructive way of generating surface plasmons without using complicated scattering theories. The advantageous features of the prism coupler led to the use of this technique in completing our experiment. The final experimental ω-β dispersion curve for the frequency range of 110 to 160 GHz was obtained through a series of Kretschmann prism coupling experiments performed at various angles of incidence with results presented in section IV of this report. A second mode was observed in the experimental dispersion spectrum caused by the interface adjacent to the prism. This mode normally does not exist in the optical frequency range due to absorption levels of the prisms encountered in the optical regions.

We have demonstrated the excitation of surface plasmons in the near-millimeter frequency range of 110-160 GHz which up to now was not reported in the literature. Excellent results were achieved. The use of highly doped n-type GaAs materials was also a first. Although extensive experiments on loss and other parameters have yet to be carried out, the success in quasi-optical method of excitation provides inspiration for continued studies on the application of surface plasmons where used in conjunction with application of magnetic fields for development of non-reciprocal millimeter-wave devices.

In parallel with the experimental analysis of structures used to generate surface waves, we

developed a numerical model employing the finite-element formulation to obtain dependable results for propagation characteristics of the waveguides which can be compared against the experimental data.

Numerical analysis of one-dimensional waveguiding structures employing surface magnetoplasmons were carried out using eight-noded isoparametric quadrilateral finite-elements with results matching those from the exact solutions precisely. Here, the finite-element formulation was derived in terms of the e_z component for the TM mode of a single air-GaAs interface exposed to a d.c. biasing magnetic field along the interface. This study was presented at the 1985 IEEE MTT-S International Microwave Symposium, see appendix A, and a more advance analysis of the topic w th complete field distributions of the modal spectrum appeared as an IEEE Transaction paper, i.e., appendix B. Although excellent results were achieved from the finite-element method, the explicit application of the boundary conditions along the interface made the formulation used in appendices A and B somewhat complicated. Another setback of finite-element method which is evident in analysis of two-dimensional structures, is the appearance of non-physical (spurious) modes which do not satisfy the divergence free condition of magnetic field, i.e., $\nabla \cdot H=0$. Therefore we developed a more general finite-element formulation in terms of the transverse components of magnetic fields which is applicable to two-dimensional rectangular waveguides having frequency-dependent permittivity tensors with off-diagonal elements. This numerical model was used to obtain the dispersion spectrum of inhomogeneously filled dielectric waveguides and optical embossed waveguides. Excellent results were achieved and are presented in section III. It may be noted that no spurious solutions were observed in our finite-element analysis.

Finally, we derived the dispersive behavior and mode shapes of an embossed rectangular waveguide employing n-type InSb material, see appendix C. This study will be submitted for publication in the near future.

III. ANALYSIS OF RECTANGULAR WAVEGUIDING STRUCTURES BY THE FINITE-ELEMENT METHOD

(N. Mohsenian)

INTRODUCTION

The widespread use of dielectric waveguides for design of components such as phase shifters, switches, modulators, and directional couplers in millimeter and optical integrated circuits has created a need for the development of numerical methods that can accurately derive the propagation characteristics of such structures. Some approximate analysis of rectangular dielectric structures have been made by several authors [1]-[4]. The study in [1] is reliable for guides where the energy is mostly contained in the core region of the structure, therefore offering good results at high frequencies and not trustworthy outcome close to cutoff frequencies of the propagating modes. This approximate method led to the effective dielectric constant technique [2] and was further developed by other researchers [3], [4] to obtain better results for the rectangular waveguiding structures utilized in the design of millimeter-wave through optical integrated circuits. There are also variational formulations applied to the solutions of surface waveguides and slab-coupled waveguides [5], [6], which in general are not suitable for problems employing anisotropic materials. Other techniques used to investigate various waveguiding structures are the transverse resonance method [7], the equivalent network approach [8], the field matching method [9], the finite-difference technique [10], [11], and the method of using the telegraphist's equation [12].

Although the approximate and numerical analysis [1]-[12] have provided good results for the propagating modes in the millimeter-wave and optical dielectric waveguides, they generally do not produce enough informations on field distributions in the model and are not applicable to canonical waveguiding structures employing semiconducting materials with complicated electrical properties. On the contrary, a numerical solution utilizing the finite-element

formulation, provides a powerful and versatile technique suitable to the analysis of practical waveguides with arbitrary shaped cross sections and various regions consisting of complex gyroelectric or gyromagnetic media. The accuracy of this numerical method in obtaining the propagation characteristics of useful structures operating at millimeter-wave through optical frequency ranges has been verified by several authors [13]-[20].

A serious difficulty associated with the finite-element formulation is the appearance of nonphysical "spurious" solutions which has been the subject of some investigations [16], [19], [21]-[23]. Here the method developed by Hayata and coworkers [22] represents an appropriate approach to the problem of eliminating the spurious modes in the dispersion spectra of planar rectangular waveguiding structures.

The purpose of this study is to develop a numerical model employing the finite-element formulation, and confirming its validity and versatility via examining the propagation modes of some useful structures and their electromagnetic field distributions accordingly. This procedure may then be applied to canonical models utilizing doped semiconductor substrates with frequency dependent permittivities to analyze surface wave excitations in the millimeter and submillimeter-wave frequency ranges. Results are given for inhomogeneously filled dielectric waveguides and optical embossed waveguides which are in agreement with exact solutions and published results.

FINITE-ELEMENT APPROACH

We consider two different waveguiding structures, the inhomogeneous dielectric waveguide and the optical embossed waveguide, which have been subject of many investigations as test cases for our model. The cross sections of the guides with the finite-element mesh superposed are depicted in Fig.1 with the electromagnetic wave propagating in the z-direction and the configuration bounded by electric walls. As discussed in the previous section, the finite-element techniques developed in terms of longitudinal or transverse field

components have resulted in many unwanted roots or singularities in their solutions. Spurious modes are believed to have irregular behavior and not satisfy the divergence-free condition of the magnetic field, i.e., $\nabla \cdot H=0$ [21]. To eliminate the spurious solutions, we will derive a finite-element formulation in terms of the components of the magnetic field with the condition $\nabla \cdot H=0$ explicitly included in the formulation. The three component curl curl equation obtained from Maxwell's equations take the form

$$\nabla \times \left(\epsilon_r^{-1} \nabla \times H \right) - \omega^2 \mu_o \epsilon_o H = 0 \qquad (1)$$

where ϵ_r is the relative dielectric constant.

We now divide the different regions of the configuration under study into eight-noded isoparametric quadrilateral elements with the interpolating functions $N_i(x,y)$ used to approximate the h_x, h_y, h_z components in the following manner: $h_x(x,y,z) \simeq [N(x,y)]\{h_x\}\, e^{-j\beta z}$, $h_y(x,y,z) \simeq [N(x,y)]\{h_y\}\, e^{-j\beta z}$, $h_z(x,y,z) \simeq j\,[N(x,y)]\{h_z\}\, e^{-j\beta z}$. Here $[N(x,y)]$ is the row vector of the interpolating functions and $\{h\}$'s are the column vectors of the nodal point values for which no boundary conditions are specified. Galerkin technique was then employed to generate the finite-element equations from (1)

$$\iint_{\mathcal{A}} \left(\epsilon_r^{-1} \left(\frac{\partial^2 h_y}{\partial y \partial x} - \frac{\partial^2 h_x}{\partial y^2} - \frac{\partial^2 h_x}{\partial z^2} + \frac{\partial^2 h_z}{\partial z \partial x} \right) - \left(\frac{\omega}{c} \right)^2 h_x \right) \cdot N_i(x,y)\, dxdy = 0 \qquad (2)$$

$$\iint_{\mathcal{A}} \left(\epsilon_r^{-1} \left(\frac{\partial^2 h_z}{\partial z \partial y} - \frac{\partial^2 h_y}{\partial z^2} - \frac{\partial^2 h_y}{\partial x^2} + \frac{\partial^2 h_x}{\partial x \partial y} \right) - \left(\frac{\omega}{c} \right)^2 h_y \right) \cdot N_i(x,y)\, dxdy = 0 \qquad (3)$$

$$\iint_{\mathcal{A}} \left(\epsilon_r^{-1} \left(\frac{\partial^2 h_x}{\partial x \partial z} - \frac{\partial^2 h_z}{\partial x^2} - \frac{\partial^2 h_z}{\partial y^2} + \frac{\partial^2 h_y}{\partial y \partial z} \right) - \left(\frac{\omega}{c} \right)^2 h_z \right) \cdot j\, N_i(x,y)\, dxdy = 0 \qquad (4)$$

The integrals are taken over the two dimensional domain $\mathcal{A}$ of the problem. Then divergence theorem was used to generate the finite-element equations in the form

$$([\mathbf{P}]-(\frac{\bar{\omega}}{\bar{\beta}})^2[\mathbb{R}])\cdot\{h_x\}+[\mathbf{C}]\cdot\{h_y\}+[\mathbb{D}]\cdot\{h_z\}+\oint_{\mathcal{B}}\left(\epsilon_r^{-1}(\frac{\partial h_y}{\partial x}-\frac{\partial h_x}{\partial y})\right) n_y\ N_i\ d\bar{l}=0 \qquad (5)$$

$$[\mathbf{C}]^T\cdot\{h_x\}+([\mathbb{E}]-(\frac{\bar{\omega}}{\bar{\beta}})^2[\mathbb{R}])\cdot\{h_y\}+[\mathbb{F}]\cdot\{h_z\}+\oint_{\mathcal{B}}\left(\epsilon_r^{-1}(\frac{\partial h_y}{\partial x}-\frac{\partial h_x}{\partial y})\right) n_x\ N_i\ d\bar{l}=0 \qquad (6)$$

$$[\mathbb{D}]^T\cdot\{h_x\}+[\mathbb{F}]^T\cdot\{h_y\}+([\mathbb{G}]-(\frac{\bar{\omega}}{\bar{\beta}})^2[\mathbb{R}])\cdot\{h_z\}+\oint_{\mathcal{B}}\left(\epsilon_r^{-1}(\frac{\partial h_z}{\partial y}-\frac{\partial h_y}{\partial z})\right) n_y\ j\ N_i\ d\bar{l}$$

$$-\oint_{\mathcal{B}}\left(\epsilon_r^{-1}(\frac{\partial h_x}{\partial z}-\frac{\partial h_z}{\partial x})\right) n_x\ j\ N_i\ d\bar{l}=0 \qquad (7)$$

Here the closed line integrals are to be evaluated along the boundary $\mathcal{B}$ between different media and also on the electric walls enclosing the waveguide with n_x and n_y being the unit normal vectors to the interface for which the line integral is calculated. It is fairly easy to show that the terms inside the line integrals represent the electric field components and due to the boundary conditions on the electric walls and the continuity of the tangential components of electric field along the interfaces, the line integrals would vanish. The i, j-th elements of the matrices which are to be evaluated for each element are given where $[\ ]^T$ indicates the transpose matrix.

$$\mathbf{B}_{ij}=\iint_{\mathcal{A}}\epsilon_r^{-1}\left(\frac{\partial N_i}{\partial\bar{y}}\ \frac{\partial N_j}{\partial\bar{y}}+N_iN_j\right)d\bar{x}d\bar{y} \qquad (8)$$

$$\mathbf{C}_{ij}=\iint_{\mathcal{A}}-\epsilon_r^{-1}\left(\frac{\partial N_i}{\partial\bar{y}}\ \frac{\partial N_j}{\partial\bar{x}}\right)d\bar{x}d\bar{y} \qquad (9)$$

$$\mathbf{D}_{ij}=\iint_{\mathcal{A}}\epsilon_r^{-1}\left(N_i\ \frac{\partial N_j}{\partial\bar{x}}\right)d\bar{x}d\bar{y} \qquad (10)$$

$$\mathbf{E}_{ij}=\iint_{\mathcal{A}}\epsilon_r^{-1}\left(\frac{\partial N_i}{\partial\bar{x}}\ \frac{\partial N_j}{\partial\bar{x}}+N_iN_j\right)d\bar{x}d\bar{y} \qquad (11)$$

$$\mathbf{F}_{ij} = \iint_{\mathcal{A}} \epsilon_r^{-1}\left(N_i \frac{\partial N_j}{\partial \bar{y}} \right) d\bar{x}d\bar{y} \qquad (12)$$

$$\mathbf{G}_{ij} = \iint_{\mathcal{A}} \epsilon_r^{-1}\left(\frac{\partial N_i}{\partial \bar{x}} \frac{\partial N_j}{\partial \bar{x}} + \frac{\partial N_i}{\partial \bar{y}} \frac{\partial N_j}{\partial \bar{y}} \right) d\bar{x}d\bar{y} \qquad (13)$$

$$\mathbf{R}_{ij} = \iint_{\mathcal{A}} N_i N_j \; d\bar{x}d\bar{y} \qquad (14)$$

Once assembled, the finite-element equations take the eigenvalue form of (15).

$$\left(\left[\mathbf{P} \right] - \left(\frac{\bar{\omega}}{\bar{\beta}}\right)^2 \left[\mathbf{Q} \right] \right) \cdot \begin{bmatrix} \{h_x\} \\ \{h_y\} \\ \{h_z\} \end{bmatrix} = 0 \qquad (15)$$

and $$\left[\mathbf{P} \right] = \begin{bmatrix} [\mathbb{B}] & [\mathbb{C}] & [\mathbb{D}] \\ [\mathbb{C}]^T & [\mathbb{E}] & [\mathbb{F}] \\ [\mathbb{D}]^T & [\mathbb{F}]^T & [\mathbb{G}] \end{bmatrix}, \quad \left[\mathbf{Q} \right] = \begin{bmatrix} [\mathbb{R}] & [0] & [0] \\ [0]^T & [\mathbb{R}] & [0] \\ [0]^T & [0]^T & [\mathbb{R}] \end{bmatrix}$$

Here $\bar{\omega}$ and $\bar{\beta}$ are the normalized frequency and propagation constant, respectively, given by, $\bar{\omega}=\omega t/c$, $\bar{\beta}=\beta t$, with t being the height of the core region for the embossed waveguide or the dimension of the square cross section of the inhomogeneous dielectric waveguide, and c is the velocity of light. The coordinates x and y were also normalized according to $\bar{x}=\bar{\beta}x/t$ and $\bar{y}=\bar{\beta}y/t$.

The finite-element dispersion spectrum obtained from the system in (15) includes spurious solutions. Therefore, we adopted the method employed by Hayata and coworkers [22] to explicitly include the relation $\nabla \cdot H=0$ in our formulation to eliminate the spurious solutions. Upon application of Galerkin technique to the divergence-free condition of the magnetic field the equations in (16) were obtained.

$$\begin{bmatrix} \{h_x\} \\ \{h_y\} \\ \{h_z\} \end{bmatrix} = \begin{bmatrix} [U] \\ [T_z]^{-1}\left[[T_x] \;\; [T_y] \right] \end{bmatrix} \bullet \begin{bmatrix} \{h_x\} \\ \{h_y\} \end{bmatrix} \qquad (16)$$

Here [U] is the unity matrix and the elements of other matrices are

$$T_{z_{ij}} = \iint_{\mathcal{A}} N_i N_j d\bar{x}d\bar{y}\ , \quad T_{x_{ij}} = -\iint_{\mathcal{A}} N_i \frac{\partial N_j}{\partial \bar{x}} d\bar{x}d\bar{y}\ , \quad T_{y_{ij}} = -\iint_{\mathcal{A}} N_i \frac{\partial N_j}{\partial \bar{y}} d\bar{x}d\bar{y}$$

Substituting (16) into our previous results, (15), and multiplying by the transpose of the coefficient matrix in (16), the final finite-element equations were generated in terms of the transverse components of the magnetic field for which the dispersion spectrum does not contain spurious modes.

$$\left([\mathbb{L}]^T \cdot [\mathbb{P}] \cdot [\mathbb{L}] - (\frac{\bar{\omega}}{\bar{\beta}})^2 [\mathbb{L}]^T \cdot [\mathbb{Q}] \cdot [\mathbb{L}]\right) \bullet \begin{bmatrix} \{h_x\} \\ \{h_y\} \end{bmatrix} = 0 \qquad (17)$$

where $$\left[\ \mathbb{L}\ \right] = \begin{bmatrix} [U] \\ [T_z]^{-1}\left[\ [T_x]\ \ [T_y]\right] \end{bmatrix}$$

For a given value of $\bar{\beta}$, the eigenvalue problem of (17) can be easily solved to derive the values of $\bar{\omega}$. However, for complicated waveguiding structures where the frequency dependence of electrical parameters of substrates are to be analyzed, the system in (17) no longer represents an eigenvalue problem. Here we generate the following finite-element equations

$$\left[\ S\ \right] \bullet \begin{bmatrix} \{h_x\} \\ \{h_y\} \end{bmatrix} = 0 \qquad (18)$$

where

$$\left[\ S\ \right] = \left[\ \mathbb{L}\ \right]^T \bullet \begin{bmatrix} [B] & [C] & [D] \\ [C]^T & [E] & [F] \\ [D]^T & [F]^T & [G] \end{bmatrix} \bullet \left[\ \mathbb{L}\ \right] \qquad (19)$$

and the i, j-th elements of matrices [B], [C], [D], [E], [F], and [G] are given

$$B_{ij} = \mathbb{B}_{ij} - (\frac{\bar{\omega}}{\bar{\beta}})^2 \mathbb{R}_{ij}\ , \ C_{ij} = \mathbb{C}_{ij}, \ D_{ij} = \mathbb{D}_{ij}\ , \ E_{ij} = \mathbb{E}_{ij} - (\frac{\bar{\omega}}{\bar{\beta}})^2 \mathbb{R}_{ij}\ , \ F_{ij} = \mathbb{F}_{ij}\ , \ G_{ij} = \mathbb{G}_{ij} - (\frac{\bar{\omega}}{\bar{\beta}})^2 \mathbb{R}_{ij}$$

A nontrivial solution exists for equation (18) if the determinant $|\ S\ | = 0$. Employing the

standard root finding techniques, one can obtain the values of $\bar{\omega}$ for a given $\bar{\beta}$.

RESULTS AND CONCLUSIONS

The eigenvalues of equation (17) and the roots of the determinant | S | resulting from (18) were both obtained to form the finite-element dispersion spectrum for the structures depicted in Fig. 1. The two approaches produced identical results with the method used in (18) applicable to the analysis of waveguides employing semiconducting materials. As the first example we derived the LSM-LSE (odd modes) of an inhomogeneously filled dielectric waveguide with ϵ_r=1.5. Eight quadrilateral elements were used to divide one-half of the cross section of the guide with the plane of symmetry assumed to be a magnetic wall, see Fig. 1(a). Good agreement was found between the finite-element results and the dispersion spectrum obtained from the exact solution of the waveguide [24], see Fig. 2. As a comparison with other finite-element formulations utilizing the variational technique [22], we calculated the first thirteen values of $\bar{\omega}$ for $\bar{\beta}$=10. Here we used eight and thirty-two quad-8 element in our method. As seen from table I, the 32-element model offers better accuracy than the 64 triangular-element model of ref. [22]. The exact solution of the problem derived from the transcendental equations is also shown [24].

TABLE I

(*Inhomogeneous dielectric waveguide with* ϵ_r=1.5)

	exact sol. from [24]	F.E. sol. in literature [22]	our F.E. sol. eight-elements	our F.E. sol. 32-elements
	ϖ	ϖ	ϖ	ϖ
LSM_{11}:	8.8090	8.8093	8.8093	8.8090
LSE_{11}:	9.3860	9.3896	9.3921	9.3873
LSM_{12}:	10.2721	10.2752	10.2790	10.2726
LSM_{13}:	11.0975	11.1038	11.1120	11.0987
LSE_{12}:	11.2566	11.2677	11.2857	11.2601
LSM_{31}:	11.4313	11.4501	11.4834	11.4358
LSE_{31}:	11.9434	11.9882	12.0358	11.9510
LSE_{13}:	12.6406	12.6686	12.7543	12.6475
LSM_{14}:	12.7691	12.8092	12.8375	12.8304
LSM_{32}:	12.8844	12.9575	12.9655	12.8902
LSE_{32}:	13.7780	*	14.0014	13.7906
LSM_{33}:	14.0181	*	14.0607	14.0249
LSM_{15}:	14.7807	*	15.1475	14.8292

Next we used thirty-two elements to obtain both the odd and even modes of an inhomogeneously filled dielectric waveguide with ϵ_r=17.7. One-half of the cross section of the guide was divided into quad-8 elements. The plane of symmetry was assumed to be a magnetic wall or an electric wall to derive the odd and even LSE-LSM modes, respectively. The first eight branches of the finite-element dispersion spectrum was compared against the exact solutions [24] and excellent agreement was achieved as shown in Fig. 3.

The second test case in our investigation was the optical embossed waveguide used in optical integrated circuits. The core of the guide has a refractive index $n_1=\sqrt{\epsilon_1}=1.5$ and a uniform substrate region with a refractive index $n_2=\sqrt{\epsilon_2}=1.45$, which is in contact with a third dielectric, air, see Fig. 1(b). One of the first applications of the finite-element method to optical waveguides was carried out by Yeh et al. [14]. The authors in [14] used 900 elements in one-half of the entire cross section, to obtain the dominent mode E_{11}^y of various embossed rectangular waveguides. The plane of symmetry along the y-axis was assumed to be a magnetic wall. Later Koshiba and coworkers obtained the same results for the E_{11}^y mode employing the finite-element method [20], and also using the equivalent network approach to calculate the first four modes of the dispersion spectrum for the same waveguide [8].

We examined the accuracy of our finite-element formulation by obtaining the dominent modes E_{11}^x and E_{11}^y for the optical waveguide analyzed in [8], [14], [20]. The finite-element grid of the problem is shown in Fig.1(b). An aspect ratio of two was used for the core region. With the proper applications of boundary conditions along the y-axis, the fundamental modes are derived. The plane of symmetry being a magnetic wall or an electric wall yields the E_{11}^y mode or E_{11}^x mode, respectively. The results of the finite-element method derived from both the eigenvalue solver and the determinant solver were satisfactory and matched each other. Sixteen elements were used to divide the cross section of the guide and obtain the fundamental modes. No spurious solutions were observed in this analysis. Then eight elements were employed to divide one-half of cross section of the guide. With the proper boundary conditions

along the y-axis, each dominent mode was derived separately. Results of the two different models are compared in table I for a few points. Finally, the two fundamental modes obtained from our analysis are compared against the results presented by the authors in [8] in Fig. 4.

TABLE II

(*optical embossed waveguide with an aspect ratio of two; here the 8-element and 16-element models represent one-half and complete cross section of the guide, respectively*)

$\bar{\beta}$	$\bar{\omega}(E_{11}^{x}$mode) 8-elements	$\bar{\omega}(E_{11}^{x}$mode) 16-elements	$\bar{\omega}(E_{11}^{y}$mode) 8-elements	$\bar{\omega}(E_{11}^{y}$mode) 16-elements
11.0	7.5272	7.5272	7.5318	7.5348
17.0	11.4827	11.4827	11.4932	11.4972
23.0	15.4512	15.4512	15.4650	15.4689
29.0	19.4298	19.4298	19.4444	19.4484
35.0	23.4147	23.4147	23.4292	23.4330

It should be noted that the values $\bar{\beta}$ and $\bar{\omega}$ were used to calculate the parameters v and b given in Fig. 4, where $v=\bar{\omega}\sqrt{\epsilon_1-\epsilon_2}\ /\pi$ and $b=\left((\bar{\beta}/\bar{\omega})^2-\epsilon_2\right)/(\epsilon_1-\epsilon_2)$. The relative dielectric constants of the core and substrate regions of the guide are represented by ϵ_1 and ϵ_2, respectively. We also derived the magnetic field distributions h_x, h_y, h_z for the lowest point calculated from the E_{11}^{y} mode. The results are shown in figures 5-7. As expected the component h_x had an even field distribution with most of its amplitude contained in the core region of the guide. Components h_y and h_z displayed odd field distributions with some peaks also showing in the core region. Overall h_x was the dominent magnetic field component and most of the energy of the electromagnetic wave seems to be traveling in the core region of the structure where index of refraction of the material is the largest. This explains the satisfactory

results we obtained while employing so few elements.

Validity and versatility of a finite-element method derived in terms of the transverse components of the magnetic field was verified via solving the propagation characteristics of some practical waveguiding structures used as test cases. Both the eigenvalue solver and the determinant solver routines developed from equations (17) and (18) produced good results and matched each other. The relation $\nabla \cdot H = 0$ was explicitly inserted into our formulation and the spurious modes were completely eliminated in the finite-element solutions. The results presented here gives us the necessary confidence to investigate complicated canonical models utilizing surface waves on semiconductor substrates. These structures can be used to design components in the millimeter and submillimeter-wave frequency ranges. The finite-element technique developed here will be applied to such models employing III-V compounds with the dispersion spectrum and modal field distributions presented in other sections of this report.

REFERENCES

[1] E. A. J. Marcatili, "Dielectric rectangular waveguide and directional coupler for integrated optics," *Bell Syst. Tech. J.*, vol. 48, pp. 2079-2102, Sept. 1969.

[2] R. M. Knox and P. P. Toulios, "Integrated circuits for the millimeter through optical frequency range," in Proc. Symp. on Submillimeter Waves, Polytechnic Inst. of Brooklyn, 1970, pp.497-516.

[3] W. McLevige, T. Itoh, and R. Mittra, "New waveguide structures for millimeter-wave and optical integrated circuits," *IEEE Trans. Microwave Theory Tech.*, vol. MTT-23, pp. 788-794, Oct. 1975.

[4] T. Itoh, "Inverted strip dielectric waveguide for millimeter-wave integrated circuits," *IEEE Trans. Microwave Theory Tech.*, vol. MTT-24, pp. 821-827, Nov. 1976.

[5] C. G. Williams and G. K. Cambrell, "Numerical solution of surface waveguide modes using transverse field components," *IEEE Trans. Microwave Theory Tech.*, vol. MTT-22, pp. 329-330, Mar. 1974.

[6] M. Ohtaka, M. Matsuhara, and N. Kumagai, "Analysis of the guided modes in slab-coupled waveguides using a variational method," *IEEE J. Quantum Electron.*, vol. QE-12, pp. 378-382, July 1976.

[7] S. T. Peng and A. A. Oliner, "Leakage and resonance effects on strip waveguides for integrated optics," *Trans. Inst. Electron. Commun. Eng. Japan*, vol. 61-E, pp. 151-154, Mar. 1978.

[8] M. Koshiba and M. Suzuki, "Vectorial wave analysis of dielectric waveguides for optical integrated circuits using equivalent network approach," *J. of Lightwave Technology*, vol. LT-4, pp. 656-664, June 1986.

[9] K. Solbach and I. Wolff, "The electromagnetic fields and the phase constants of dielectric image lines," *IEEE Trans. Microwave Theory Tech.*, vol. MTT-26, pp. 266-274, Apr. 1978.

[10] E. Schweig and W. B. Bridges, "Computer analysis of dielectric waveguides: A finite difference method, " *IEEE Trans. Microwave Theory Tech.*, vol. MTT-32, pp. 531-541, May 1984.

[11] K. Bierwirth, N. Schulz, and F. Arndt, "Finite difference analysis of rectangular dielectric waveguide structures," *IEEE Trans. Microwave Theory Tech.*, vol. MTT-34, pp. 1104-1114, Nov. 1986.

[12] K. Ogusu, "Numerical analysis of the rectangular dielectric waveguide and its modifications," *IEEE Trans. Microwave Theory Tech.*, vol. MTT-25, pp. 874-885, Nov. 1977.

[13] Z. J. Csendes and P. Silvester, "Numerical solution of dielectric loaded waveguides: I-finite-element analysis," *IEEE Trans. Microwave Theory Tech.*, vol. MTT-18, pp. 1124-1131, Dec. 1970.

[14] C. Yeh, K. Ha, S. B. Dong, and W. P. Brown, "Single-mode optical waveguides," *Applied optics*, vol. 18, pp. 1490-1504, May 1979.

[15] M. Ikeuchi, H. Sawami, and H. Niki, "Analysis of open-type dielectric waveguides by the finite-element iterative method," *IEEE Trans. Microwave Theory Tech.*, vol. MTT-29, pp. 234-239, Mar. 1981.

[16] N. Mabaya, P. E. Lagasse, and P. Vandenbulcke, "Finite-element analysis of optical waveguides," *IEEE Trans. Microwave Theory Tech.*, vol. MTT-29, pp. 600-605, June 1981.

[17] M. Aubourg, J. P. Villotte, F. Godon, and Y. Garault, "Finite-element analysis of lossy waveguide application to microstrip lines on semiconductor substrate," *IEEE Trans. Microwave Theory Tech.*, vol. MTT-31, pp. 326-330, Apr. 1983.

[18] B. M. A. Rahman and J. B. Davies, "Finite-element analysis of optical and microwave waveguide problems," *IEEE Trans. Microwave Theory Tech.*, vol. MTT-32, pp. 20-28, Jan. 1984.

[19] M. Hano, "Finite-element analysis of dielectric-loaded waveguides," *IEEE Trans. Microwave Theory Tech.*, vol. MTT-32, pp. 1275-1279, Oct. 1984.

[20] M. Koshiba, K. Hayata, and M. Suzuki, "Improved finite-element formulation in terms of the magnetic field vector for dielectric waveguides," *IEEE Trans. Microwave Theory Tech.*, vol. MTT-33, pp. 227-233, Mar. 1985.

[21] B. M. A. Rahman and J. B. Davies, "Penalty function improvement of waveguide solution by finite elements," *IEEE Trans. Microwave Theory Tech.*, vol. MTT-32, pp. 922-928, Aug. 1984.

[22] K. Hayata, M. Koshiba, M. Eguchi, and M. Suzuki, "Vectorial finite-element method without any spurious solutions for dielectric waveguiding problems using transverse magnetic-field component," *IEEE Trans. Microwave Theory Tech.*, vol. MTT-34, pp. 1120-1124, Nov. 1986.

[23] T. Angkaew, M. Matsuhara, and N. Kumagai, "Finite-element analysis of waveguide modes: A novel approach that eliminates spurious modes," *IEEE Trans. Microwave Theory Tech.*, vol. MTT-35, pp. 117-123, Feb. 1987.

[24] R. E. Collin, *Field theory of guided waves.* New York: McGraw-Hill, 1960.

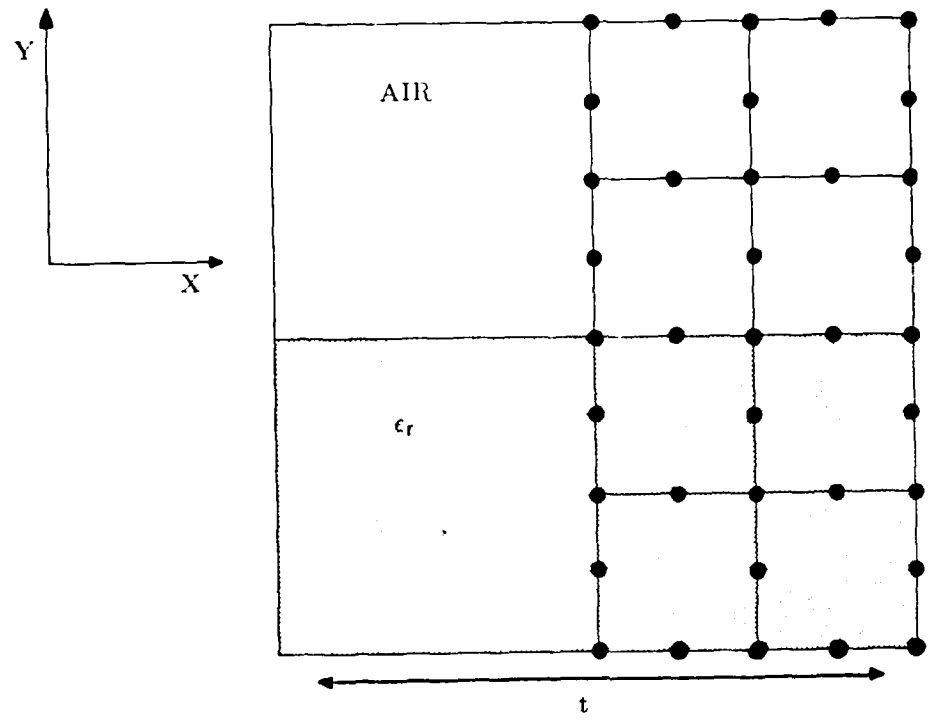

Fig.1(a) Finite-element grid for the inhomogeneously filled dielectric waveguide.

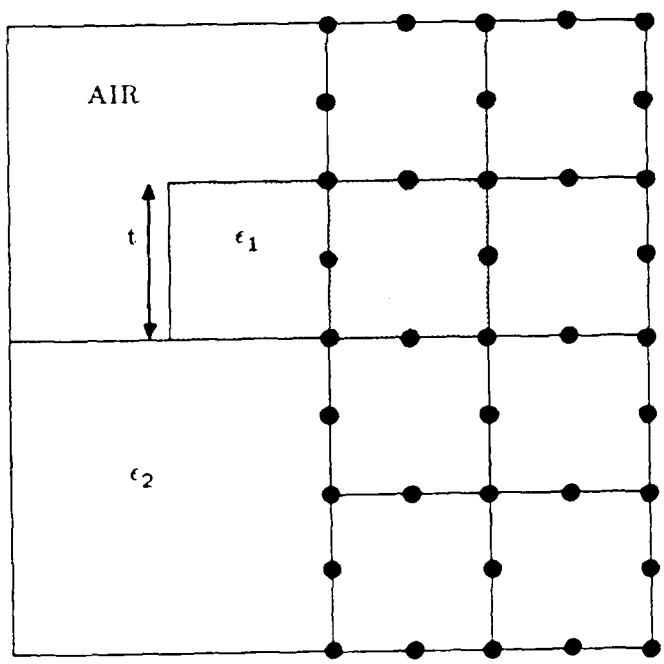

Fig.1(b) Finite-element grid for the optical embossed waveguide.

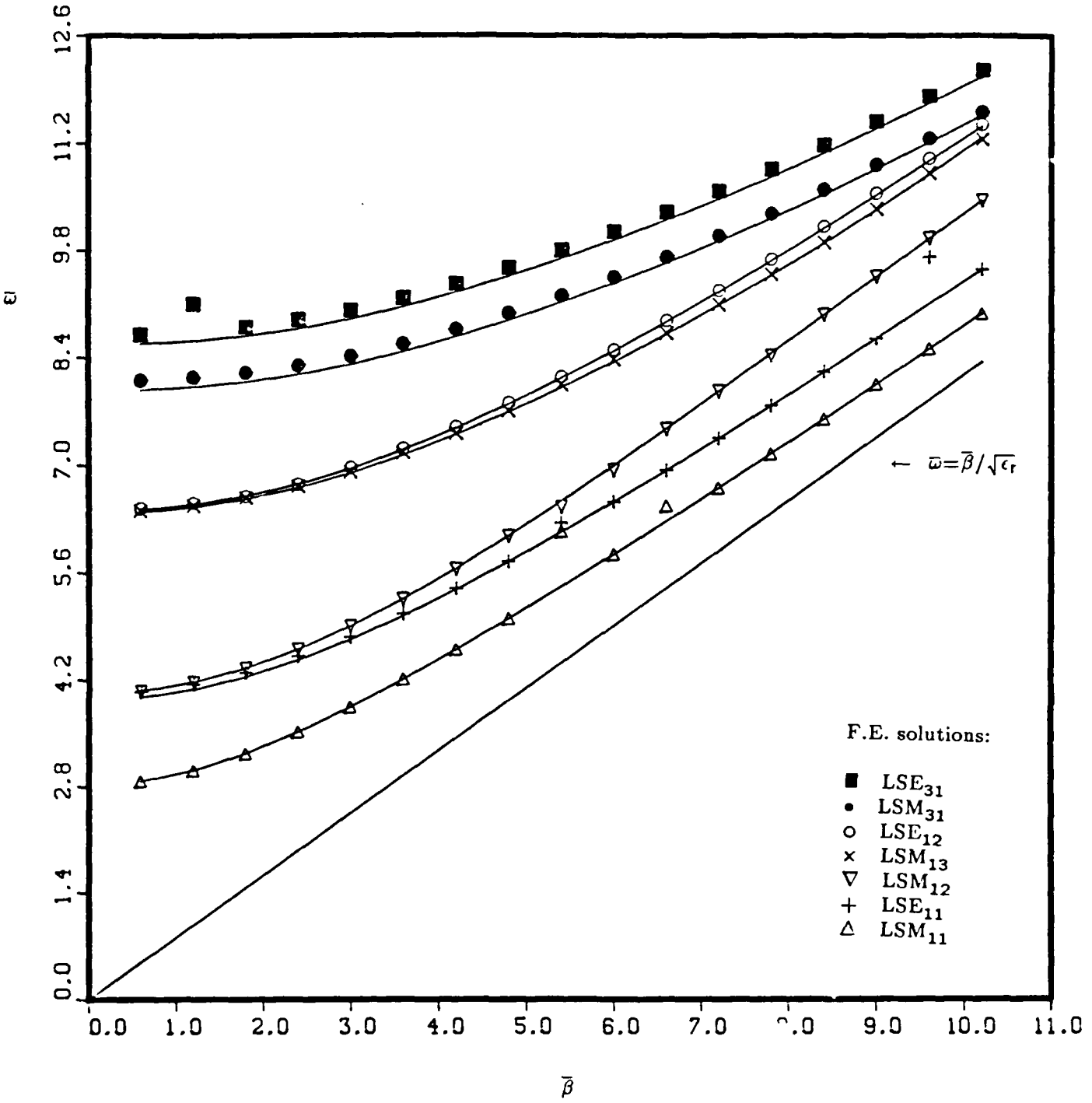

Fig.2. Finite-element and exact dispersion spectra of an inhomogeneously filled dielectric waveguide with $\epsilon_r=1.5$ while employing 8 elements. Solid lines represent the exact solutions.

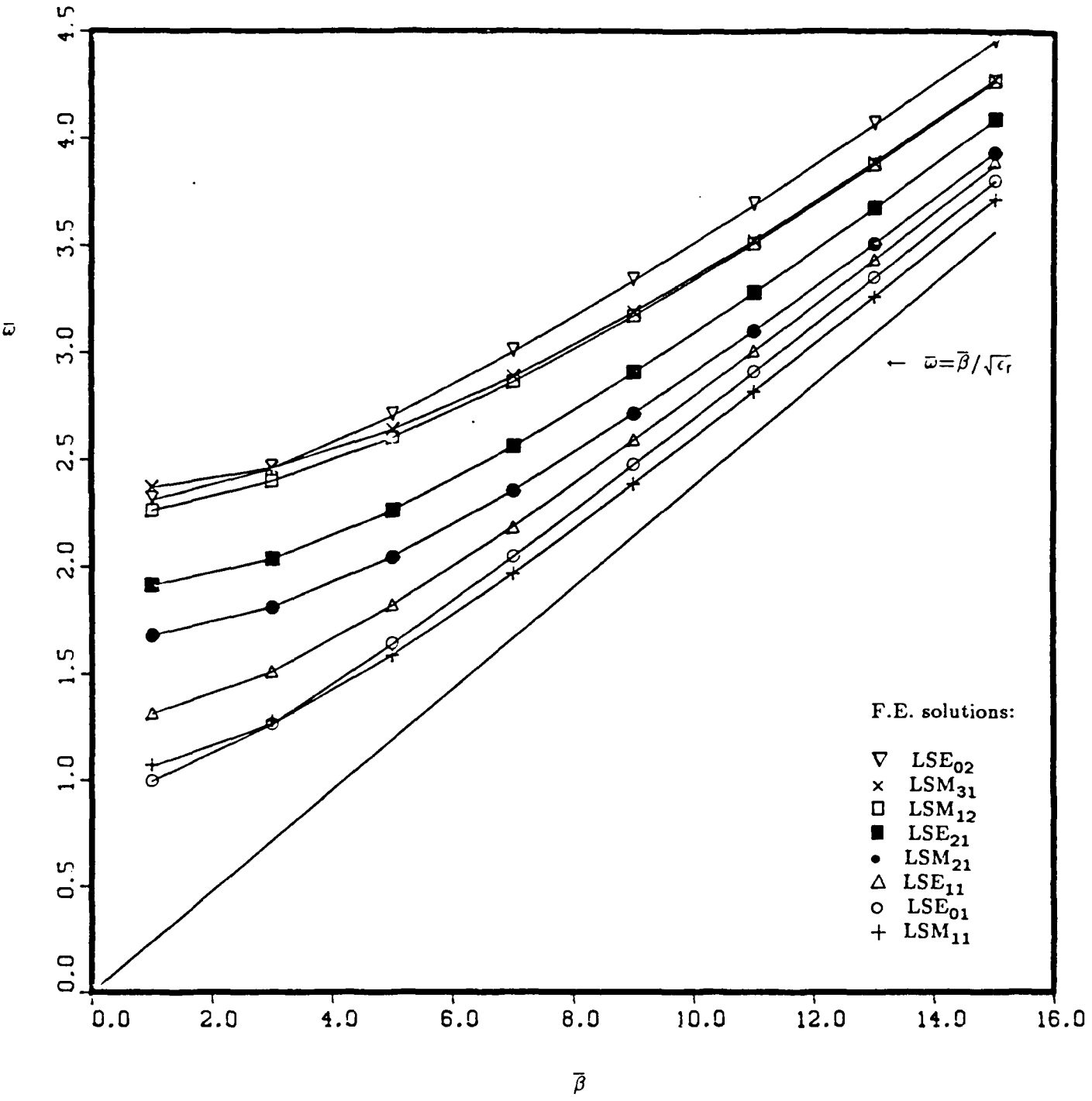

Fig.3. Finite-element and exact dispersion spectra of an inhomogeneously filled dielectric waveguide with $\epsilon_r=17.7$ while employing 32 elements. Solid lines represent the exact solutions.

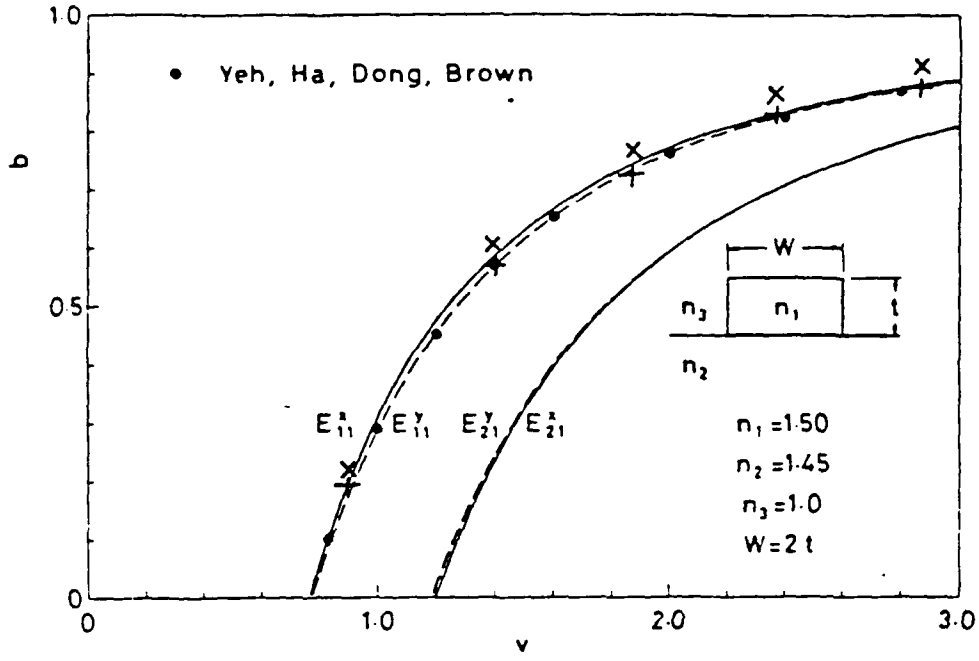

Fig.4. Finite-element dispersion characteristics for an optical embossed waveguide.

+ *represents* E^y_{11} *mode for our F.E. model.*

× represents E^x_{11} mode for our F.E. model.

• represents results from F.E. method of [14].

Solid and dashed lines represent results from equivalent network approach [8].

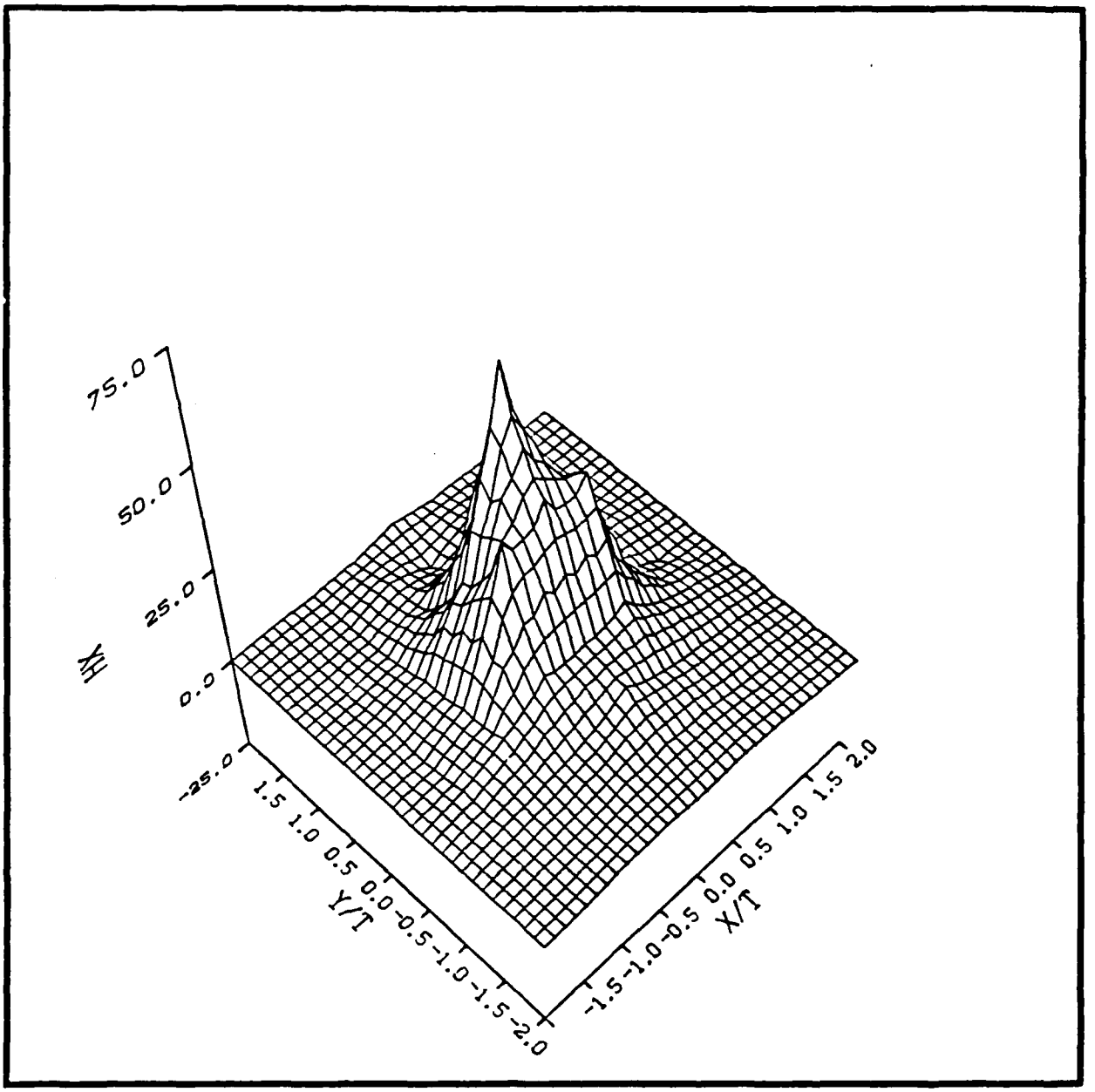

Fig. 5. h_x field distribution of the optical waveguide for E_{11}^{y} mode, v=.921, b=.195.

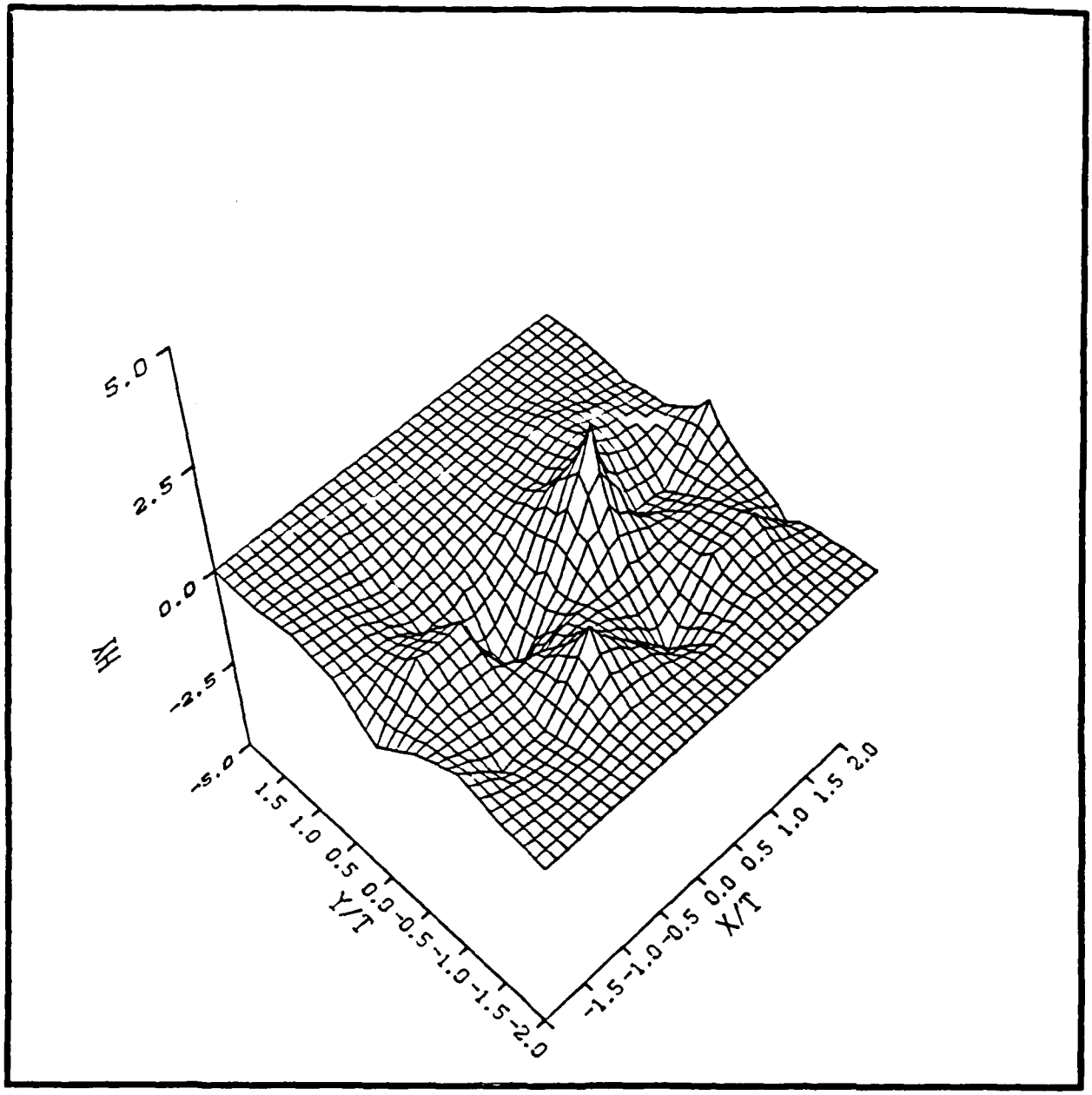

Fig. 6. h_y field distribution of the optical waveguide for E_{11}^{y} mode, v=.921, b=.195.

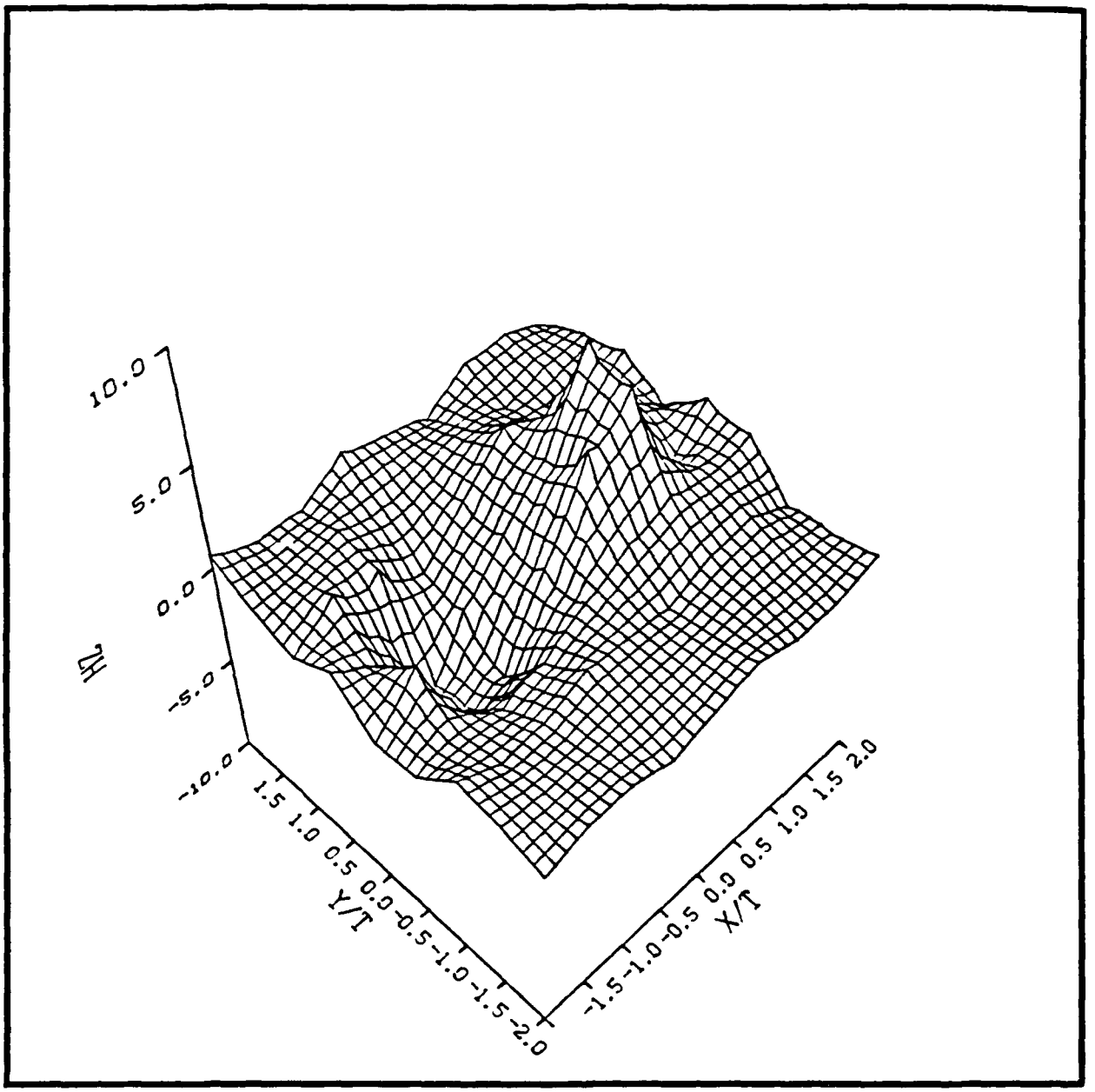

Fig. 7. h_z field distribution of the optical waveguide for E_{11}^{y} mode, v=.921, b=.195.

IV. EXPERIMENTAL EXCITATION OF SURFACE PLASMONS ON n-TYPE GaAs SUBSTRATES IN THE 110-160 GHz FREQUENCY BAND

(Dong-Hyun Hwang)

INTRODUCTION

Due to the advancement of communication technology, there exist a need for development and operation of nonreciprocal devices in the millimeter and submillimeter-wave frequency ranges. Waveguiding structures employing surface magnetoplasmons on semiconducting substrates have shown great promise for developing planar integrated nonreciprocal devices that can obtain the circuit functions performed by ferrite decices [1].

Experimental studies in surface plasmons are limited to works in the optical frequencies [2]-[5]. Even at these frequencies, very few obtained experimental dispersion relations of surface plasmons on high mobility semiconductors [2]. In this work, we will investigate quasi-optical techniques for the generation of surface plasmon waves on n-type GaAs substrates in the frequency range of 110 to 160 GHz. Results for the experimental dispersion curve will be compared to the theoretical predictions for a heavily doped n-type GaAs material at room temperature. Analyzed are the prism and grated couplers as methods for excitation of surface waves and their possible application when used in conjunction with application of magnetic fields for nonreciprocal device application. Although plasmon generation on GaAs substrate has been reported for optical frequencies [6], no experimental investigation has been carried on in the frequency range of 110-160 GHz. This work will provide the first step in experimenting with materials capable of control of plasma density. The application of surface plasmons could provide a new array of millimeter-wave devices with loss comparable to ferrite devices at lower frequencies.

SURFACE PLASMONS

A- *Surface polaritons*

As defined by Wallis et al. [7], a polariton is an electromagnetic wave coupled through phonon, plasmon, magnon or other type of excitation to condensed matter. In the literature, the term electromagnetic surface waves generally refer to guided modes propagating in a thin film on top of a metal substrate (see Fig.1). This type of surface wave is not a polariton and can be distinguished by examining its ω-β dispersion curve as shown in Fig. 2. In this paper, the phenomena of interest for guiding and controlling millimeter waves are surface plasmons, a member of the surface polariton family. This type of surface wave, for an isotropic n-type semiconductor, has the unique dispersion curve which lies entirely to the right of the light line in vacuum and is asymptotic to the surface plasma frequency (see Fig.3).

The theoretical dispersion of millimeter-wave surface plasmons in n-type GaAs was derived by Nurmikko et al. [8], for an isotropic electron gas taking into consideration a simple Drude contribution to the dielectric constant.

$$\epsilon(\omega) = \epsilon^{(o)} - \frac{\omega_p^2}{\omega(\omega+i/\tau)} = \epsilon_s' + i\epsilon_s'' \qquad (1)$$

Where $\epsilon^{(o)}$ is the static dielectric constant of the material, ω_p is the plasma frequency, and τ is the momentum relaxation time. Equation (1) can be separated into real and imaginary parts so,

$$\epsilon(\omega) = \epsilon_s' + i\epsilon_s''$$

$$\text{where} \quad \epsilon_s' = \mathrm{Re}[\epsilon^{(o)}] - \frac{\omega_p^2}{\omega^2+(1/\tau)^2} \quad \text{and} \quad \epsilon_s'' = \mathrm{Im}[\epsilon^{(o)}] - \frac{\omega_p^2}{\tau\omega(\omega^2+(1/\tau)^2)} \qquad (2)$$

Plotting $\mathrm{Re}[\epsilon(\omega)]$, we see it has large negative values at liquid nitrogen temperatures (77°K) with a carrier concentration equivalent to the plasma frequency of $\omega_p=10^{13}$ rad/s for the frequency band of 110-170 GHz. For the same plasma frequency, but at room temperature (300°K), the real permittivity remains positive (see Fig.4). To obtain a surface plasmon wave, it is necessary for one of the media's effective permittivity to posses a sufficiently large negative real part. This requirement will be explained in the next section when the

electromagnetic theory of surface polaritons is discussed. Since at room temperature the effective real permittivity is only slightly positive ($\simeq$3.0), adjustments in the carrier concentration and lowering of the temperature to increase mobility will lower the permittivity into the negative region. Although it is possible to obtain a desired range of values for the carrier concentration through plasma injection, it would be difficult to measure the exact carrier density contributed by this process. A problem also arises if optical injection methods are used. The depth of penetration for the newly formed plasma layer will be substantially less than the length of the millimeter wave, so the surface plasmon guiding structure becomes a three or even four medium layer, complicating the theory further. For our immediate purpose, a highly doped ($\simeq 10^{18}/cm^3$) substrate will be used to generate a lower portion of the dispersion curve without introducing concern over plasma injection problems.

B- *Electromagnetic theory of surface polaritons*

We consider a single planar interface of infinite extent which separates two media characterized by frequency-dependent dielectric constants $\epsilon_a(\omega)$ and $\epsilon_b(\omega)$ for x>0 and x<0, respectively. If the magnetic field is eliminated from Maxwell's curl equations, the electric field E satifies the equation

$$\nabla\times\nabla\times E + \frac{1}{c^2}\frac{\partial^2 D}{\partial t^2} = 0 \qquad (3)$$

We seek a solution to eq. (3) in which the electric field propagates in the z-direction and decreases exponentially with increasing distance from the interface. So, the equations for the electric fields in the two regions can be written as

$$E_a = E_a^{\,o}\, e^{-\alpha_a x}\, e^{i(kz-\omega t)} \quad , \quad x>0 \qquad (4)$$

$$E_b = E_b^{\,o}\, e^{\alpha_b x}\, e^{i(kz-\omega t)} \quad , \quad x<0$$

substituting eqs.(4) into (3), we obtain the decay constant for each region.

$$\alpha_a^{\,2} = k^2 - \epsilon_a(\omega)\frac{\omega^2}{c^2} \quad , \quad \alpha_b^{\,2} = k^2 - \epsilon_b(\omega)\frac{\omega^2}{c^2} \qquad (5)$$

Applying the boundary conditions, at x=0 leads to the relations

(tangential): $E_{ay}^{\,o}=E_{by}^{\,o}$, $E_{az}^{\,o}=E_{bz}^{\,o}$ (6) and (normal): $\epsilon_a(\omega)/\epsilon_b(\omega)=-\alpha_a/\alpha_b$ (7)

In addition, from the continuity of the tangential components of B, the following is obtained.

$$(\alpha_a + \alpha_b) E_{ay}^{o} = 0 \qquad (8)$$

Since the decay constants α_a and α_b must be positive, $E_{ay}^{o} = 0$. Therefore for surface polaritons only TM mode propagation exists. Using eqs. (5) and (7), the well-known dispersion relation is obtained [7]-[9].

$$k^2 = \frac{\omega^2}{c^2} \frac{\epsilon_a(\omega)\, \epsilon_b(\omega)}{\epsilon_a(\omega) + \epsilon_b(\omega)} \qquad (9)$$

Equation (7) indicates that $\epsilon_a(\omega)$ and $\epsilon_b(\omega)$ must have opposite signs at the frequency ω. The medium with negative $\epsilon(\omega)$ is termed "surface active". In the case of an air interface for ϵ_b, $\epsilon_a(\omega)<-1$. So this justifies the statement in section A regarding the requirement for a media to have an effective real permittivity of negative value.

C- *Theory for highly doped GaAs*

For a doping level of order of 10^{18} /cm^3, GaAs exhibits an effective dielectric constant with large negative values for the real part of the permittivity in the near millimeter wave range of 110 to 170 GHz. To obtain the effective permittivity, we have to calculate the plasma frequency and the relaxation time from the carrier concentration. The plasma frequency is defined by

$$\omega_p^2 = \frac{ne^2}{\epsilon_o m^*} \qquad (10)$$

where n is the carrier concentration of the material. Since for the doping level of 10^{18}, the plasma frequency ω_p is about 2.18×10^{14} rad/s, the operating bandwidth is well below the asymptotic value of the surface plasma frequency ω_{ps}. The relaxation time τ, can be deduced from the DC conductivity $\sigma(0)$, if τ is assumed to be frequency independent. Since the frequency-dependent conductivity is defined by

$$\sigma(\omega) = \frac{ne^2\tau}{m^*} \frac{1}{1 - i\omega\tau} \qquad (11)$$

and we obtain the DC conductivity by setting $\omega=0$, $\sigma(0)=ne^2\tau/m^*$. M/A-Com, the manufacturer of the GaAs wafers, indicated an overall edge and center resistivity of 2.6×10^{-3} Ω-cm for the Si-doped samples. From the resistivity, an impurity concentration of 8×10^{17} /cm^3 can be deduced from the curve in Sze [10] for room temperature (T=300°K) n-type GaAs.

This value is very close to the carrier concentration of $10^{18}/cm^3$ indicated by the manufacturer, so we can reasonably assume all the impurities are ionized at room temperature. With $n=10^{18}$ $/cm^3$ and $\sigma(0)=384.6$ $/\Omega$-cm, a vlaue of $\tau=9.169x10^{-14}$ sec is obtained. The corresponding change in the real part of the permittivity ϵ_s' in eq.(2) can be calculated as a function of ω for the obtained ω_p and τ. Since $1/\tau$ is large compared to the operating ω range, the $\Delta\epsilon_s'$ is almost a constant at about -385. This yields an effective real permittivity of $\epsilon_s' \simeq$-382 if $Re[\epsilon^{(o)}]$ is assumed to be 13.0. The change in the imaginary permittivity is $\Delta\epsilon_s'' \simeq$-4030. If $Im[\epsilon^{(o)}]=1000$ is assumed, the complex effective permittivity for the frequency range of 110-170 GHz is about $\epsilon_s \simeq$-382 - i3030. Using this constant effective permittivity, the dispersion relation is simplified.

The dispersion relation for surface plasmons is given by Ward et al. [11] where the propagation constant for an air interface is given by

$$\beta = \frac{\omega}{c}\sqrt{\frac{(A+\sqrt{A^2+B^2})}{2D}} \qquad (12)$$

where $A=|\epsilon|^2 + \epsilon'$, $B=|\epsilon|^2 + \epsilon''$, $D=|\epsilon + 1.0|^2$ (13)

and $\epsilon=\epsilon'+\epsilon''$ is the effective dielectric constant of GaAs. The theoretical dispersion curve for a sample with a carrier concentration of $10^{18}/cm^3$ is a constant line slightly to the right of the light line for the frequency range of 110-170 GHz. In the case of $n=10^{18}/cm^3$, $\omega_p=2.18x10^{14}$ rad/s and for $\tau=9.17x10^{-14}$ s, the propagation constant has the relation, $\beta=(\omega/c)$ 1.098. If a simple model is used without taking the Drude model into consideration, the dispersion relation is not altered by a great amount, since $\beta \simeq (\omega/c)$ 1.026.

THEORY OF EXCITATION OF THE SURFACE WAVES

A- *Grating coupler theory*

In grating couplers, the surface wave must be accompanied by space harmonics in the grating region because of the periodic nature of the structure. These harmonics have

propagation constants given by

$$\beta_m = \beta_o + \frac{2m\pi}{d} \qquad m = 0, \pm 1, \pm 2, \ldots \ldots \tag{14}$$

where β_o is closely equal to the surface wave propagation constant if the periodic structures are considered to be small perturbation and d the periodic spacing. The phase matching condition can be satisfied if $k \sin\theta = \beta_m$ (15)

where θ is the incident beam angle to the periodic structures.

Experiments with grating couplers on semiconductors such as GaAs [6] and InSb [2] were conducted earlier. The construction of a dispersion curve $\omega(\beta)$, involves the determination of eigenfrequencies ω_r, which depends on the grating profiles. Experimentalists have encountered the well known Wood's anomalies for gratings. This is illustrated in Fig.5. Theory and experiment have shown that the modulation depth h of the periodic structures contributes significantly to the shape of the dispersion curve [12], [13]. Since the experiment is performed using high index line strips of rectangular shape polymer material as the periodic corrugation, better coupling is expected than for grooves drawn on the substrate surface. The only difference in theory between grooves and high index structures is a refractive index term n_p, multiplied for the material used as grating structures on the left hand side of eq. (15). So $\beta_m = n_p\, k \sin\theta$ and $n_p \simeq 1.60$ for polymer dielectrics at the operating frequency range of 110 to 170 GHz. The maximum achievable efficiency of coupling for such periodic structures is 80.1% [14]. This condition is obtained for the optimum αw_o value of 0.68, where

$$w_o = w \sec\theta \tag{16}$$

w is the half beam-width of a Gaussian beam and α is the leakage factor. The leakage factor depends very much on the height of the grating [15]. If the length of the period d, is half of the wavelength, and h, the height is about 0.1 mm at λ=2.0 mm, the leakage factor is approximately 3.75/m. The constraint on the beam width for this range of wavelength is

$$0 < w < 18.1 \text{ cm} \qquad \text{for } 0 < \theta < \pi/2 \tag{17}$$

so for practical high efficiency coupling at 0.1 mm of grating height, about 1° to 5° of

incidence angle will be optimal to obtain a reasonable beam width from a waveguide horn. Since we are involved in experimenting at considerably shorter wavelength than is the case for microwaves, most of the theory is obtained from optics. However, various experiments will have to be conducted to obtain a reasonable interpretation for the quasi-optical theory applied to the millimeter-wave range.

B- *Prism coupler theory*

The use of attenuated total reflection (ATR) method for wave excitation has been a common technique in waveguide optics [16], [17]. More common terminologies used are the prism coupling or optical tunneling techniques. The surface plasmon excitation technique was first suggested by Otto [18] and followed by a modified technique by Kretschmann [19] for thin samples. The theories behind this method of surface plasmon excitation are basically identical to that of guided optics. In guided optics, the dielectric layer is bounded by a top and bottom layer and the incident wave travels along a zig-zag path exhibiting total reflection at both layers. The wave in surface plasmon is bounded on top by an active surface and below extends to infinity. Both configurations have to match the propagation constant at the base of the prism to the guided wave mode or the surface plasmon propagation constant. In the guided wave case, the theory becomes more complicated as consideration of various allowable modes for the dielectric thickness limits the material selection for the prism coupler. This restriction is more evident in semiconductor guides where the refractive indexes range from 3.0 to 4.0. Since, to excite a guided mode, the prism coupler's refractive index has to exceed the guide's effective refractive index, optical range wave guiding had to be achieved through end coupling. The use of millimeter waves provide new flexibilities in selecting prism couplers for semiconductor guides. This is due to the reduced effective refractive index contributed by the carriers.

The Otto or guided wave configuration has a gap between the prism and the guide. This gap is usually of the order of the wavelength and it is usually considered to be air, although index matching dielectrics can be used to fill the gap. The Otto configuration works through a

phenomenon refered to as frustrated total internal reflection. The ATR technique utilizes the evanescent tail formed through the prism to couple to the surface wave (both surface plasmon and guided wave). Since surface waves are non-radiative, the propagation constant required is to the right of the light line in the ω-β diagram. This can be achieved by forming an incident wave above the critical angle of the prism-gap interface. When the incident wave is totally reflected, the reflected intensity shows a dip at the resonant coupling condition. This loss in energy corresponds to the energy conversion into surface wave. The dispersion relation, for a resonant angle of incidence θ_i, can be expressed by $\beta(\omega)=\omega/c\ n_p \sin \theta_i$.

EXPERIMENT AND RESULTS

A- *Experiment setup*

The source of the millimeter wave was a Micro-Now model 705B millimeter wave sweeper with a model 170 BWO tube. The output power averaged about 10 mW for the frequency band of 110-170 GHz. Our measurements were performed using a bolometer. A signal generator was used to modulate the tube at 1kHz. The modulation was triggered by a TTL signal and was connected to the amplitude modulation input (AM). The TTL signal was also connected to the reference input of a phase locked amplifier, (EG&G Princeton Applied Research model 5207). The modulated millimeter wave output was connected to a Hughes model 45728H-1000 attenuator with a range of 0 to 50 dB of attenuation and a maximum insertion loss of 2dB. A directional coupler was followed by the attenuator. The Hughes coupler model 45328H-1210 is a 3 port split block style general purpose coupler with a low frequency band crossguide coupling value of 10dB. The second line output from the coupler was connected to the leveler input of the generator. The main line was connected to a waveguide horn. The pyramidal horn has a 24dB gain at mid band. The reflected and surface transmitted signals were detected by a flat broadband detector connected to a receiver waveguide horn. The detector has a minimum sensitivity of 100 mV/mW. Signal detection was

achieved by using the phase lock-in amplifier. The general schematic of the setup is shown in Fig.6.

B- *Periodic grating experiment*

In this experiment, the M/A-Com GaAs sample was placed at 45° and reflective intensity measurements between the polished samples and the sample with periodic lines of 2mm were compared (see Fig.7). The lines were 2mm wide, 0.1mm thick and composed of cellophane. The millimeter wave sweeper was swept from 140 to 170 GHz. Initial comparison showed a dip at about 163.6 GHz in the reflected intensity for the sample with the periodic structure (see Fig.8). To check for surface wave coupling, the receiver was placed at the edge of the sample to obtain signal detection. The receiver detected two signals with strong intensities at 146.3 and 163.6 GHz (see Fig.9). The experiment was repeated with power leveling and with a directional coupler and we obtained a sweep of a narrower bandwidth (158 to 164 GHz). The results, as depicted in Fig.10, show a drop in intensity at 163.6 GHz for the grated sample as compared to the polished sample. Also, there is strong detection of a signal at the edge of the sample at the same frequency. Another experiment with d=1.5mm was conducted at 23°. Since the periodic length was not in the $\lambda/2$ regime, very weak coupling was observed for this case. The results are evident in figures 11-12. The reflection drop at 160.7 GHz is not as well defined as in the previous case and the end signal detection is disturbed by noise levels as strong as the signal itself. Another experiment was carried out with the enhanced gratings being three times greater in height than in the previous case. The sweep frequency was narrowed to a range of 158.4 to 164.5 GHz. The results are depicted in Fig.13 which shows an increase in the number of end coupling peaks. In this case, the detection of the particular coupling frequency is hampered by an increased number of harmonics or noise. This particular experiment shows that a complicated diffraction and reflection theory would have to be taken into account. Although a few very involved theories are published, to pursue these would be too much of a distraction from our immediate desire of observing surface plasmon waves.

Although there is a strong evidence of surface plasmon generation at 2mm of grating distance, the height and shape of the particular grating structure influences to a high degree the detection procedure for the surface wave. A more practical and nondestructive method is the prism coupling configuration which will be discussed in the next section. The grating coupler dips obtained will be compared with the prism coupled surface wave in the ω-β diagram. The reason for this is to eliminate any doubts in our grating data as to it being of higher or lower harmonic origin. A comparison will illustrate the more accurate method of surface wave generation for a particular frequency range. The final reasoning for not utilizing the periodic structure method is the presence of the scattered of waves which contribute to a high level of noise.

C- *Prism coupling experiment*

In comparison to grating couplers, prisms provide a non-destructive way of generating surface plasmons. It also eliminates the need to worry about the complicated scattering theories needed for grating profiles. So, Wood's anomalies should not be encountered as in the previous experiments conducted using enhanced periodic structures. The method used in this experiment is shown in Fig.14. The setup is referred to as the Kretschmann configuration [19]. This configuration differs from the traditional Otto configuration because the gap between the prism and the metal is eliminated. To use this method, the thickness of the surface active material has to be restricted to less than the order of the operating wavelength (usually $\lambda/10$). Since the wafer of the GaAs is 25mils or 0.0635cm, the operation in the frequency range of 110 to 170 GHz results in a surface active thickness of order of $\lambda/4$.

When performing this experiment, the prism was separated by a distance of 16cm from the source horn. This was to ensure far zone operation and plane wave incidence could be assumed ($2D^2/\lambda$). Experiments were conducted for reflection angles of 37°, 45°, 51°, and 57° at the prism base. Millimeter wave sweeps were performed for two bandwidths of 110 to 136 GHz and 136 to 159 GHz. Distinctive sweeps at four differing angles of incidence were

performed. The experiments were conducted both with and without the GaAs. The data is shown in figures 15 to 18 and the resulting sweep was normalized to obtain the plane polarized reflection coefficient for each case. As observed in figures 19 to 22, various minimums are to be observed for the two bandwidths of 110-136 GHz and 136-159 GHz. Careful consideration of these minimum points is required to interpret the data correctly. First, the obtained minimums are used to calculate the propagation constant β, which will help determine the correct minimums when plotted against the normalized plane polarized reflection coefficient. The obtained minimas were labeled and normalized to obtain the frequency of the minimum for each angle of incidence. Theoretically, the surface plasmon wave is generated when the reflection coefficient approaches zero. In the experiment performed, the minimum normalized value obtained was about 0.05 or -13.0dB. As variation in the incident angle is introduced, the reflection coefficient changes. The desired angle of observation is that which yields the minimum reflection at a given frequency. For this experiment the accuracy of the angle of incidence is limited to about $\pm 2^{\circ}$ and if a more accurate method of angular measurement was available, near zero levels of normalized minimum should be observed. Some minimums will be closely matched to the incidence angle and most points will be in the vicinity of this angle. Interpolation of angles is necessary to yield the full continuous ω-β curve.

In table I, the points A through M showed the most clearly distinguished minima when plotted against the propagation constant. The minimum usually occurrs for the case of a 45° angle of incidence, with the only exception occurring for point M which was at 51°. Consequently, table I was plotted for four bandwidths as depicted in figures 23 to 26. When the data was plotted in Fig.27 in the form of an ω-β diagram, it showed a very close match to the theory presented for highly doped GaAs material. The 'x' points indicate dispersion points obtained using periodic couplers. It can be observed, that prism coupling provides greater accuracy when performing the experiment.

TABLE I

Experimental data for minimum reflection points

Point	Frequency (GHz)	β (θ=37°)	β (θ=45°)	β (θ=51°)	β(rad/cm) (θ=54°)
A	115.49	23.29	27.37	30.08	32.46
B	116.38	23.47	27.58	30.31	32.71
C	120.20	24.24	28.48	31.30	33.78
D	122.93	24.79	29.13	32.01	34.55
E	127.13	25.64	30.13	33.11	35.73
F	129.23	26.06	30.62	33.66	36.32
G	130.04	26.23	30.82	33.87	36.55
H	131.49	26.52	31.16	34.24	36.96
I	135.86	27.40	32.19	35.38	38.18
J	141.80	28.60	33.60	36.93	39.85
K	145.05	29.25	34.37	37.78	40.77
L	151.89	30.63	36.00	39.56	42.69
M	157.95	31.85	37.43	41.13	44.39

The slight shift in the experimental data could mostly be accounted for by the errors contributed during the angular measurements. It could also be due to inaccurate assumptions of the refractive index of the prism (n_p=1.6). But it is not likely for a variation in the refractive index due to frequency dependence to be sufficiently large. In the periodic coupler case substantial retardation was observed. The cause of this phenomenon could be attributed to various causes. Wood's anomalies could contribute a major factor, but extensive studies and experiments would have to be carried out to prove this.

Further considerations must be given of points not mentioned in table I and R_p vs. β figures. These are N, O, P for the lower bandwidth of 110 to 136 GHz and Q, R, S for the higher band of 136 to 159 GHz. The six points mentioned show strong reduction of R_p against a frequency sweep. The lack of definite dips in the R_p vs. β plots prevent these points from being analyzed with accuracy. Interpolation will have to be used to estimate the approximate angle of incidence. In the case of point N, substantial reduction in the reflection coefficient was observed for θ=51° than θ=45°. But at θ=45° there was still about 0.7 reduction of the reflectivity, so the angle of incidence which would excite a surface plasmon would be closer to 51° but not by a large margin. The estimation for point N will be taken as θ=48°, this can be interpreted as for $\omega=0.7825\times10^{12}$ rad/s (f=124.54, point N) β=31.01 rad/cm. This value is slightly greater than the expected value, but it is within admissible margin of error. The same evaluation applies to point O with an estimated θ of 41°, $\omega=0.805\times10^{12}$rad/s at this point with a β of 28.16 rad/cm. Point P is unique because, as the reflection angle is increased, the reflection coefficient drops. It has a high value of estimated minimum and it is the first point branching out into second curve for the dispersion relation. With an estimated θ of 55°, point P yields to a propagation value of 38.5 rad/cm. The existence of a second mode becomes more evident when points R and S show more than one excitation angle for a single frequency. Both points R and S start at a minimum and increase to a maximum reflection around 45° and drop back to another minimum at about 55°. This point will not be included due to this

uncertainty. It is probably influenced by material absorption property rather than the excitation of a surface wave. Finally, the tabulated data for the additional modal points are in table II, and the final dispersion curve including these points, is depicted in Fig.28.

Table II

Additional data with second modal points into consideration

Point	Frequency (GHz)	Minimum Angles M_1	M_2	β_1 (rad/cm)	β_2 (rad/cm)
N	124.54	48°	---	31.01	--------
O	128.10	41°	---	28.16	--------
P	132.66	55°	---	38.50	--------
Q	Discarded Point				
R	147.31	39°	58°	31.10	41.86
S	157.31	40°	59°	33.88	45.19

The second set of points to the right of the dispersion curve indicate another mode contributed by the prism substrate boundary. Normally this mode is not observed in the optical regions. If no major experimental errors exist, the only reasonable explaination for this mode is its generation by the interface adjacent to the prism. Two methods of possible verification can be suggested. First, increase the sweeper frequency to obtain a fuller dispersion curve. Second, reduce the doping density to lower the plasma frequency. The latter will also have an effect as to the range of the observable dispersion curve. If any hypothesis of the experimental errors could be made, it will be mainly due to angular measurement errors. For example, the first angle of incidence of 37° is very close to the critical angle of the prism. This error in measuring and operating in the critical angle region could have contributed to the unexpected second mode. The final suggestion for anybody repeating this experiment would be the use of a goniometer or other accurate angular measurement device. Since our experiment, were carried

out at room temperature, the next step would be to experiment under cryogenic conditions.

CONCLUSION

Surface plasmon generation was accomplished using quasi-optical techniques. Verification was obtained through end coupling detection for the periodic coupler case, and generating R_p vs. frequency and R_p vs. β plots for the prism coupler. A better match between theory and experiment was obtained for the prism coupler. Through the experiments, the retardation effects for periodic or grating couplers were observed. The difficulty in distinguishing the correct harmonic was a problem when the profile height was tripled. Unlike the periodic coupler, the prism coupler had the advantage of generating various propagation constants for a given type of prism.

It has been shown that the non-destructive methods employed here not only is convenient, but also provides a relatively accurate detection of the surface wave dispersion characteristic. The additional mode encountered could prove to be an interesting topic for further study. In the case of optical couplers for experiments conducted on metal surfaces, the absorption levels of the prisms encountered in the optical regions prevent such modes from existing.

Finally, the generation of surface plasmons at the frequency range of 110-160 GHz has not been demonstrated before. The use of a highly doped n-type GaAs for such an experiment is also a first. The gap between the optical and microwave field needs to be explored for further advancement of millimeter wave devices and systems.

REFERENCES

[1] D. M. Bolle and S. Talisa, *IEEE Trans. Microwave Theory Tech.*, MTT-29, p.91 (1981)

[2] N. Marschall, B. Fischer, and H. J. Queisser, *Phy, Rev. Lett.*, vol. 27, p.95 (1971)

[3] V. V. Bryksin, D. Mirlin, and I. I. Reshina, *Sov. Phys. JETP Lett.*, vol. 16, p.315 (1972)

[4] A. Hartstein and E. Burstein, *Solid State Comm.*, vol. 14, p.1223 (1974)

[5] E. D. Palik, R. Kaplan, R. W. Gammon, H. Kaplan, R. F. Wallis, and J. J. Quinn, *Phys. Rev.*, vol. B13, p.2497 (1976)

[6] B. Fischer and N. Marschall, *Proceedings of the 10th International Conference on the Physics of Semiconductors*, S. P. Keller, J. C. Hensel, and F. Stern, eds., p.845 (1970)

[7] R. F. Wallis and C. A. Se'benne, Handbook on Semiconductors, M. Balkanski Ed., vol. 2, Ch.3, (1980)

[8] A. V. Nurmikko, D. M. Bolle, and S. Talisa, *Int. J. Inf.*, vol. 1, p. 3 (1980)

[9] A. Otto, Optical Properties of Solids-New Developments, B. Seraphin Ed., vol. 2, Ch. 12, (1975)

[10] S. M. Sze, Physics of Semiconductor Devices, p. 33 (1981)

[11] C. A. Ward, R. J. Bell, R. W. Alexander, and G. S. Kovener, *Appl. Opt.*, vol. 13, p. 2378 (1979)

[12] B. Laks, D. L. Mills, and A. A. Maradudin, *Phys. Rev-B*, vol. B23, p. 4965 (1981)

[13] J. Hagglund and F. Sellberg, *J. Opt. Soc. Am.*, vol. 56, p. 1031 (1966)

[14] T. Tamir and H. J. Berton, *J. Opt. Soc. Am.*, vol. 61, p. 1397 (1971)

[15] T. Tamir, Topics in Applied Physics - "Integrated Optics", vol. 7, p. 113 (1979)

[16] R. Ulrich, *J. Opt. Soc. Am.*, vol. 60, p. 1337 (1970)

[17] J. H. Harris and R. Shubert, *IEEE Trans. Microwave Theory Tech.*, vol. MTT-19, p. 269 (1971)

[18] A. Otto, *Z. Physik*, vol. 181, p. 232 (1965)

[19] E. Kretschmann, *Z. Physik*, vol. 241, p. 313 (1971)

[20] R. F. Harrington, Time-harmonic Electromagnetic Fields, Ch. 4, (1961)

[21] D. L. Lee, Electromagnetic Principles of Integrated Optics, Ch. 4, (1986)

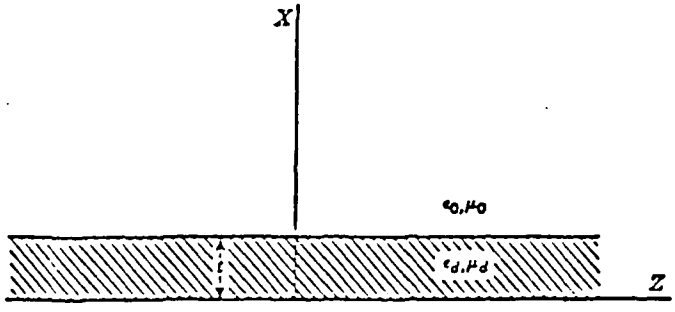

A dielectric-coated conductor.

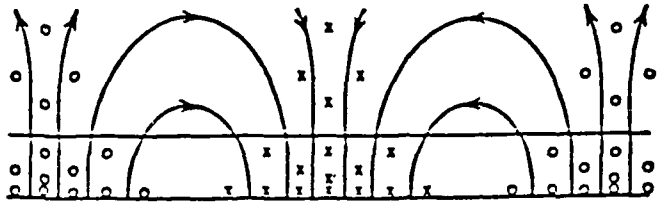

The TM_0 mode pattern for the coated conductor ($\mathcal{E}$ lines solid.)

Figure 1-(from Harrington [20])

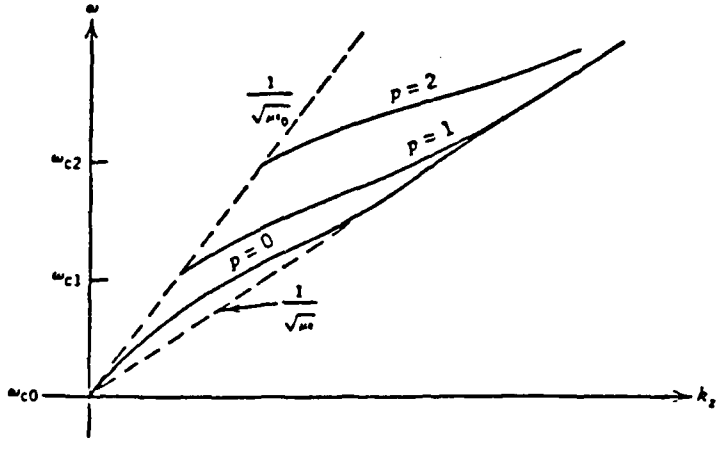

Dispersion relation for first three guided modes.

Figure 2 (from Lee [21])

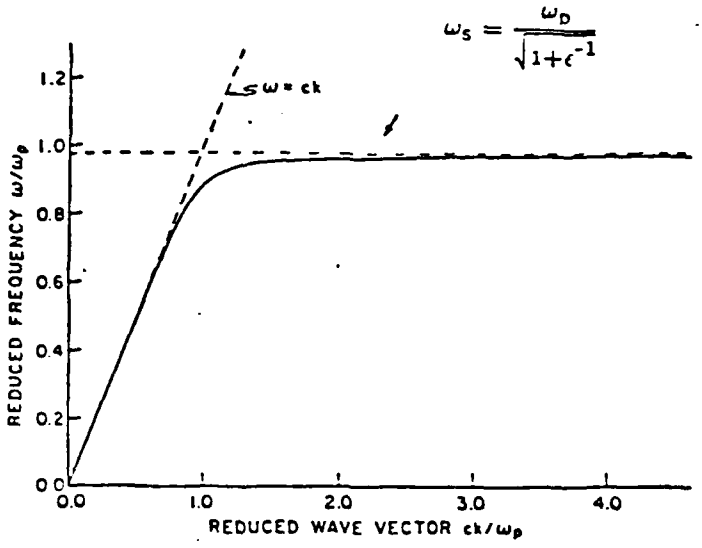

Dispersion curve for surface plasmon polaritons in n-type InSb.

Figure 3- (from Wallis *et al.* [7])

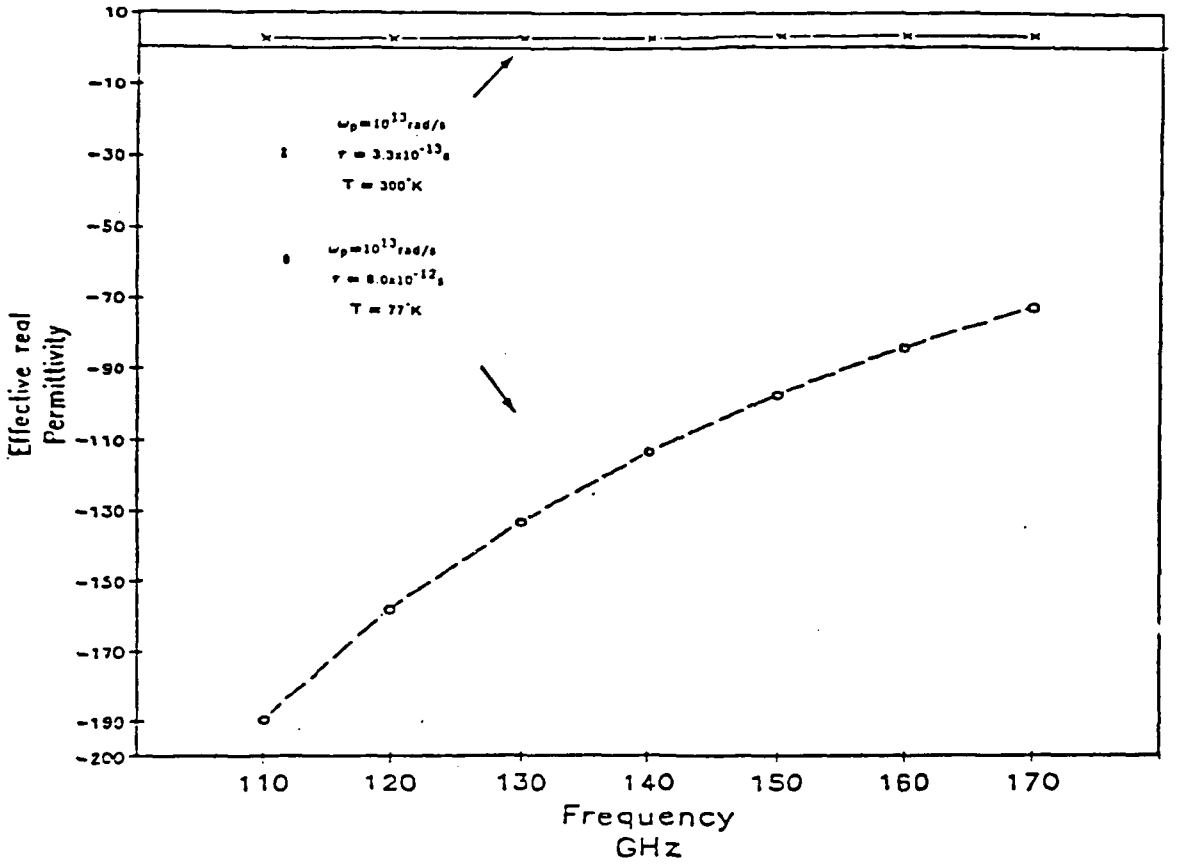

Figure 4– Effective real permittivity of n-type GaAs

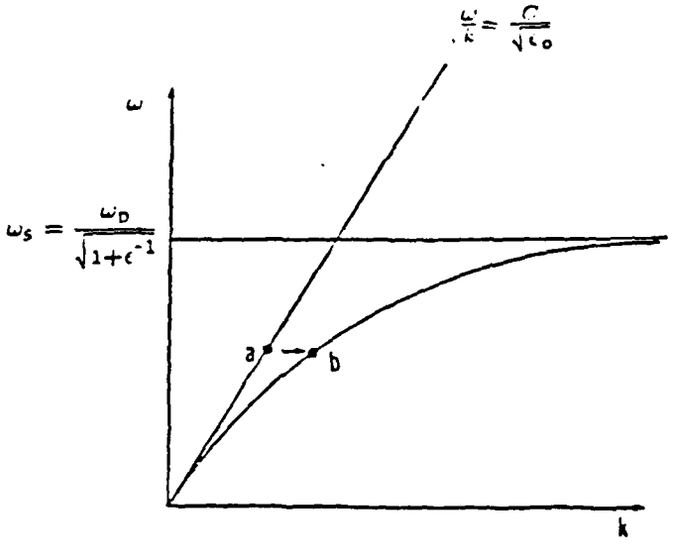

Figure 5- Description of Wood's anomalies

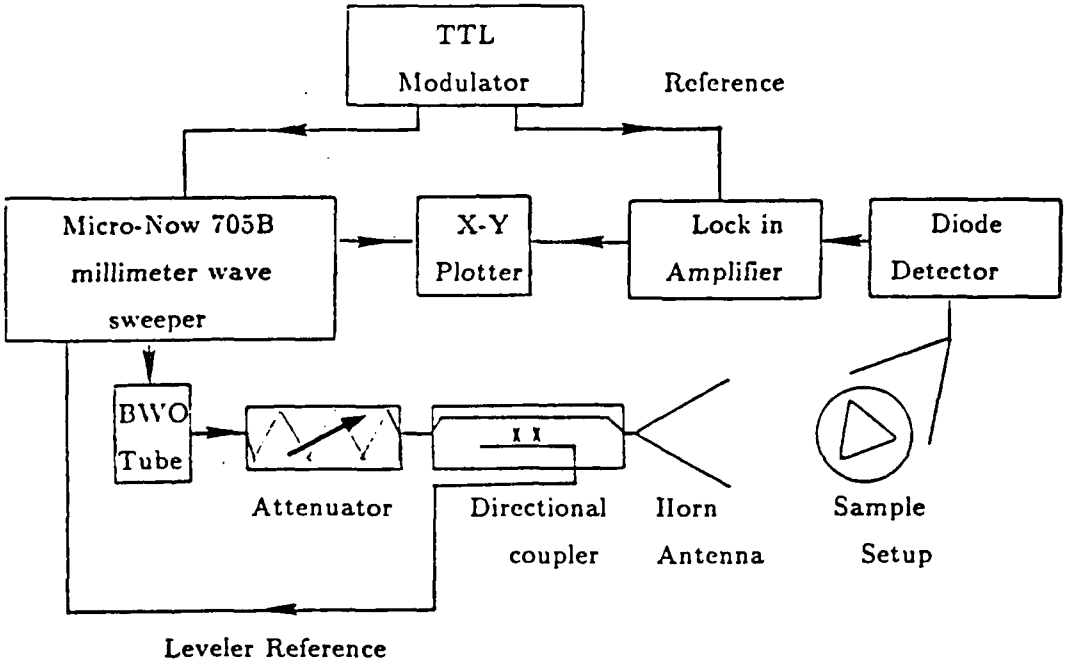

Figure 6- Block diagram of experimental setup

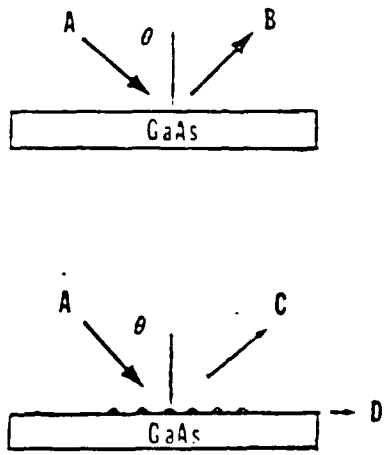

Figure 7- Sample comparison experiment

A - Incident beam from source

B - Reflected beam from polised sample

C - Reflected beam from sample with periodic structures

D - Surface wave beam

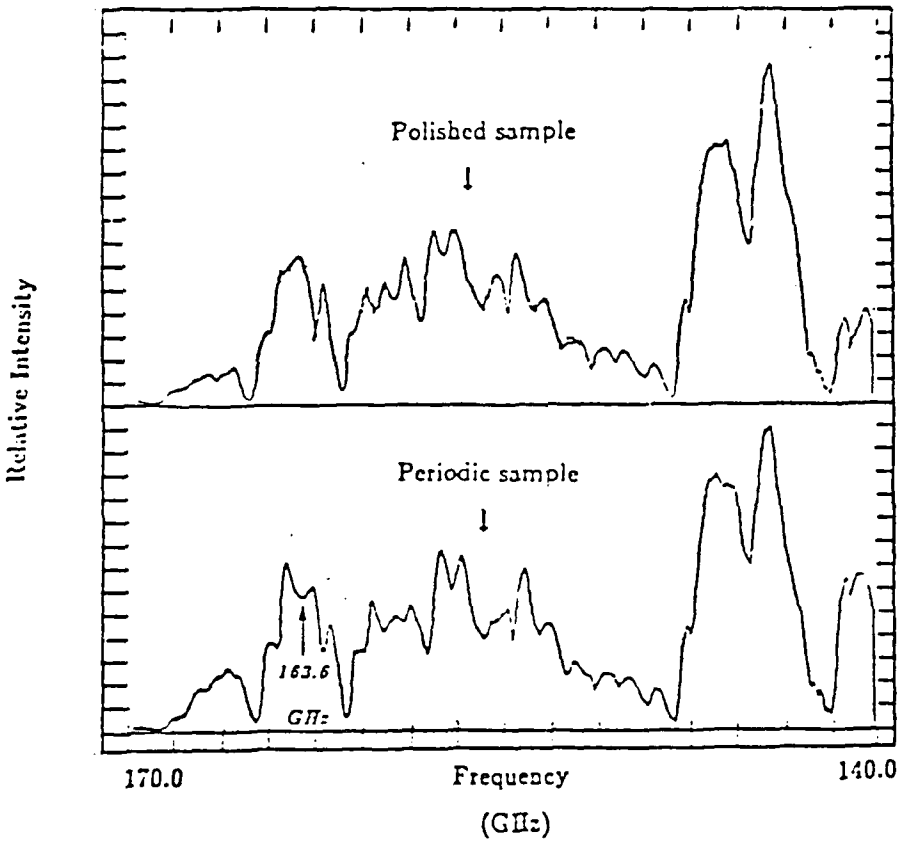

Figure 8- Comparison of intensity of reflected beams

(For $\theta = 45^\circ$ and $d = 2$ mm)

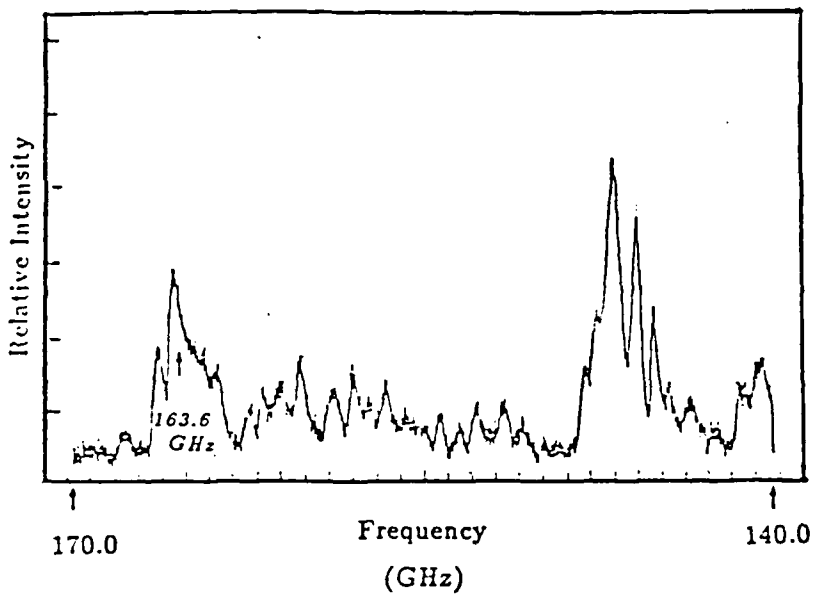

Figure 9- End detection for coupled wave

(For θ=45° and d=2mm)

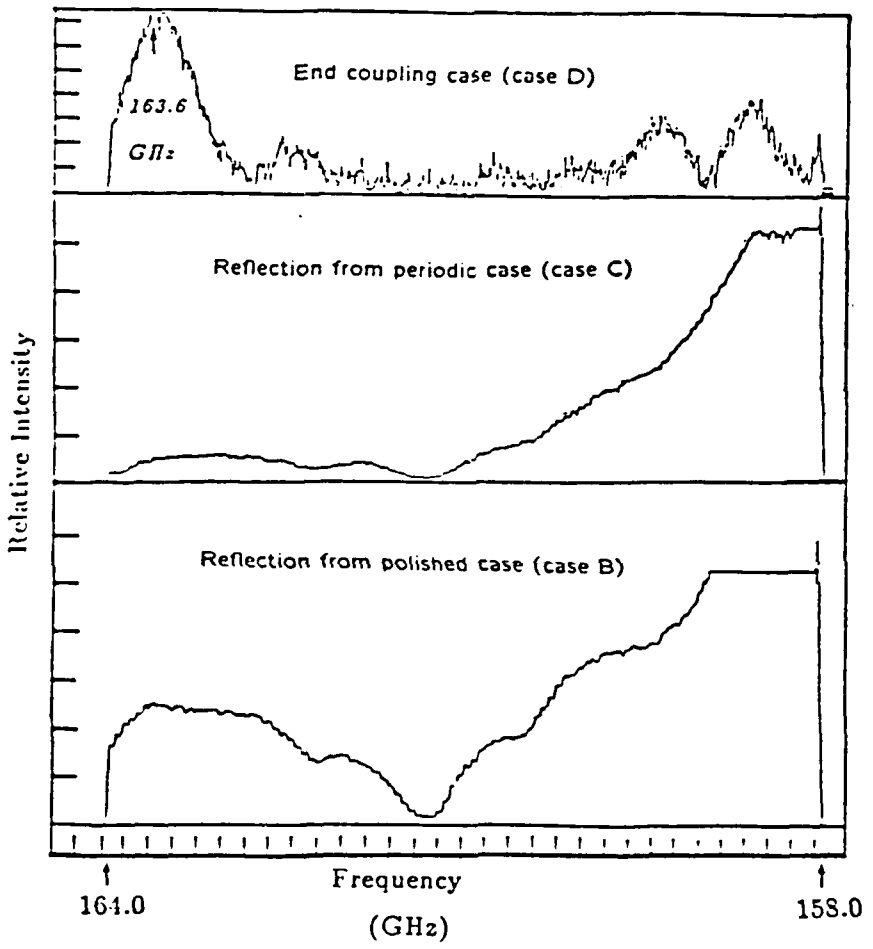

Figure 10- Sweep at a narrower bandwidth

(*For* $\theta = 45^{\circ}$ *and* $d = 2mm$)

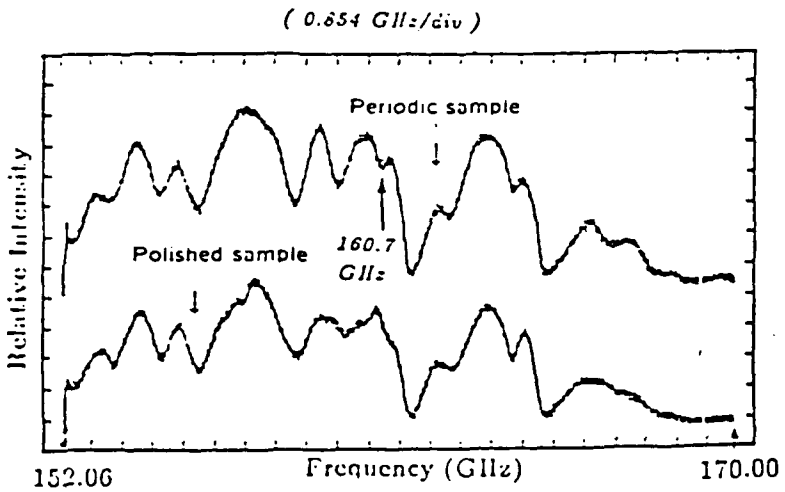

Figure 11- Comparison of intensity of reflected beams

(For θ= 23° and d=1.5mm)

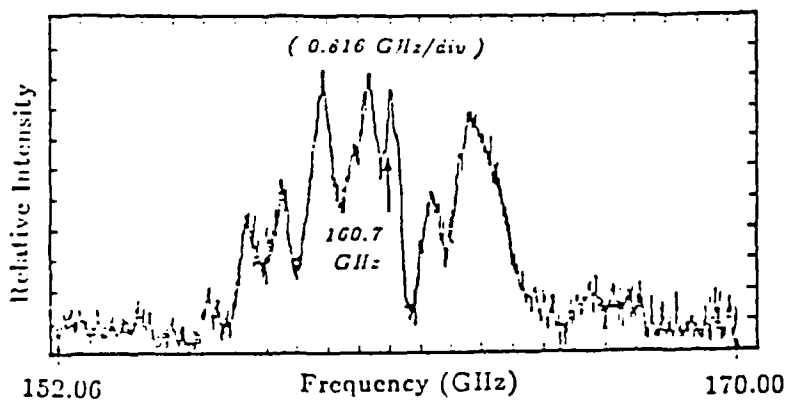

Figure 12- End coupling intensity of sample with periodic structures

(For θ= 23° and d=1.5mm)

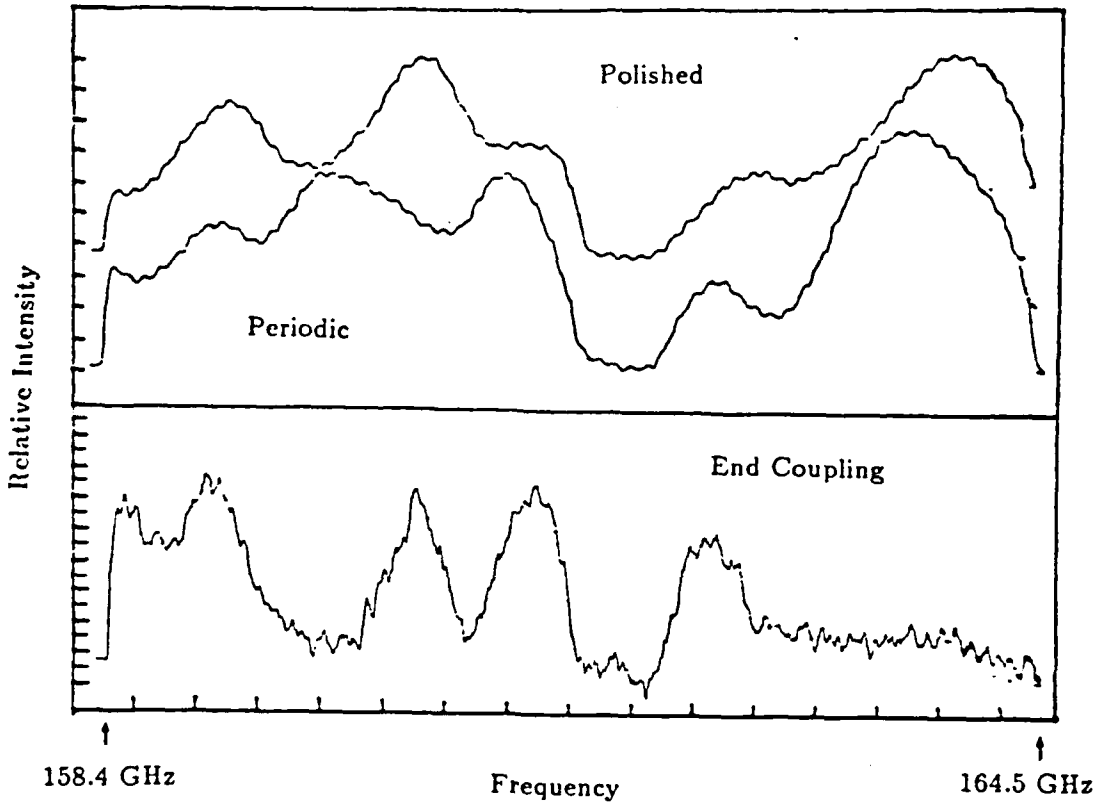

Figure 13- Higher grating profile coupling intensity (158.4-164.5 GHz)
(θ=23° , d=1.5mm)

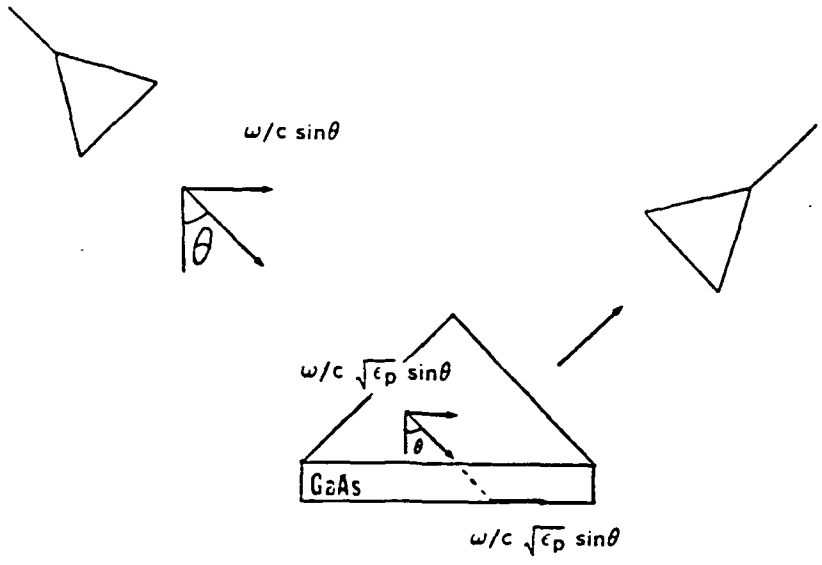

Figure 14- The Kretschmann configuration

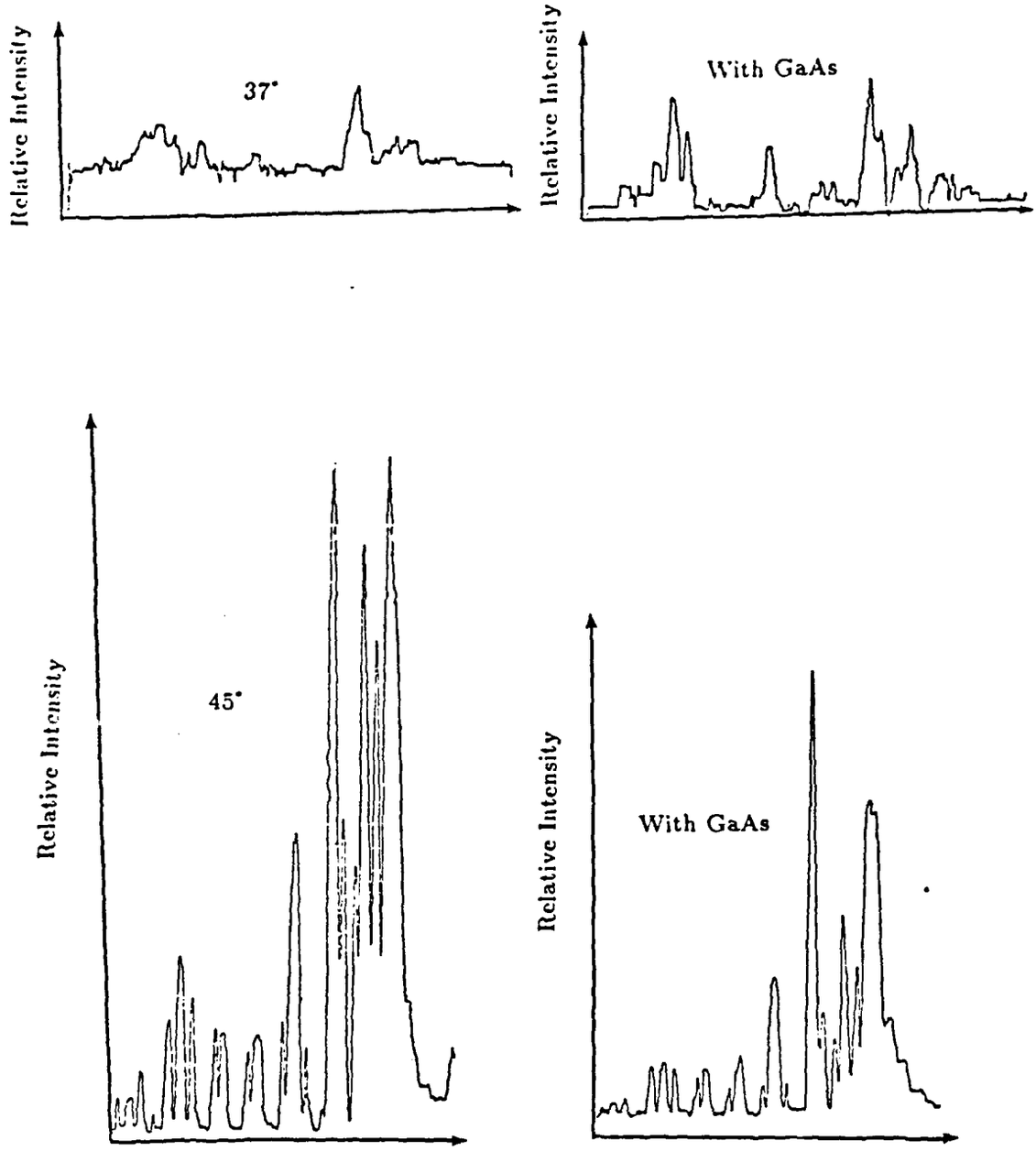

Figure 15- Prism coupler intensity comparison (110-136 GHz)

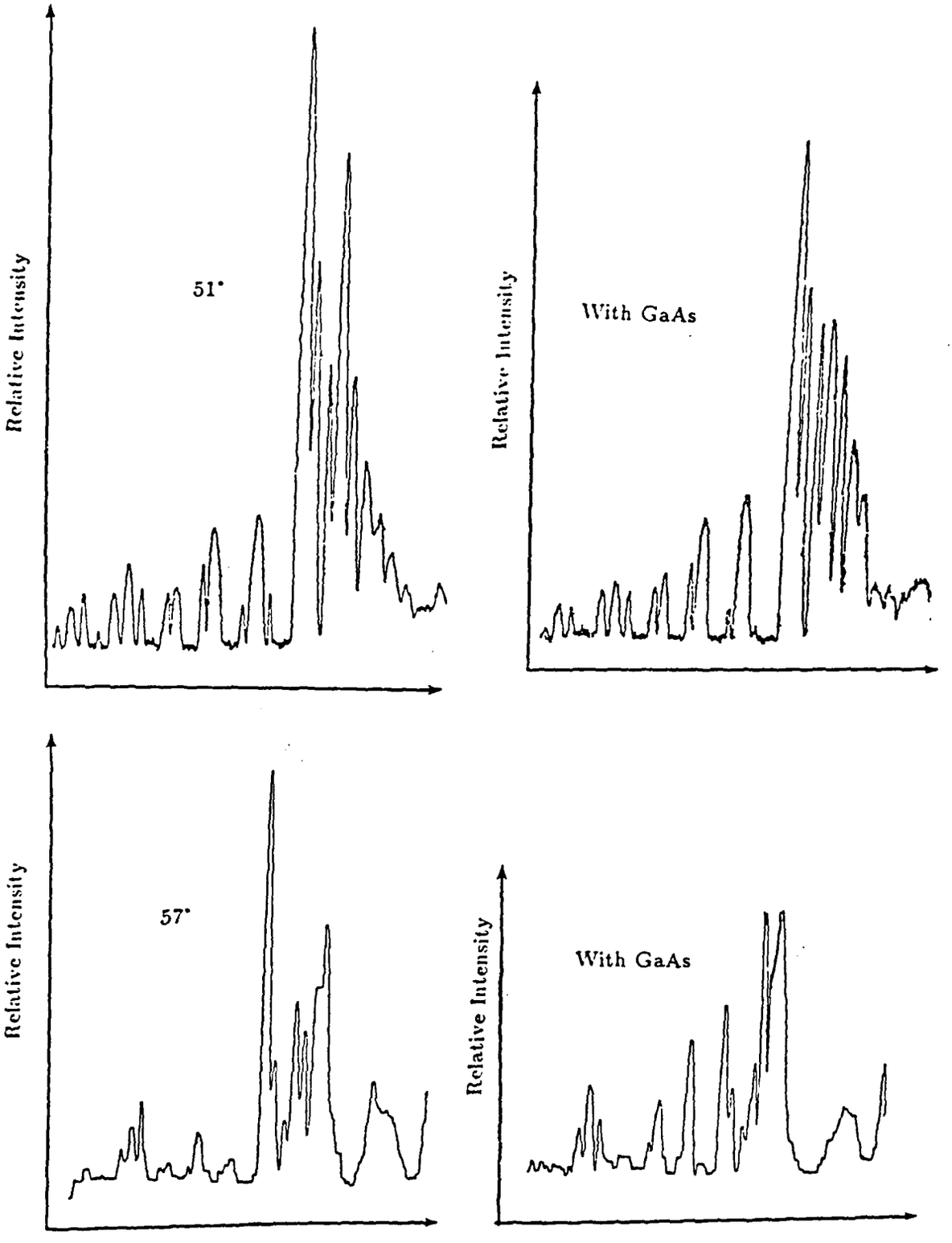

Figure 16- Prism coupler intensity comparison (110-136 GHz)

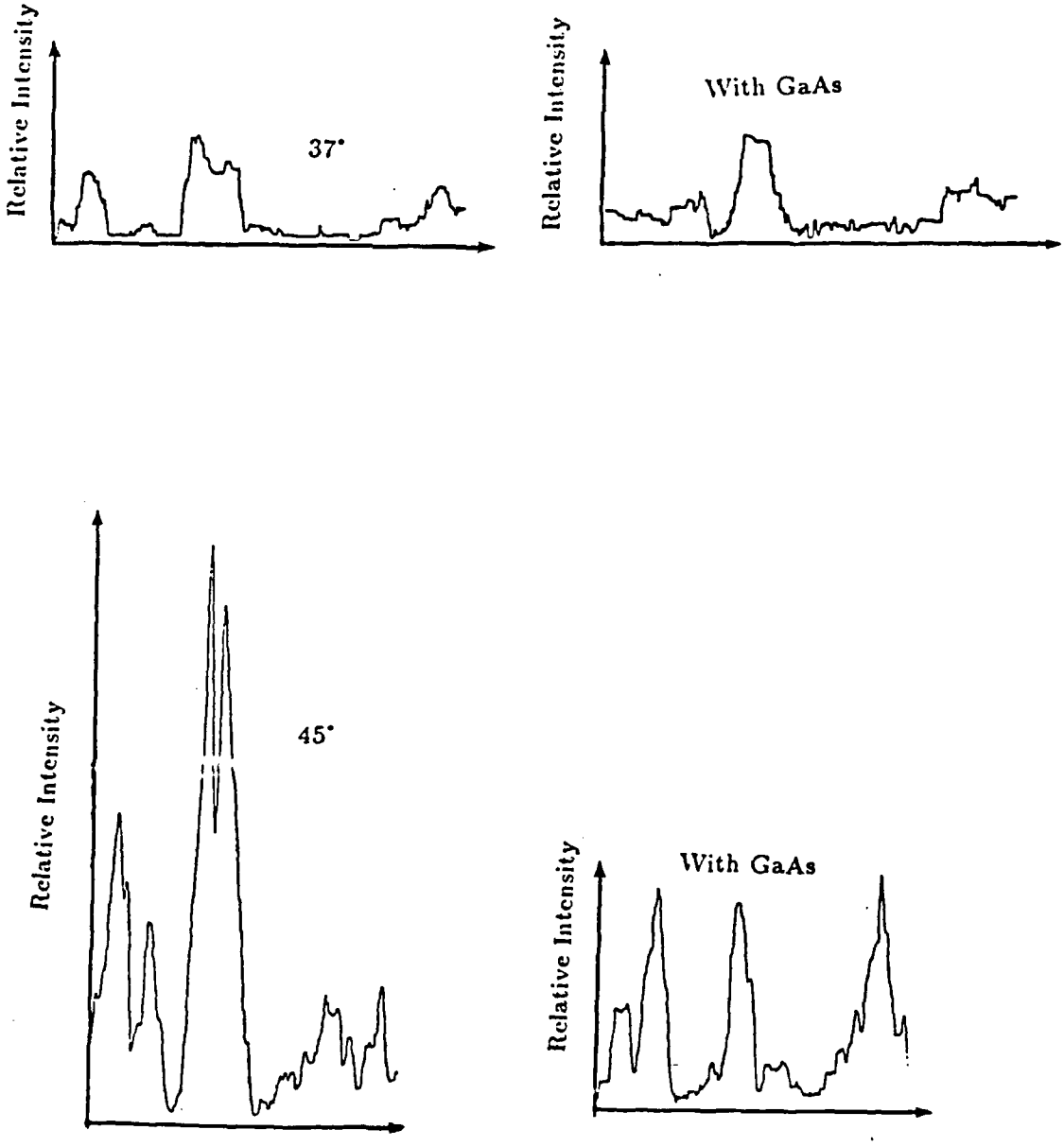

Figure 17- Prism coupler intensity comparison (136-157 GHz)

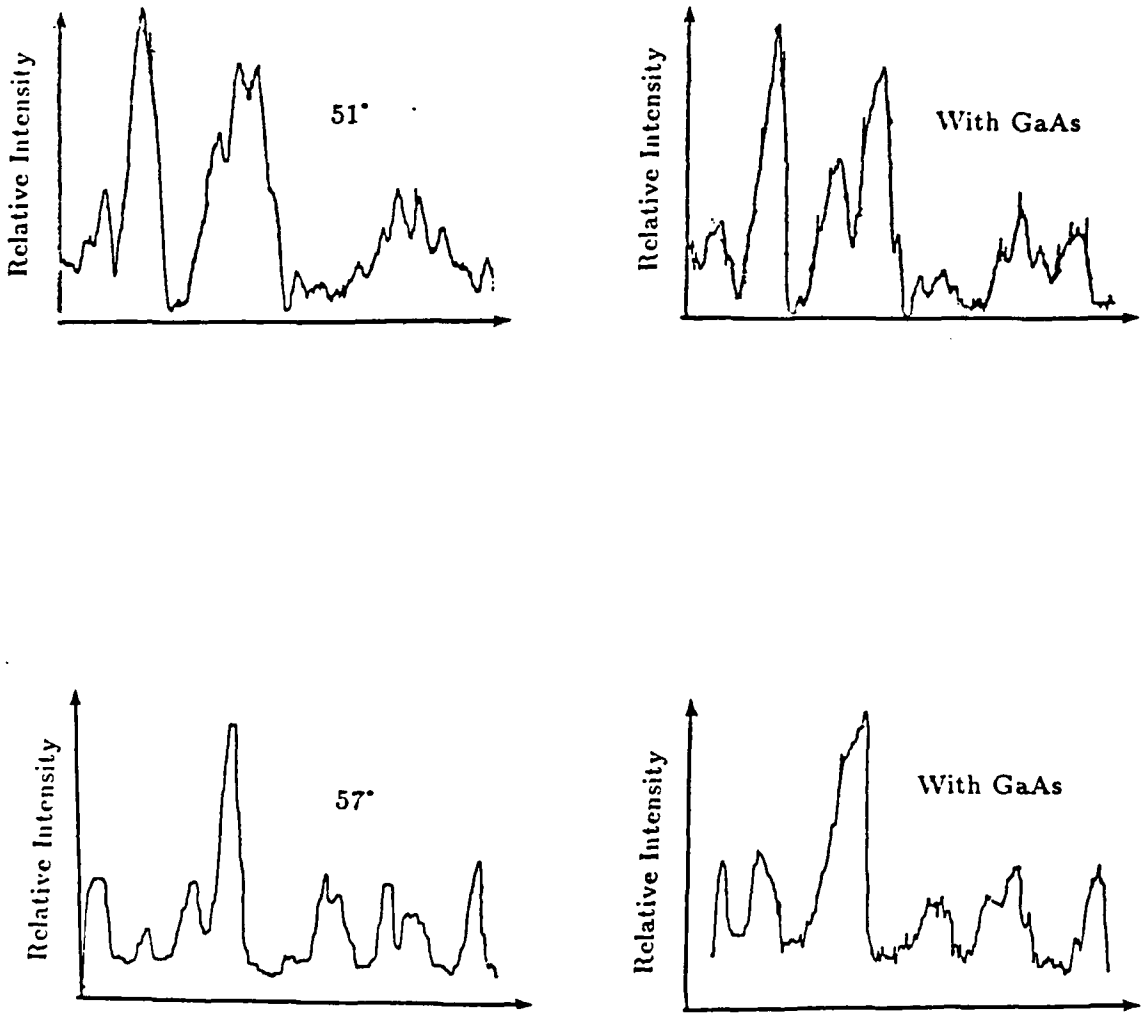

Figure 18- Prism coupler intensity comparison (136-157 GHz)

Normalized Reflection Coefficient

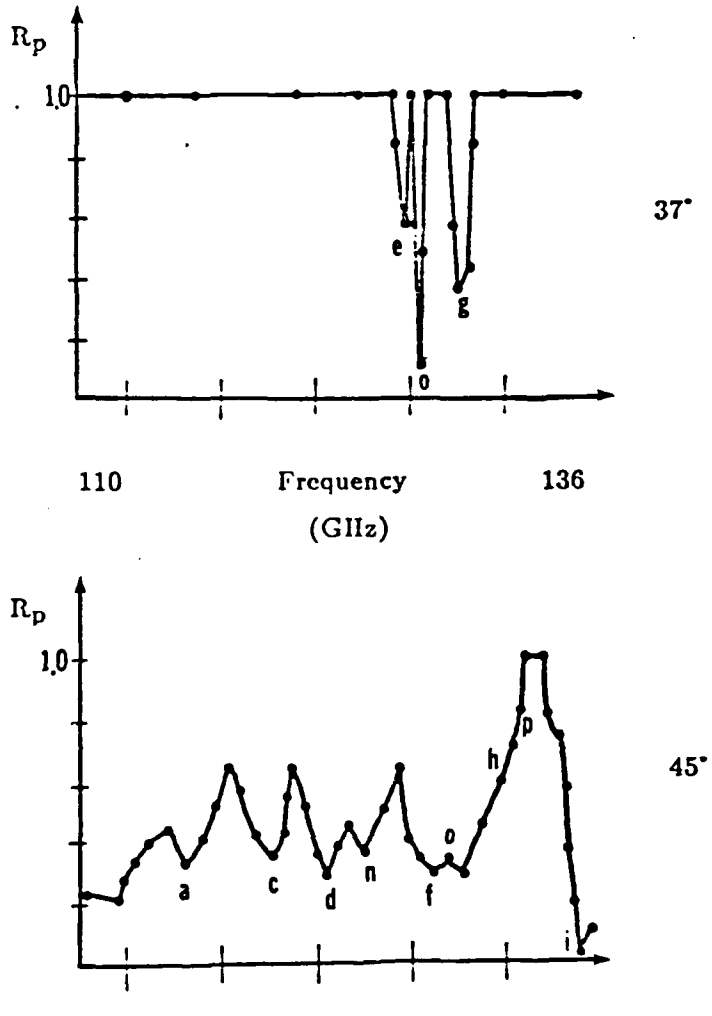

Figure 19- R_p vs. Frequency (θ=37°, 45°, 110- 136 GHz)

Normalized Reflection Coefficient

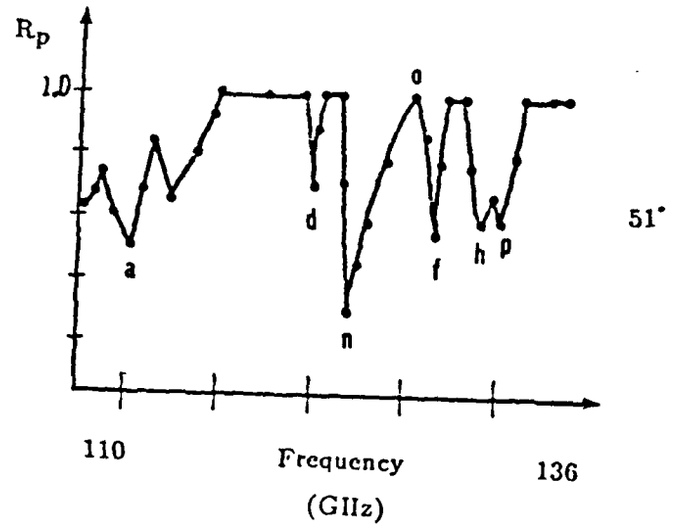

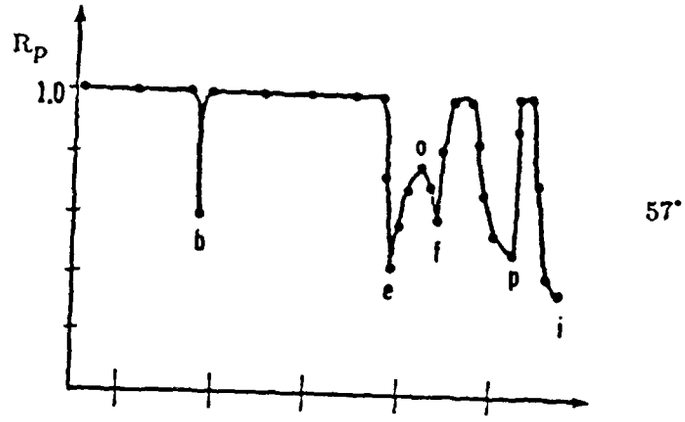

Figure 20- R_p vs. Frequency (θ=51°, 57°, 110- 136 GHz)

Normalized Reflection Coefficient

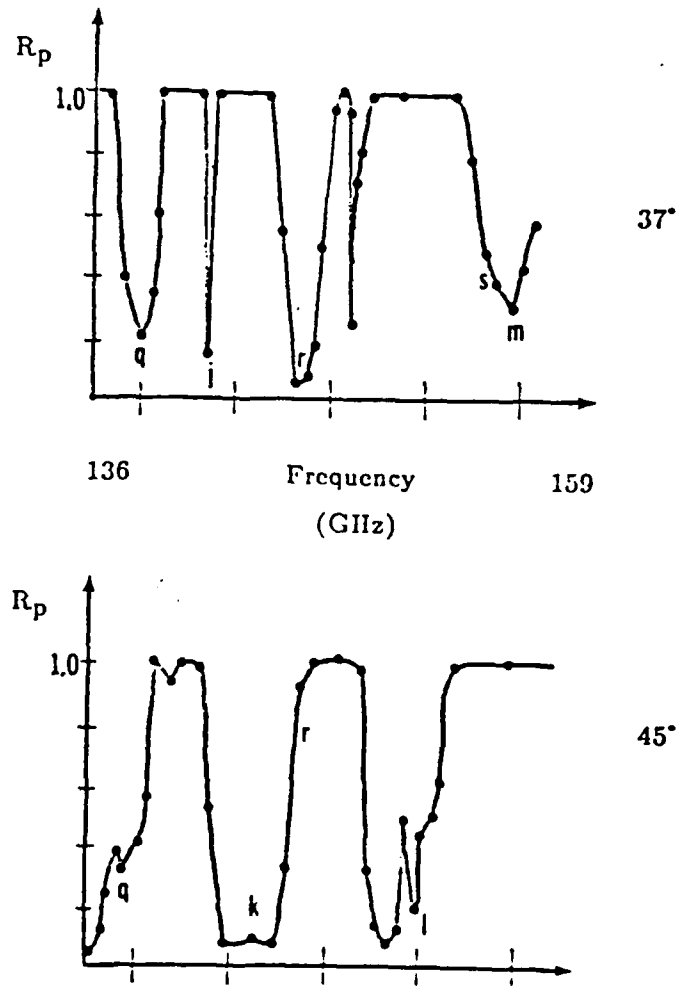

Figure 21- R_p vs. Frequency (θ=37°, 45°, 136- 159 GHz)

Normalized Reflection Coefficient

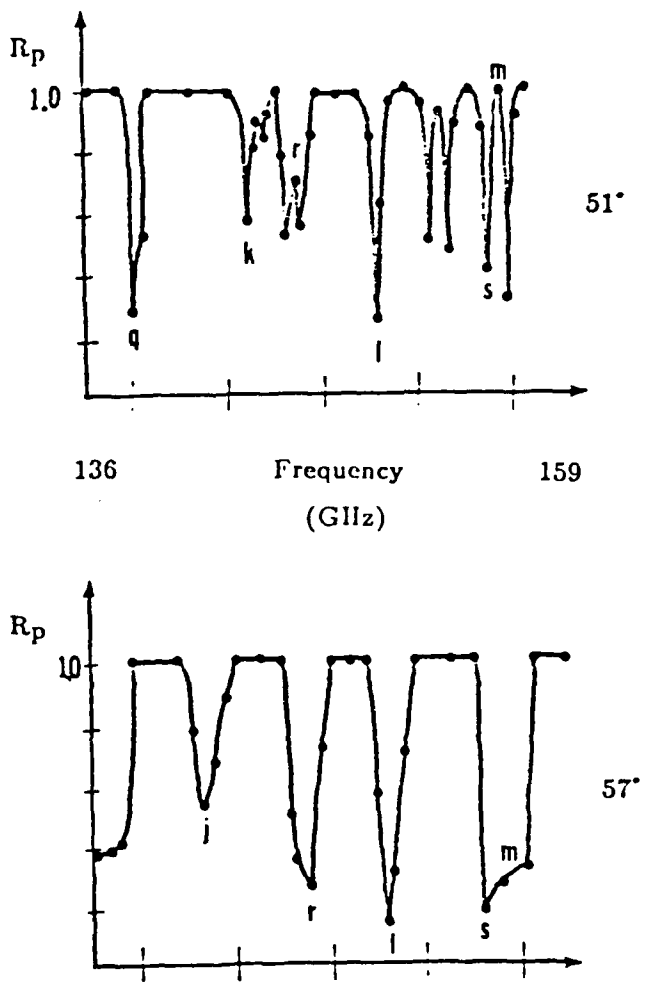

Figure 22- R_p vs. Frequency (θ=51°, 57°, 136- 159 GHz)

R_p vs. β

Normalized Reflection Coefficient

For 115.49 to 122.93 GHz

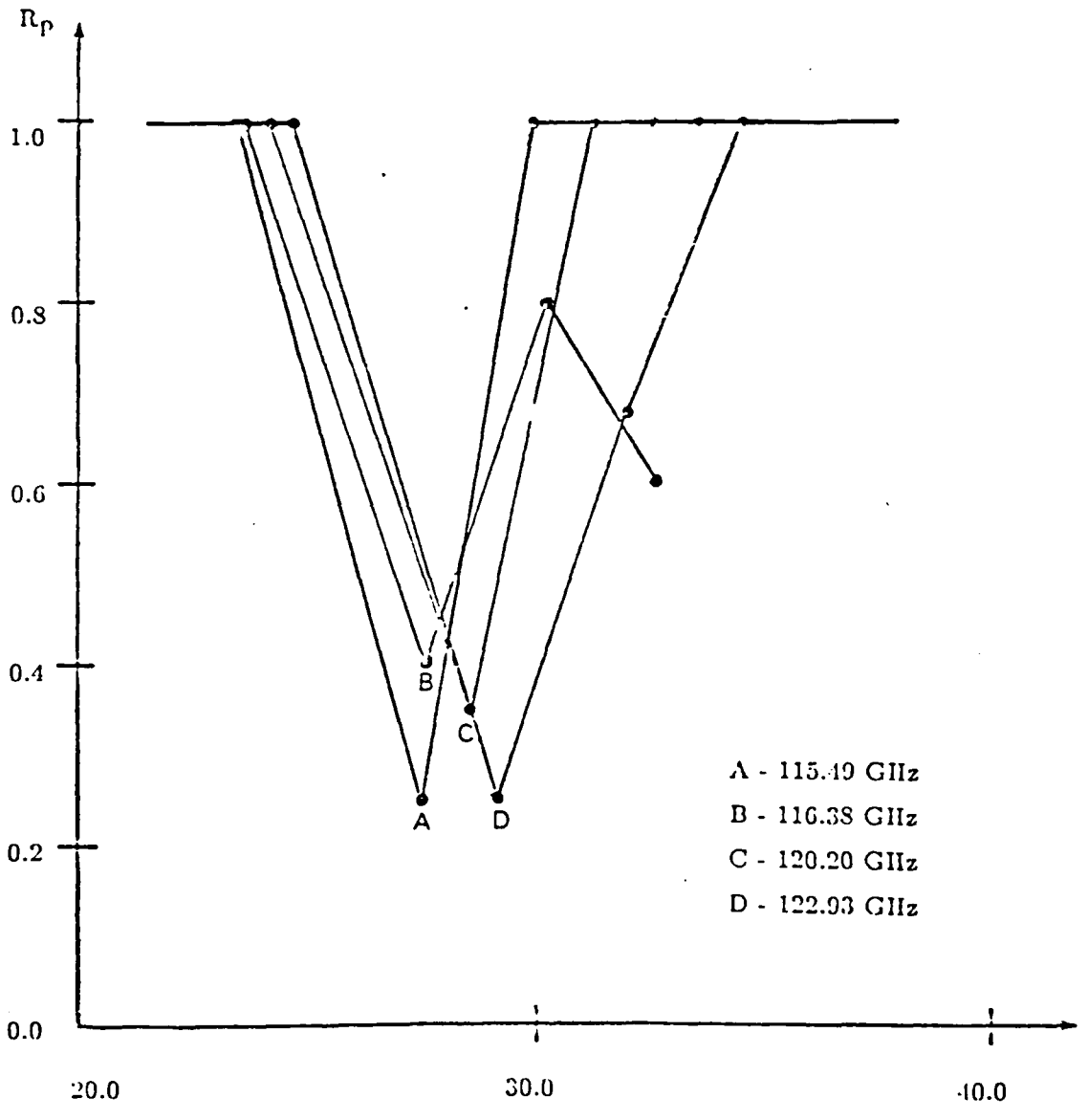

Figure 23- - R_p vs. β (115-123 GHz)

R_p vs. β

Normalized Reflection Coefficient

For 122.93 to 130.01 GHz

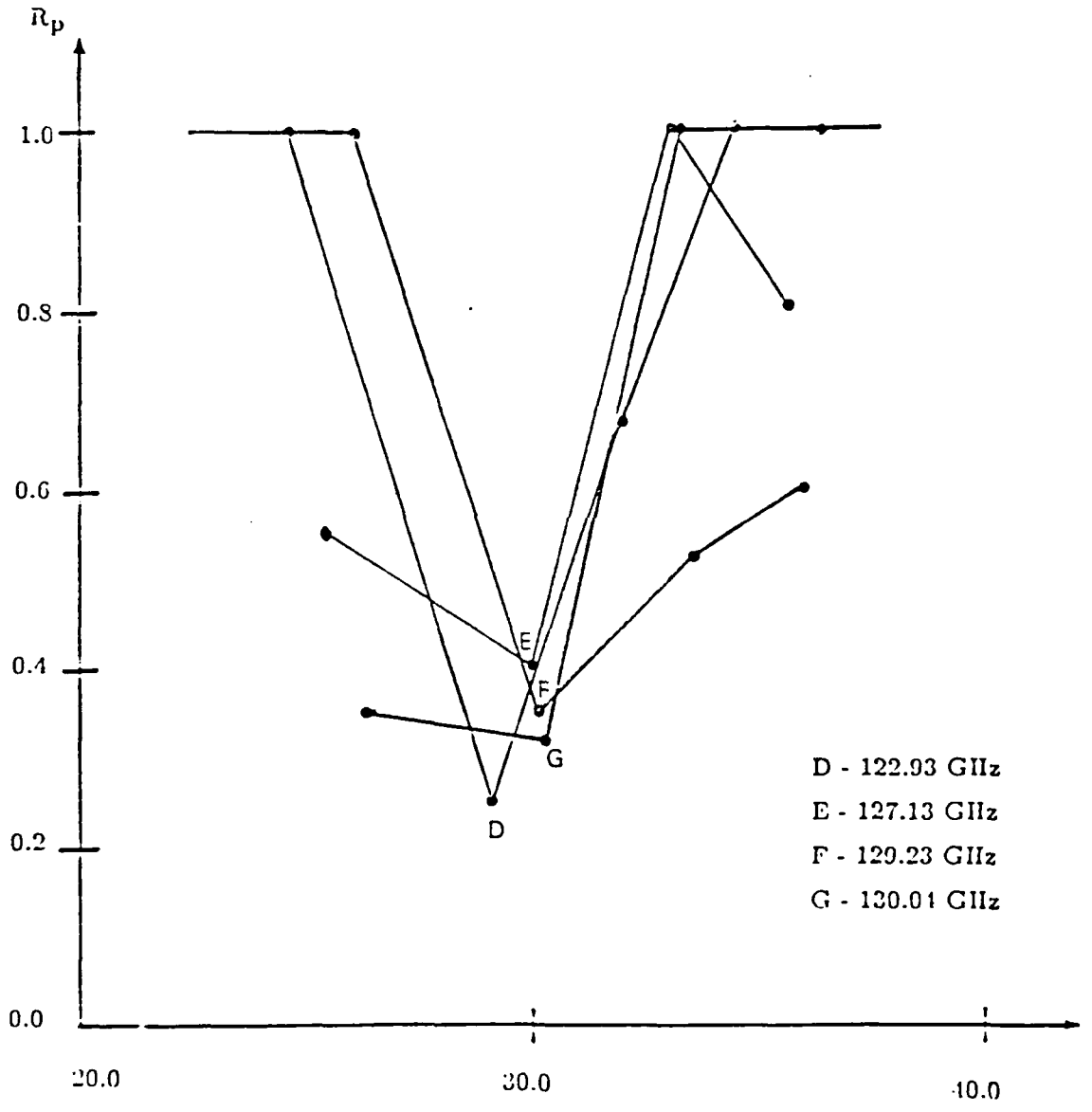

Figure 24 - R_p vs. β (123 : 0 GHz)

R_p vs. β

Normalized Reflection Coefficient

For 130.04 to 141.80 GHz

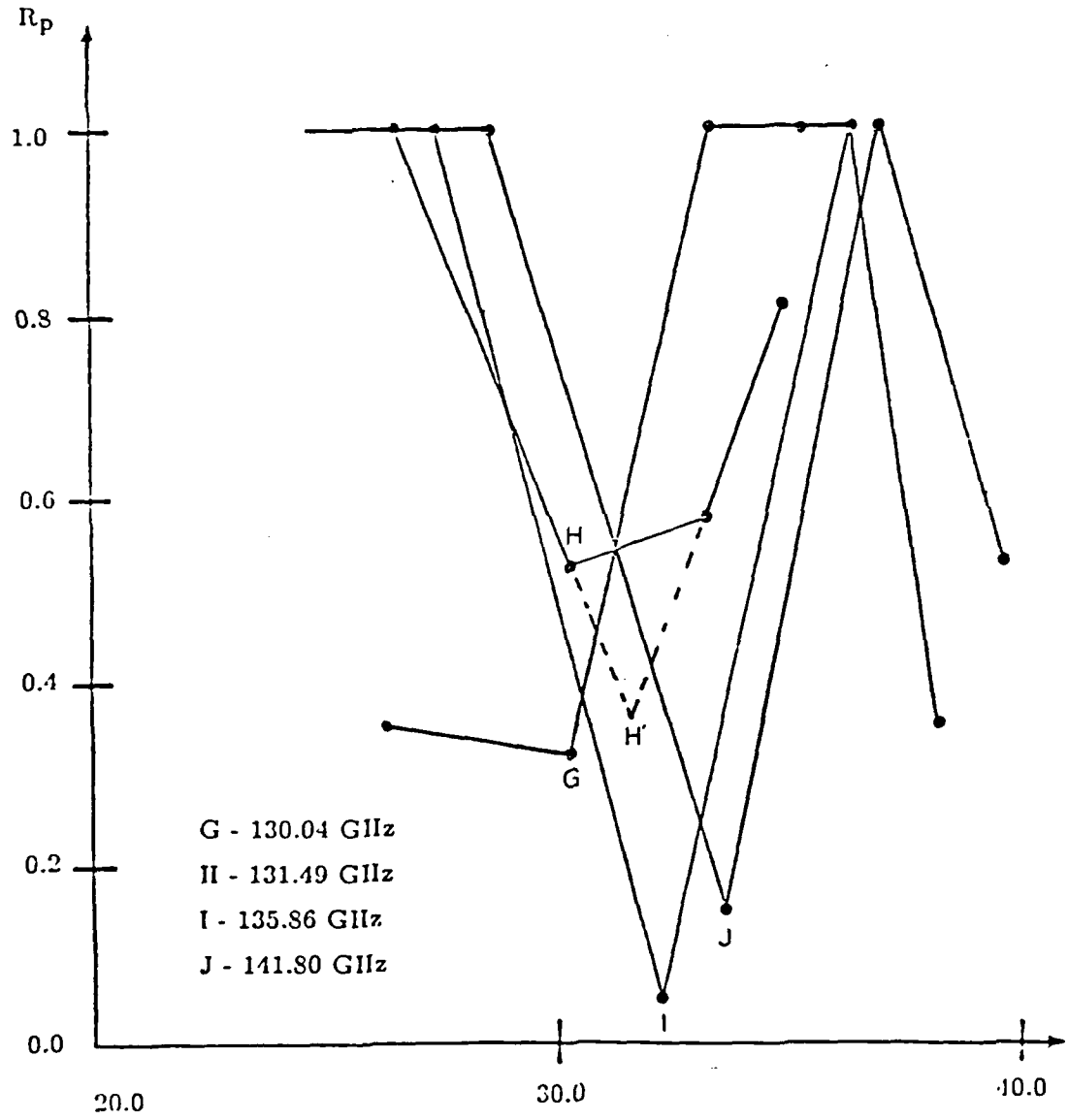

Figure 25 - R_p vs. β (130-142 GHz)

R_p vs. β

Normalized Reflection Coefficient

For 141.80 to 157.95 GHz

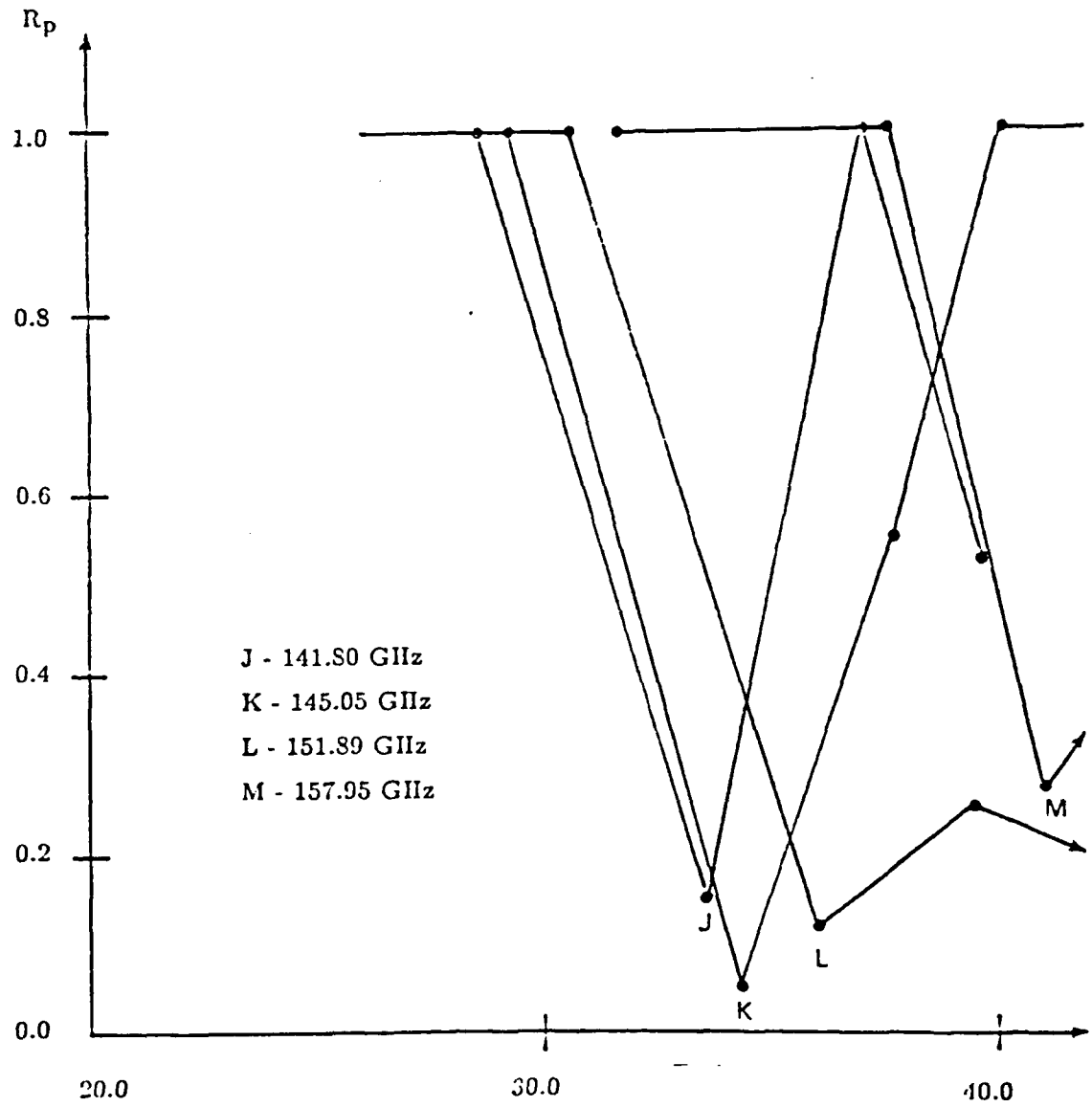

Figure 26 - R_p vs. β (142-158 GHz)

ω-β Dispersion Curve

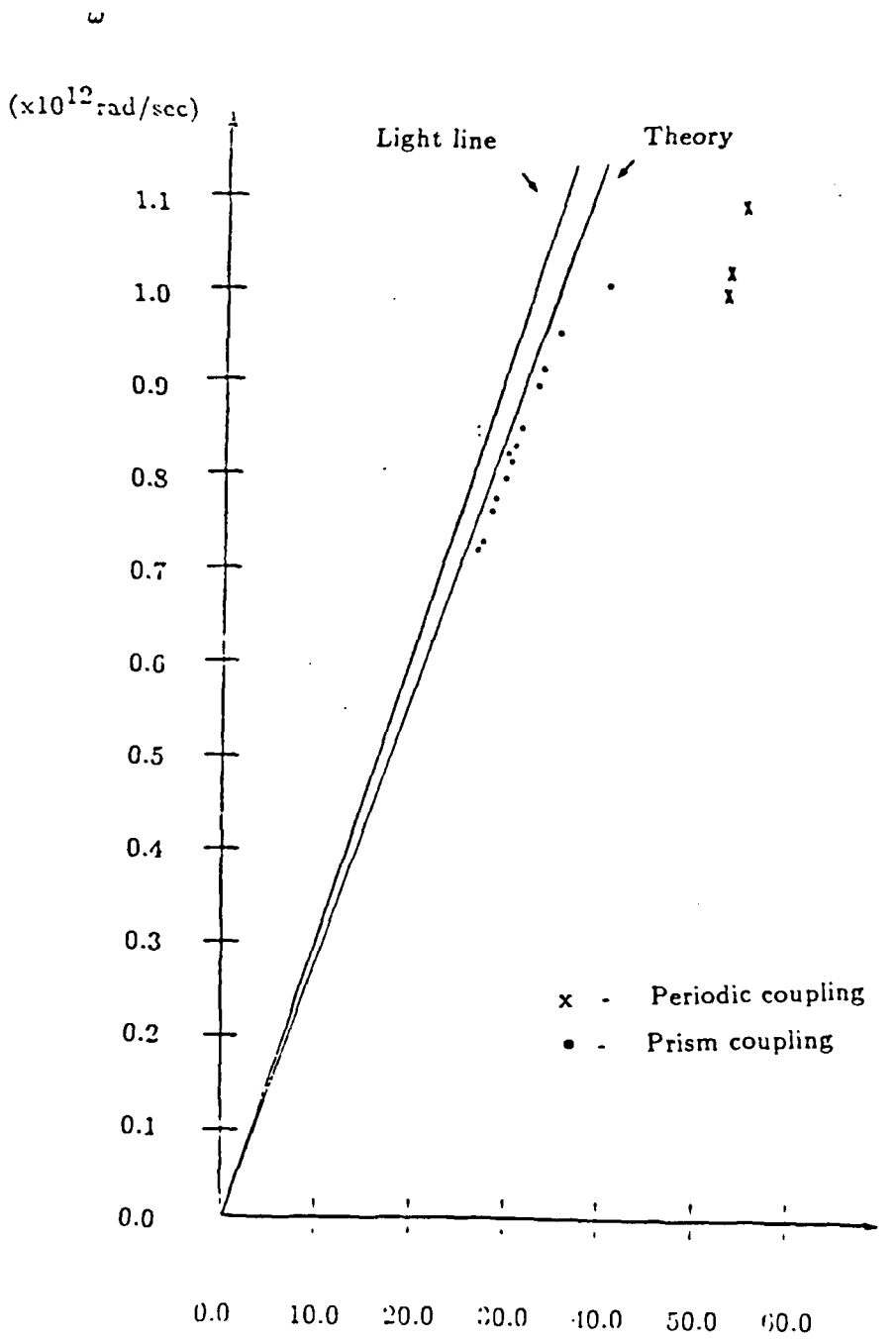

Figure 27 - ω-β Dispersion curve from experiment

ω-β Dispersion Curve

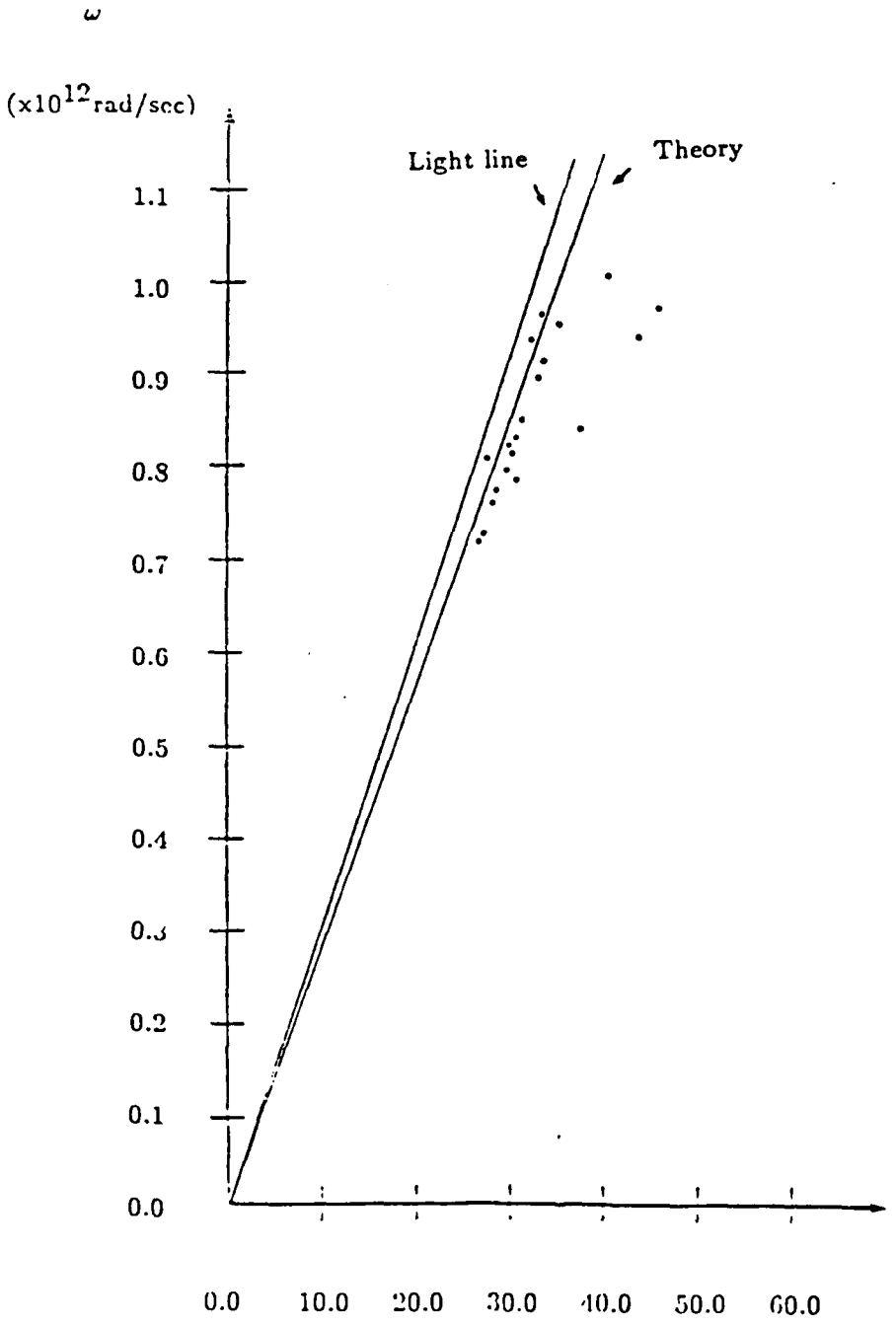

Figure 28 - Final ω-β Dispersion curve form experiment

V. FUTURE PLANS

With the satisfactory results achieved from the finite-element model for various dielectric waveguides and also structures with isotropic semiconducting materials, the next step is to introduce a dc biasing field in our two-dimensional structure employing semiconducting medium to study the nonreciprocal behavior of the dispersion spectrum caused from the interaction of the magnetic field with the plasma material. Both the embossed and embedded waveguiding structures utilizing surface plasmon on III-V semiconducting compounds such as InSb and GaAs are needed to be analyzed. Proper electrical and geometrical parameters are required to achieve nonreciprocity in the near-millimeter frequency bands of 140 & 220 GHz. The structures proposed here represent a suitable canonical model for design of quasi-optical devices such as isolators, circulators, and phase shifters. Once theoretical predictions are obtained from the finite-element formulation for component design in the near-millimeter wave frequency range, we will have numerical results to compare against the experimental data.

The success in quasi-optical method of surface plasmon excitation and theory verification for millimeter waves provides motivation for continued experimental research in this field. The next logical step to follow would be on the improvement in measurement and parameter control techniques to obtain a closer match between theory and experiment. Also an interesting topic for further study is the second unexpected mode appearing in the experimental dispersion curve due to the interface between the prism and GaAs. To verify this mode, we may increase the sweeper frequency or lower the plasma frequency of GaAs via reducing the doping density.

Loss measurements are desireable for the surface plasmon wave with specific attention on the separation of the two modes observed in the experimental dispersion curve. The proposed experimental setup utilizes the Kretschmann configuration to form decoupled modes at top and bottom boundary of the semiconductor, and an Otto configuration to decouple the surface wave. By varying the spacing between the two prisms of the configurations, the loss of the

surface wave due to bulk attenuation of GaAs and air will be obtained and compared against theoretical results.

Finally, the last step is to carry on the experimental procedure at cryogenic temperatures with loss calculations. Once satisfactory results are achieved, the investigation of millimeter wave surface polaritons in semiconductors in the presence of external magnetic fields are required to develop quasi-optical nonreciprocal devices.

APPENDIX A

"FINITE-ELEMENT ANALYSIS APPLIED TO GYROELECTRICALLY LOADED WAVEGUIDING STRUCTURES"

(IEEE MTT-S International Microwave Symposium, June 1985)

FINITE-ELEMENT ANALYSIS APPLIED TO GYROELECTRICALLY LOADED WAVEGUIDING STRUCTURES

N. Mohsenian*, Student Member, IEEE, T. J. Delph†,

and D. M. Bolle‡, Fellow Member, IEEE

Abstract

A finite-element formulation has been used to obtain the dispersion relation for a single dielectric-semiconductor interface bounded by two perfectly conducting planes. This system represents a suitable canonical problem for the design of non-reciprocal devices such as circulators, isolators, and phase shifters. The finite-element solution for the dispersive behavior was compared against the exact solution for the lowest real branches, and excellent agreement was found between the two.

---

*Department of Computer Science and Electrical Engineering, Lehigh University, Packard Laboratory #19, Bethlehem, Pa. 18015.

†Department of Mechanical Engineering and Mechanics, Lehigh University, Packard Laboratory #19, Bethlehem, Pa. 18015.

‡D.M.Bolle was with CSEE Department of Lehigh University until August 1,1988. He is presently at New York Polytechnic Institute.

INTRODUCTION

In recent years interest in various waveguiding structures in the millimeter (mm) and submillimeter (smm) wavelength, i.e., 100-1000 GHz, has been growing. The development of this technology requires a parallel development of more accurate computational techniques. The finite-element method provides an attractive approach to the problem of obtaining the dispersive behavior of the waveguide. The effectiveness of this method has led many researchers to apply it to different electromagnetic field problems, [1].

The single dielectric-semiconductor interface model considered in this paper is a suitable canonical problem for the design of non-reciprocal devices such as circulators, isolators, and phase shifters. Propagation characteristics of structures used to obtain such circuit functions have been analyzed in [2], [3].

THE WAVEGUIDING STRUCTURE

Consider the dielectric-semiconductor single interface sided by two perfectly conducting planes shown in Fig. 1, with a superimposed finite-element mesh. A high quality n-type GaAs material has been taken as the substrate for the semiconductor region. The system is assumed to be exposed to a uniform d.c. magnetic field along the y-direction, with time-harmonic wave propagation in the z-direction. Only TM modes will be considered in the present analysis since TE modes do not have significant interaction with the semiconducting material.

We take the permeability μ_0 to be a constant for both regions. The permittivity ϵ is a scalar constant for the dielectric medium, but becomes a tensor for the semiconducting material. For a biasing magnetic field in the y-direction, the dielectric tensor takes the following form, [3].

$$\epsilon_2(\omega) = \begin{bmatrix} \xi & 0 & -j\eta \\ 0 & \zeta & 0 \\ j\eta & 0 & \xi \end{bmatrix} \qquad (1)$$

where $\xi=\epsilon^{(o)}-\frac{\omega_p^2(\omega-j\nu)}{\omega[(\omega-j\nu)^2-\omega_c^2]}$, $\zeta=\epsilon^{(o)}-\frac{\omega_p^2}{\omega(\omega-j\nu)}$, $\eta=\frac{-\omega_p^2\omega_c}{\omega[(\omega-j\nu)^2-\omega_c^2]}$

and ω_p is the plasma frequency, ν the collision frequency, and ω_c the cyclotron frequency, $\omega_c=eB_o/m^*$. For the isotropic case, $\omega_c=0$ and the tensor elements reduce to

$$\xi=\zeta=\epsilon^{(o)}-\frac{\omega_p^2}{\omega(\omega-j\nu)} \quad \text{and } \eta=0.$$

From Maxwell's equations, uncoupled two-dimensional partial differential equations were derived for e_z. These equations have the common form

$$\frac{\partial^2 e_z}{\partial x^2}+M_1\frac{\partial^2 e_z}{\partial y^2}+M_2 e_z=0 \qquad (2)$$

where $M_1=\frac{\zeta(\gamma^2+\omega^2\mu_o\epsilon_o\xi)}{\xi(\gamma^2+\omega^2\mu_o\epsilon_o\zeta)}$ and $M_2=\gamma^2+\frac{\omega^2\mu_o\epsilon_o(\xi^2-\eta^2)}{\xi}$

for the semiconducting medium and $M_1=1$, $M_2=\gamma^2+\omega^2\mu_o\epsilon_o\epsilon_1$ for the dielectric medium. Moreover the magnetic field component h_y is given in terms of e_z by

$$h_y=\left(\frac{-j\omega\epsilon_o\xi}{\gamma^2+\omega^2\mu_o\epsilon_o\xi}\right)\left(\frac{\partial e_z}{\partial x}+\frac{j\eta\gamma}{\xi}e_z\right) \qquad (3)$$

in the semiconducting medium and

$$h_y=\left(\frac{-j\omega\epsilon_o\epsilon_1}{\gamma^2+\omega^2\mu_o\epsilon_o\epsilon_1}\right)\frac{\partial e_z}{\partial x} \qquad (4)$$

in the dielectric medium.

The dielectric-semiconductor interface was taken to be lossless ($\nu=0$). Assuming there are no y-variations ($\partial/\partial y=0$), a TM mode solution exists in the vicinity of the interface (components h_y, e_x, e_z). The electromagnetic field boundary condition at the perfectly

conducting plane requires that $n \times E = 0$. The dispersion relation is obtained from imposing this boundary condition and requiring continuity of e_z and h_y at the interface. The result is

$$\left(\frac{\epsilon_1}{k_1}\right) \mathrm{Coth}(k_1 P_1) = \left(\frac{\xi k_2}{\gamma^2 + \omega^2 \mu_o \epsilon_o \xi}\right) \mathrm{Coth}(k_2 P_2) - \left(\frac{j\eta\gamma}{\gamma^2 + \omega^2 \mu_o \epsilon_o \xi}\right) \qquad (5)$$

with $\quad k_1^2 = -\gamma^2 - k_o^2 \epsilon_1; \quad k_2^2 = -\gamma^2 - k_o^2 \epsilon_e(\omega)$

Here $\gamma = \alpha + j\beta$ is the complex propagation constant, and $k_o^2 = \omega^2 \mu_o \epsilon_o$, $\epsilon_e(\omega) = \frac{\xi^2 - \eta^2}{\xi}$. Furthermore, α is the attenuation constant, ϵ_o the permittivity of vacuum, ϵ_1 the relative dielectric constant of the dielectric medium, $\epsilon^{(o)}$ the static dielectric constant of the semiconducting medium, ϵ_e the effective dielectric constant of the semiconducting medium, P_1 the width of the dielectric medium, and P_2 the width of the semiconducting medium.

FINITE-ELEMENT FORMULATION

The finite-element mesh for this problem is shown in Fig. 1. The finite-element interpolating functions utilized were those for the eight-noded isoparametric quadrilateral element, [4]. Both the dielectric and the semiconducting regions were divided into three equally-spaced elements. The finite-element equations were generated from equation (2) by means of the Galerkin formulation

$$\iint_{\mathcal{A}} \left(\frac{\partial^2 e_z}{\partial x^2} + M_1 \frac{\partial^2 e_z}{\partial y^2} + M_2 e_z\right) N_i(x,y)\, dxdy = 0 \qquad (6)$$

where the $N_i(x,y)$ are the finite-element interpolating functions, and the index i ranges over those nodal points at which the value of e_z is not specified by the boundary conditions. We now introduce the finite-element approximation $e_z = [N(x,y)]\{e_z\}$, where $[N(x,y)]$ is the row vector of interpolating functions and $\{e_z\}$ the column vector of nodal point values. An application of the divergence theorem now yields the finite-element equations in the form

$$[A]\{e_z\} - \oint_{\bar{B}} \left(\frac{\partial e_z}{\partial x} n_x + M_1 \frac{\partial e_z}{\partial y} n_y\right) N_i \, ds = 0 \tag{7}$$

The i,j-th element in the coefficient matrix [A] is given by

$$A_{ij} = \iint_{\mathcal{A}} \left(\frac{\partial N_i}{\partial x} \frac{\partial N_j}{\partial x} + M_1 \frac{\partial N_i}{\partial y} \frac{\partial N_j}{\partial y} - M_2 N_i N_j\right) dxdy \tag{8}$$

and is evaluated by 3×3 point Gaussian integration. The line integral in equation (7) is to be evaluated around the boundary $\bar{B}$ of the finite-element mesh, and (n_x, n_y) are the components of the unit normal vector to $\bar{B}$. When assembling the finite-element equations from element contributions, as is usually done, the integral is to be evaluated around the boundary $\bar{B}_e$ of each element. The boundary conditions $e_z=0$ at $x=-P_1$, P_2, as well as the condition $\partial e_z/\partial y=0$ on the top and bottom sides of $\bar{B}$, can easily be shown to lead to the vanishing of the line integral along these portions of $\bar{B}$. Moreover interelement compatability conditions between adjacent elements in the same medium lead to a vanishing net contribution when the line integral is evaluated over the common interelement boundary. This is not true, however, along the interface between the dielectric and semiconducting regions, where special care must be taken.

Let n be one of the three values of the index i corresponding to the three interface nodes. Further denote the values of e_z in the dielectric and semiconducting regions of $e_z^{(1)}$ and $e_z^{(2)}$ respectively. Along the interface we must have both continuity of e_z, $e_z^{(1)}=e_z^{(2)}$, and the continuity of h_y. The latter condition, from equations (3) and (4), gives that

$$\frac{\partial e_z^{(1)}}{\partial x}\Big|_{x=o} = \left(R_1 \frac{\partial e_z^{(2)}}{\partial x} + R_2 e_z^{(2)}\right)\Big|_{x=o} \equiv C \tag{9}$$

where $R_1 = \dfrac{\xi(\gamma^2+\omega^2\mu_o\epsilon_o\epsilon_1)}{\epsilon_1(\gamma^2+\omega^2\mu_o\epsilon_o\xi)}$ and $R_2 = \left(\dfrac{j\eta\gamma}{\xi}\right)R_1$

We now write the n-th finite-element equation separately for both the dielectric and semiconductor regions. These are, respectively (with summation convention implied)

$$A_{nj}^{(1)} e_{zj}^{(1)} = Cd_n$$
$$A_{nj}^{(2)} e_{zj}^{(2)} - \left(\frac{R_2}{R_1}\right) b_{nj}\, e_{zj}^{(2)} = \frac{Cd_n}{R_1} \qquad (10)$$

where $d_n = \int_{-\alpha}^{\alpha} N_n(0,y)\, dy$ and $b_{nj} = \int_{-\alpha}^{\alpha} N_n(0,y)\, N_j(0,y)\, dy$. Eliminating C between equation (10) and requiring continuity of e_z at the interface now yields for the n-th equations

$$\left(A_{nj}^{(1)} + R_1 A_{nj}^{(2)} - R_2 b_{nj}\right) e_{zj} = 0 \qquad (11)$$

Equations (11) represent the finite-element equations corresponding to the interface nodes. The remaining finite-element equations have the form of equation (7), with the line integral vanishing for these equations. When assembled, the finite-element equations have the form $[A^*]\{e_z\}=0$. A nontrivial solution then requires that

$$| A^* | = 0 \qquad (12)$$

which represents the finite-element dispersion equation for the problem. Given a value of ω, one may obtain corresponding values of γ by standard numerical root-finding techniques.

RESULTS AND CONCLUSIONS

Equations (5) and (12) represent respectively the exact dispersion relation and the finite-element approximation. Both equations were solved numerically using a standard technique, the bisection method, for the following physical constants: $\epsilon^{(o)}=13$, $\epsilon_1=1$, $\omega_p=10^{13}$ rad/sec, $\omega_c=10^{12}$ rad/sec, $P_1=80\mu m$, $P_2=100\mu m$. Figure 2 shows the lowest positive and negative real branches of the dispersion spectrum obtained from the exact and finite-element dispersion equations for $|\beta| < 2$, for a normalized propagation constant defined by $\bar{\beta}=P_2\beta$ and a normalized frequency given by $\bar{\omega}=\omega P_2/c$. It can be seen that the agreement between the two is excellent. In fact, three-digit agreement was typically noted in the numerical results.

Figures 3 and 4 show the distribution of e_z at two points each along the positive and negative branches, one taken in the linear portion of each curve and the other in the flattened

portion of the curve. The value of e_z at the interface was normalized to unity. Again excellent agreement between the results of the exact solutions and the finite-element approximation may be noted.

To summarize, we have applied the finite-element method to the problem of obtaining the dispersion characteristics of a relatively simple, one-dimensional waveguiding structure. Excellent results were obtained. The primary advantage of the finite-element method is, of course, its ability to treat problems of practical interest involving complicated two-dimensional geometries and correspondingly complicated electric and magnetic field distributions. The results given here indicate that the finite-element method holds great promise for these applications, and in particular for the analysis of complex gyroelectrically and gyromagnetically loaded waveguiding structures.

REFERENCES

[1]- M. V. K. Chari and P. P. Silvester, Finite-Elements in Electrical and Magnetic Field Problems, Wiley, New York (1980).

[2]- W. L. K. Hwang, Applications of surface magnetoplasmons on semiconductor substrates, Ph.D. Thesis, Department of Electrical and Computer Engineering, Lehigh University (1983).

[3]- S. H. Talisa and D. M. Bolle, "Fundamental considerations in millimeter and near-millimeter component design employing magnetoplasmons", *IEEE Trans. Microwave Theory Tech.*, vol. MTT-29, pp. 916-923, 1981.

[4]- K. H. Huebner and E. A. Thornton, The Finite-Element Method For Engineers, Second Ed., Wiley-Interscience, New York (1982).

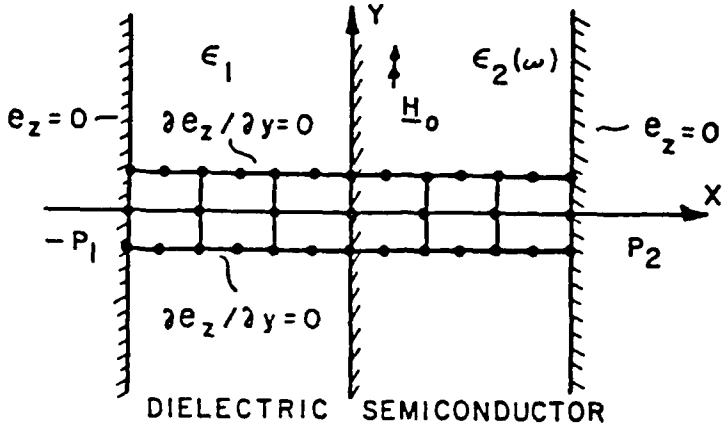

Fig. 1 - Dielectric-Semiconductor Single Interface.

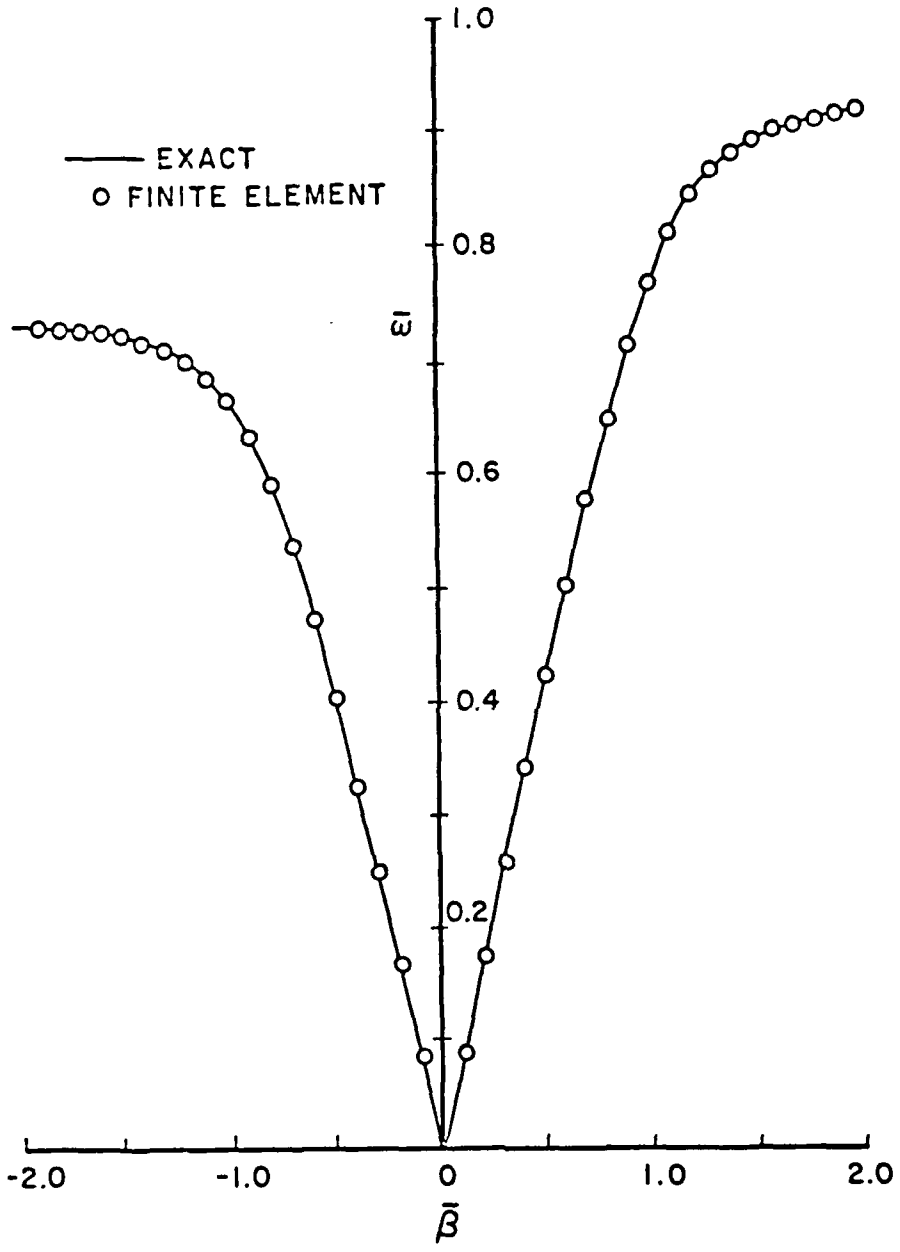

Fig.2- Exact and Finite-Element Dispersion Spectra.

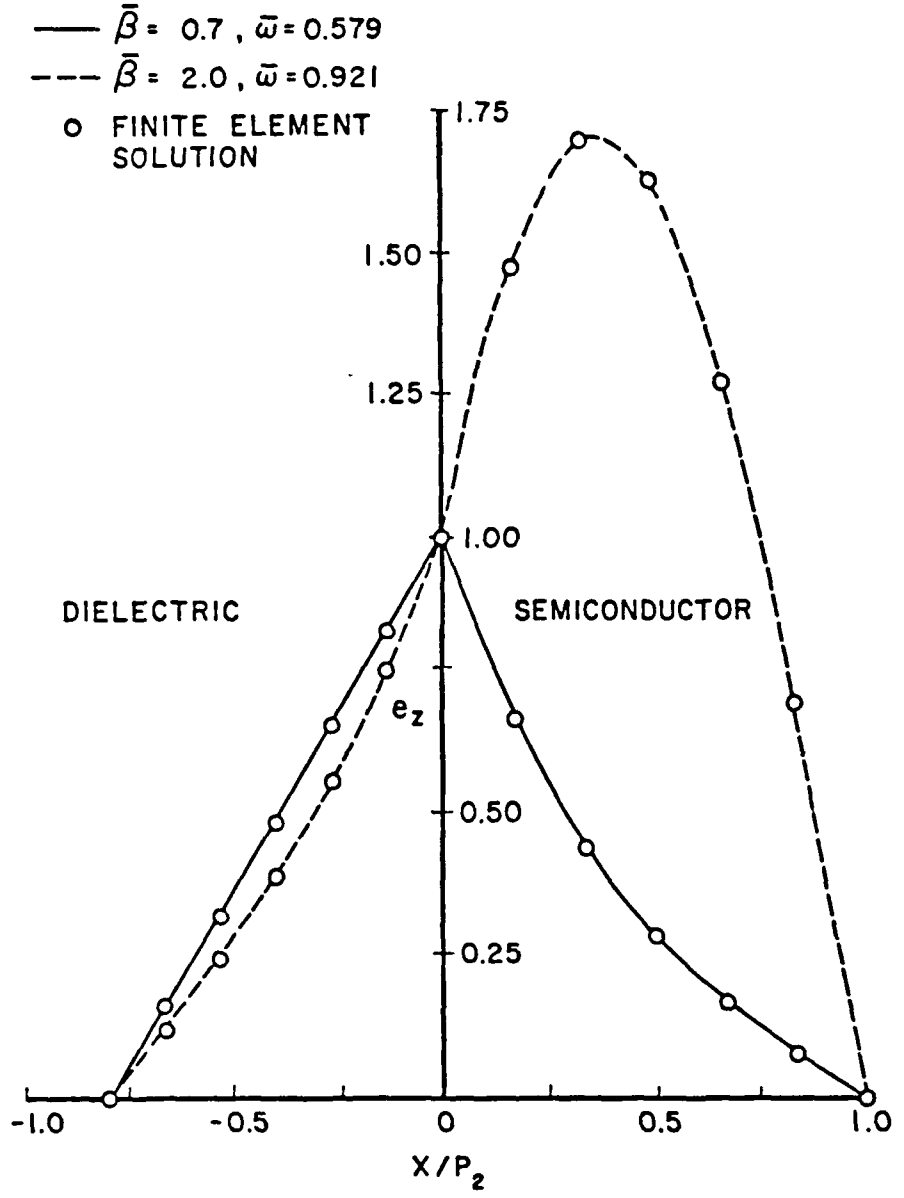

Fig.3-Distribution of e_z at Two Points Along Positive Branch.

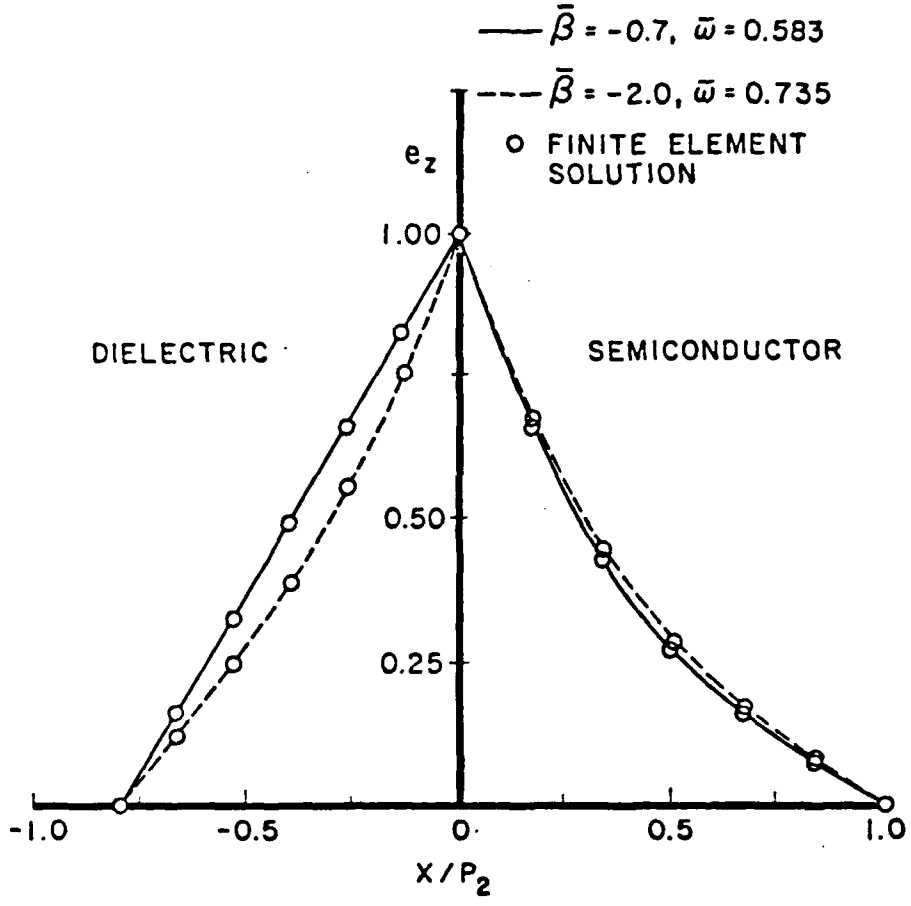

Fig.4-Distribution of e_z at Two Points Along Negative Branch.

APPENDIX B

"ANALYSIS OF WAVEGUIDING STRUCTURES EMPLOYING SURFACE MAGNETOPLASMONS BY THE FINITE-ELEMENT METHOD"

(IEEE Transactions on Microwave Theory and Techniques, April 1987)

ANALYSIS OF WAVEGUIDING STRUCTURES EMPLOYING SURFACE MAGNETOPLASMONS BY THE FINITE-ELEMENT METHOD

N. Mohsenian*, Student Member, IEEE, T. J. Delph†,

and D. M. Bolle‡, Fellow Member, IEEE

This work was supported in part by the Army Research Office under Grant DAAG29-85-K-0081.

---

*Department of Computer Science and Electrical Engineering, Lehigh University, Packard I aboratory #19, Bethlehem, Pa. 18015.

†Department of Mechanical Engineering and Mechanics, Lehigh University, Packard Laboratory #19, Bethlehem, Pa. 18015.

‡D.M.Bolle was with CSEE Department of Lehigh University until August 1,1988. He is presently at New York Polytechnic Institute.

ABSTRACT

The dispersion relation and electromagnetic field distributions for a gyroelectrically loaded waveguiding structure are obtained utilizing finite-element techniques. The structure considered consists of two layers, one a dielectric and the other a semiconductor, bounded by two perfectly conducting planes. The finite-element solution for the lowest real branches in the dispersion spectrum was compared against a numerical solution of the exact dispersion equation, and excellent agreement was found between the two. The structure, exhibiting nonreciprocal behavior, provides a suitable canonical model for the design of circuit components such as circulators, isolators, and phase shifters.

I. Introduction

The use of surface magnetoplasmons on semiconductor substrates shows promise in the development of components that can substitute for ferrite devices in the millimeter and submillimeter wave ranges [1]-[3]. Analytical studies of canonical structures employing surface magnetoplasmons have been reported in [4]-[6]. As the geometry of gyroelectrically loaded waveguides becomes more complicated, the problem of obtaining the dispersive behavior and the distribution of field intensities in the structure demands more sophisticated techniques. One particularly attractive means of dealing with this problem is the finite-element technique. This method has been successfully applied to microwave and optical waveguides, e.g., [7]. In this paper, we present a finite-element formulation for TM-mode wave propagation in a dielectric-semiconductor waveguide.

II. The Waveguiding Structure

We consider the two layer dielectric-semiconductor structure, sided by two perfectly conducting planes, shown in the insert of Fig. 1. A finite-element mesh is shown superposed. The thickness of the dielectric layer is taken to be P_1, while that of the semiconductor layer is P_2. The substrate for the semiconductor region is assumed to be a high-quality, moderately doped n-type GaAs material with a carrier concentration of $n \simeq 2.1\times10^{15}$ cm^{-3}, equivalent to a plasma frequency of $\omega_p=10^{13}$ rad/s. The permeability μ is taken to be a constant for both regions. A uniform dc magnetic field corresponding to a cyclotron frequency $\omega_c=10^{12}$ rad/s ($B_o=3810$ G) is assumed to be applied parallel to the interface. For a biasing magnetic field in the y-direction, the permittivity ϵ remains a constant for the dielectric medium, but becomes an asymmetric tensor for the semiconducting medium, [4]-[6], having the form

$$\epsilon_2(\omega) = \begin{bmatrix} \xi & 0 & -j\eta \\ 0 & \zeta & 0 \\ j\eta & 0 & \xi \end{bmatrix} \qquad (1)$$

where $\xi=\epsilon^{(o)}-\dfrac{\omega_p^2(\omega-j\nu)}{\omega[(\omega-j\nu)^2-\omega_c^2]}$, $\zeta=\epsilon^{(o)}-\dfrac{\omega_p^2}{\omega(\omega-j\nu)}$, $\eta=\dfrac{-\omega_p^2\omega_c}{\omega[(\omega-j\nu)^2-\omega_c^2]}$

Here, $\epsilon^{(o)}$ is the static dielectric constant of the semiconducting medium, ω is the frequency of electromagnetic wave propagation, and ν is the collision frequency. Finally, the semiconductor and dielectric here are taken to be lossless, implying $\nu=0$.

In the present analysis, we will consider only TM wave modes, because TE modes do not exhibit interesting interactions with the semiconducting material. This implies that only the h_y, e_x, and e_z field components are nonvanishing. We now assume time-harmonic wave propagation in the z direction with frequency ω and propagation constant $\gamma=\alpha+j\beta$, so that $e_z=e_z(x,y)\, e^{j\omega t-\gamma z}$. With these assumptions, an uncoupled partial differential equation may be derived for e_z from Maxwell's equations. This equation has the general form

$$\frac{\partial^2 e_z}{\partial x^2} + M_1\frac{\partial^2 e_z}{\partial y^2} + M_2 e_z=0 \qquad (2)$$

where for the semiconducting medium

$$M_1=\frac{\zeta(\gamma^2+\omega^2\mu_o\epsilon_o\xi)}{\xi(\gamma^2+\omega^2\mu_o\epsilon_o\zeta)} \qquad M_2=\gamma^2+\frac{\omega^2\mu_o\epsilon_o(\xi^2-\eta^2)}{\xi}$$

and for the dielectric medium

$$M_1=1 \qquad M_2=\gamma^2+\omega^2\mu_o\epsilon_o\epsilon_1.$$

Here, ϵ_o and μ_o are the vacuum permittivity and permeability, and ϵ_1 is the relative dielectric constant of the dielectric medium.

The waveguiding structure shown in Fig. 1 is, of course, strictly one-dimensional, so that $\partial()/\partial y=0$. Solving Maxwell's equations and applying the boundary conditions at the planes and at the interface, we obtain the dispersion equation, which is

$$\left(\frac{\epsilon_1}{k_1}\right)\mathrm{Coth}(k_1P_1)=\left(\frac{\xi k_2}{\gamma^2+\omega^2\mu_o\epsilon_o\xi}\right)\mathrm{Coth}(k_2P_2)\cdot\left(\frac{j\eta\gamma}{\gamma^2+\omega^2\mu_o\epsilon_o\xi}\right) \qquad (3)$$

where

$$k_1^2 = -\gamma^2 - k_o^2\epsilon_1 \qquad k_2^2 = -\gamma^2 - k_o^2\epsilon_e(\omega) \qquad k_o^2 = \omega^2\mu_o\epsilon_o \qquad \epsilon_e(\omega) = \frac{\xi^2 - \eta^2}{\xi}$$

III. Finite-Element Formulation

Because the governing equation (2) for the e_z field component is uncoupled and because the other field components are easily expressible in terms of e_z through Maxwell's equations, e_z was chosen as the dependent variable for the finite-element formulation. For the sake of generality, the finite-element equations will be derived in two-dimensional terms using (2), even though the problem to be treated is strictly one-dimensional. In the present case, the finite-element equations are most conveniently generated by means of the Galerkin formulation. This yields

$$\iint_{\mathcal{A}} \left(\frac{\partial^2 e_z}{\partial x^2} + M_1 \frac{\partial^2 e_z}{\partial y^2} + M_2 e_z \right) N_i(x,y)\, dxdy = 0 \qquad (4)$$

where the $N_i(x,y)$ are the finite-element interpolating (shape) functions for the problem, and the index i ranges over those nodal points at which no geometric boundary conditions are imposed for e_z. The interpolating functions are used to approximate $e_z(x,y)$ in the following manner: $e_z(x,y) \simeq [N(x,y)]\{e_z\}$, where $[N(x,y)]$ is the row vector of interpolating functions and $\{e_z\}$ is the column vector of nodal point values. An application of the divergence theorem now yields the finite-element equations in the form

$$[T]\{e_z\} - \oint_{\overline{B}} \left(\frac{\partial e_z}{\partial x} n_x + M_1 \frac{\partial e_z}{\partial y} n_y \right) N_i\, ds = 0 \qquad (5)$$

The i,jth element in the coefficient matrix [T] is given by

$$T_{ij} = \iint_{\mathcal{A}} \left(\frac{\partial N_i}{\partial x} \frac{\partial N_j}{\partial x} + M_1 \frac{\partial N_i}{\partial y} \frac{\partial N_j}{\partial y} - M_2 N_i N_j \right) dxdy \qquad (6)$$

The line integral in (5) is to be evaluated around the boundary $\bar{B}$ of the area $\mathcal{A}$ under consideration, with (n_x,n_y) being the components of the unit normal vector to $\bar{B}$. The finite-element equations are assembled from the element contributions to (5), the boundary integral being evaluated around the boundary $\bar{B}_e$ of each element. It is not difficult to show that the line integral vanishes everywhere except along the interface between the dielectric and semiconducting regions, where special care must be taken. Let n be one of the values of the index i corresponding to the interface nodes. Further, denote the values of e_z in the dielectric and semiconducting regions of $e_z^{(1)}$ and $e_z^{(2)}$, respectively. Along the interface, we must have both continuity of e_z, $e_z^{(1)}=e_z^{(2)}$, and continuity of h_y. The latter condition, from Maxwell's equations, gives

$$\frac{\partial e_z^{(1)}}{\partial x}\Big|_{x=o} = \left(R_1 \frac{\partial e_z^{(2)}}{\partial x} + R_2 e_z^{(2)}\right)\Big|_{x=o} \equiv C \qquad (7)$$

where

$$R_1=\frac{\xi(\gamma^2+\omega^2\mu_o\epsilon_o\epsilon_1)}{\epsilon_1(\gamma^2+\omega^2\mu_o\epsilon_o\xi)} \qquad R_2=\left(\frac{j\eta\gamma}{\xi}\right)R_1$$

We now write the nth finite-element equation separately for both the dielectric and the semiconducting region. Taking account of the fact that $n_x=\pm 1$, $n_y=0$ along the interface, and making use of (7), we have, respectively (with summation convention for repeated subscripts implied),

$$T_{nj}^{(1)}\, e_{zj}^{(1)} = Cd_n \qquad (8)$$

$$T_{nj}^{(2)}\, e_{zj}^{(2)} - \left(\frac{R_2}{R_1}\right) b_{nj}\, e_{zj}^{(2)} = \frac{Cd_n}{R_1} \qquad (9)$$

where

$$d_n=\int_{-\delta}^{\delta} N_n(0,y)dy \qquad b_{nj}=\int_{-\delta}^{\delta} N_n(0,y)N_j(0,y)dy.$$

Here δ and $-\delta$ represent the y coordinates of the nodes on the top and bottom of the elements, taken to be $\delta=15\mu m$. Eliminating C between (8) and (9) and requiring continuity of e_z at the interface, $e_{zn}^{(1)}=e_{zn}^{(2)}$, now yields for the nth equation

$$\left(T_{nj}^{(1)} + R_1 T_{nj}^{(2)} - R_2 b_{nj}\right) e_{zj} = 0 \qquad (10)$$

Equation (10) represent the finite-element equations corresponding to the interface nodes. The remaining finite-element equations have the form of (5), with the line integral vanishing for these equations. It is worth noting that the inclusion of the terms with coefficients R_1 and R_2 in (10) renders the resulting finite-element coefficient matrix $[T^*]$ nonsymmetric, even though the basic coefficient matrix $[T]$ in (5) is symmetric. When assembled, the finite-element equations have the form $[T^*]\{e_z\}=0$. A nontrivial solution then requires that

$$| T^* | = 0 \qquad (11)$$

Equation (11) represents the finite-element dispersion equation for the problem. Given a value of ω, one may obtain corresponding values of γ by evaluating $|T^*|$ numerically and employing standard numerical root-finding techniques.

IV. Results

Numerical results for the dispersion spectrum, using a numerical root-finding technique, were obtained from both the exact dispersion relation given by (3) and the approximate finite-element formulation given by (11). Two different combinations of layer thicknesses were considered. In case (1), $P_1=80\mu m$ and $P_2=100\mu m$, and in case (2), $P_1=320\mu m$ and $P_2=50\mu m$. Furthermore, it was assumed that $\epsilon_1=1$, $\epsilon^{(o)}=13$. For the finite-element analysis, the two layers were divided into three equisized elements (Fig.1) using eight-noded isoparametric quadrilateral elements. Fig.1 shows the resulting dispersion spectra for both combinations of thicknesses in terms of a normalized propagation constant defined by $\bar{\beta}=P_2\beta$ and a normalized frequency given by $\bar{\omega}=\omega P_2/c$, where c is the velocity of light. Nonreciprocal effects are evident in both branches of the spectrum. It can be seen that excellent agreement exists between the spectra computed from the exact dispersion relation and the approximate finite-element result.

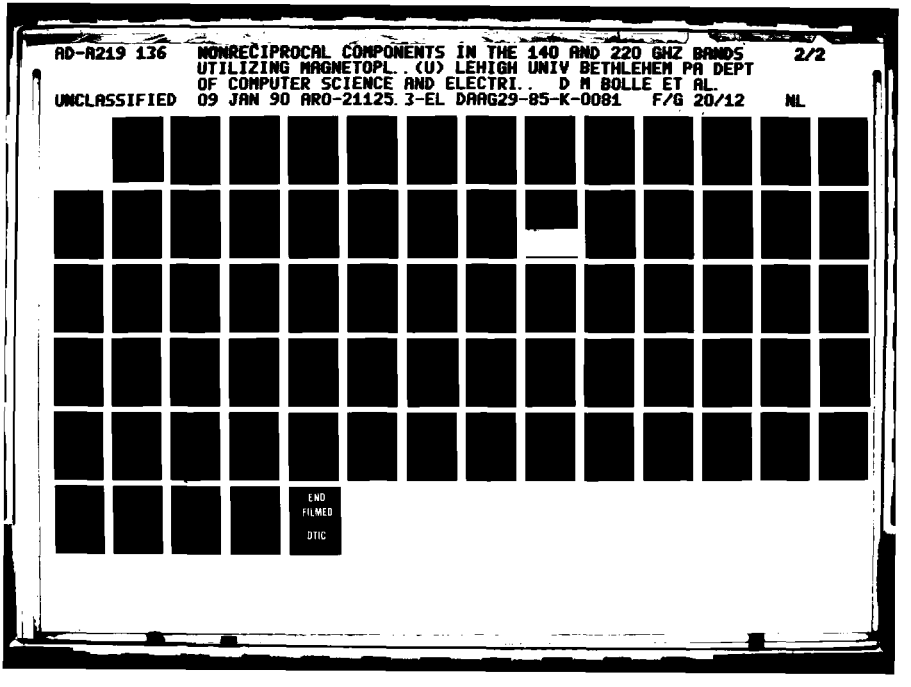
AD-A219 136
NONRECIPROCAL COMPONENTS IN THE 140 AND 220 GHZ BANDS
UTILIZING MAGNETOPL..(U) LEHIGH UNIV BETHLEHEM PA DEPT
OF COMPUTER SCIENCE AND ELECTRI.. D M BOLLE ET AL.
UNCLASSIFIED 09 JAN 90 ARO-21125.3-EL DAAG29-85-K-0081 F/G 20/12
2/2
NL
END
FILMED
DTIC

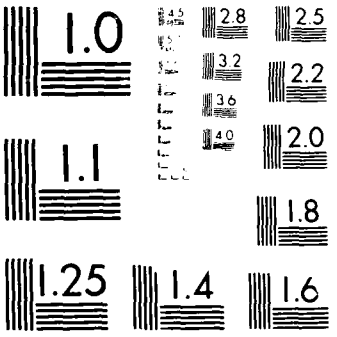

MICROCOPY RESOLUTION TEST CHART
NATIONAL BUREAU OF STANDARDS 1963-A

At low frequencies, a reverse-propagating mode was obtained in both cases, with the bulk of its energy traveling in the semiconducting medium. For small values of $\bar{\omega}$, this branch becomes asymptotic to the light line of the semiconducting medium; i.e., $\bar{\omega} \rightarrow -\bar{\beta} / \sqrt{\xi^{(o)}}$ as $\bar{\omega} \rightarrow 0$, where $\xi^{(o)}$ is defined by: $\xi^{(o)} = \epsilon^{(o)} + (\omega_p / \omega_c)^2$. The absence of a forward-prpagating mode over this frequency range may be explained through examining the configuration of the field distributions shown in Fig.2(a). If such a mode existed, most of its energy would need to be concentrated in the semiconducting medium and to be traveling in the positive z direction. The field components of the dielectric medium would display the same behavior as those derived for the reverse mode. To justify the direction of the signal, the e_x component should exhibit a negative amplitude in the semiconducting medium. But for the given electrical parameters of this problem, the tensor elements ξ and η yield positive values and these conditions do not allow the fulfilling of the continuity of the normal component of the D field. Consequently, there exists only a unidirectional mode, which propagates in the reverse direction over this frequency range, i.e., $\bar{\omega} < 0.17$. When losses are introduced, this mode will suffer sustantial attenuation; therefore, the remaining branches of the spectrum are the ones of primary interest.

In both cases, the lower branches of the forward and reverse propagation modes become asymptotic to the light line, i.e., $\bar{\omega} \rightarrow \pm \bar{\beta}$ as $\bar{\omega} \rightarrow 0$. However, for higher frequencies, the forward mode extends into a region where the quantity k_2^2 becomes negative. In this region, the transverse field components have a trigonometric variation in the semiconducting medium. The upper branches lie entirely in this region, and are called the "volume" modes [5], [6].

Also observed in case (2) is a change of slope in the lower branch of the reverse-propagating mode. This may be understood through the field displacement behavior of the mode in the structure. Here, unlike case (1), the transverse component of the magnetic field clings to the plane at $x = P_2$ for $\bar{\beta} < -0.6$, as shown in Fig.2(b). For this portion of the branch, the direction of the energy flow is reversed, and with the energy traveling in the positive

direction, a change in the slope of the branch is obtained.

Of interest is the fact that there exists a frequency band above the lower reverse mode which contains only a forward mode. This offers the possibility of designing components such as isolators and circulators having a small attenuation constant when losses and a more realistic geometry are considered. For the particular set of geometric and electrical parameters used here, this frequency band was calculated to be 358 GHz<f<411 GHz for case (1) and 377 GHz<f<396 GHz for case (2), with the former case having a 15-percent bandwidth.

Fig.2 shows the modal field distributions for the components (e_z, e_x, h_y) derived from both the exact and finite-elements (F.E.) solutions. Here, for comparison purposes only, the h_y component was normalized by the factor η_0 for the lower branch and by the factor $\eta_0/10$ for the unidirectional branch, where η_0=376.82 Ω is the impedance of free space. The value of e_z at the interface is normalized to unity. For the linear region of the lower branches in both cases, most of the energy is seen to be contained within the dielectric medium, while the energy is essentially uniformly distributed throughout the structure as these branches move away from the light line. The upper branches in case (1) also exhibit similar energy distributions, but the behavior of case (2) is somewhat different. Here, the bulk of the energy shifts to the semiconducting medium, while at the very low end of the upper branches a fairly uniform distribution of energy may be noted. Finally, the field structures of the components (e_z, e_x, h_y) derived from the finite-element formulation are shown in Fig.3 at time t=0. These patterns do not attempt to show the relative field strengths, but only the directions. However, the relative field strengths between the two media can be observed in the previous figure.

V. Conclusions

A numerical analysis based on the finite-element formulation has been presented for a canonical, one-dimensional, gyroelectrically loaded waveguiding structure. The agreement between the finite-element solution and that obtained from the exact dispersion equation can be seen to be excellent and was, in fact, good to three significant figures. The primary

advantage of the finite-element method is, of course, its ability to treat problems of practical interest involving complicated two-dimensional geometries and correspondingly complicated electric and magnetic field distributions. The results given here indicate that the finite-element method holds substantial promise for such applications, and gives the necessary confidence for its use in the analysis of electromagnetic wave propagation in much more complex gyroelectrically and gyromagnetically loaded waveguiding structures, where exact methods of analysis are not available.

REFERENCES

[1]- R. E. Hayes and W. G. May, "The use of semiconductors in nonreciprocal devices for submillimeter wavelengths," in *Proc. Symp. Submillimeter Waves* (Polytechnic Inst. Brooklyn), 1970, pp. 237-250.

[2]- M. Kanda and W. G. May, "Hollow-cylinder waveguide isolators for use at millimeter wavelengths," *IEEE Trans. Microwave Theory Tech.*, vol. MTT-22, pp. 913-917, Nov. 1974.

[3]- M. Kanda and W. G. May, "A millimeter-wave reflection-beam isolator," *IEEE Trans. Microwave Theory Tech.*, vol. MTT-23, pp. 506-508, June 1975.

[4]- W. L. K. Hwang, "Application of surface magnetoplamons on semiconductor substrates," Ph.D. thesis, Dept. Computer Sci. & Elec. Eng., Lehigh University, Bethlehem, PA, 1983.

[5]- D. M. Bolle and S. H. Talisa, "Fundamental considerations in millimeter and near-millimeter component design employing magnetoplasmons," *IEEE Trans. Microwave Theory Tech.*, vol. MTT-29, pp. 916-923, Sept. 1981.

[6]- S. H. Talisa and D. M. Bolle, "Performance predictions for isolators and differential phase shifters for the near-millimeter wave ranges," *IEEE Trans. Microwave Theory Tech.*, vol. MTT-29, pp. 1338-1343, Dec. 1981.

[7]- B. M. A. Rahman and J. B. Davies, "Finite-element analysis of optical and microwave waveguide problems," *IEEE Trans. Microwave Theory Tech.*, vol. MTT-32, pp. 20-28, Jan. 1984.

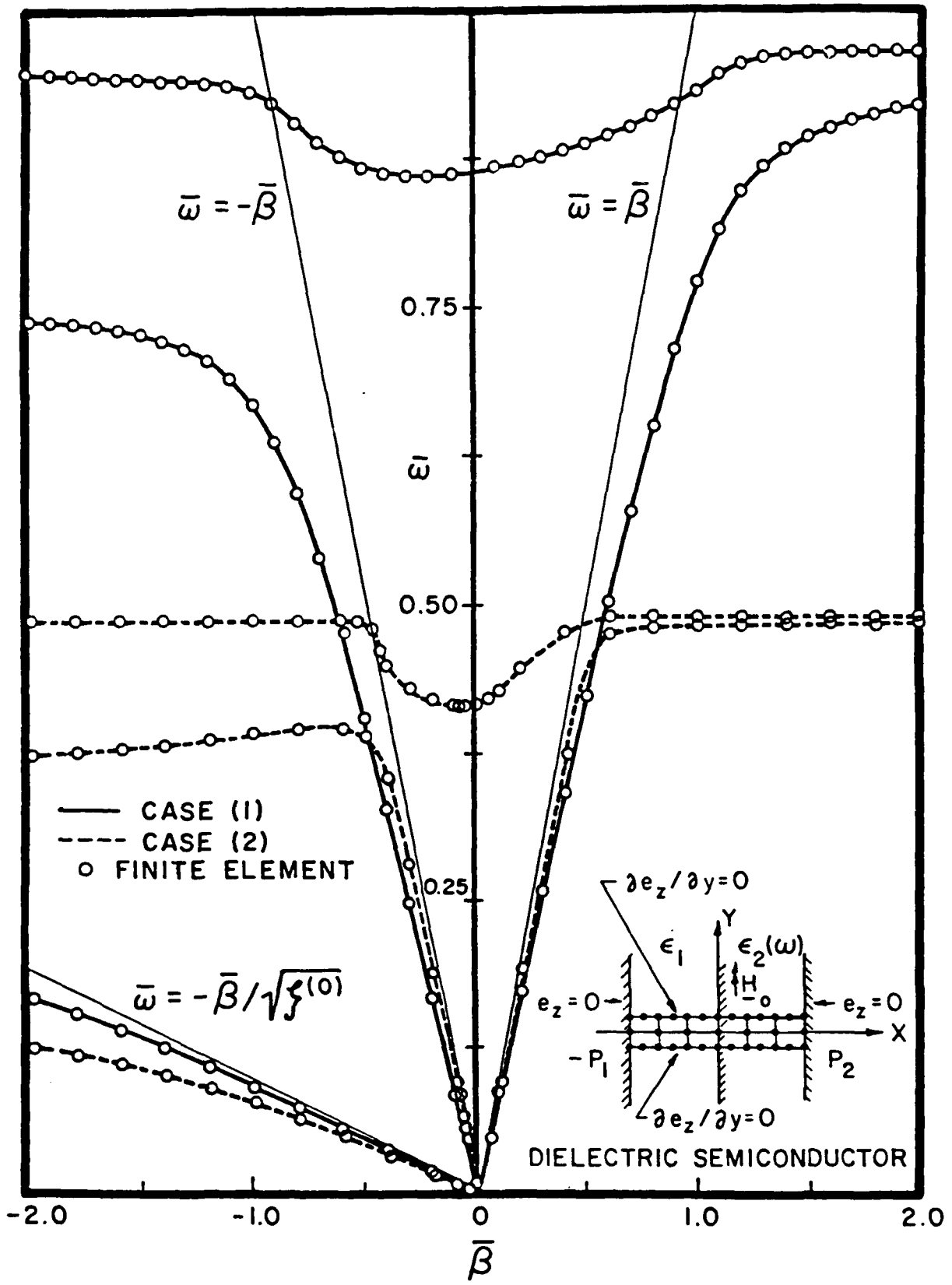

Fig.1. Exact and finite-element dispersion spectra of a dielectric-semiconductor single interface for case (1):P_1=80μm, P_2=100μm and case(2):P_1=320μm,P_2=50μm

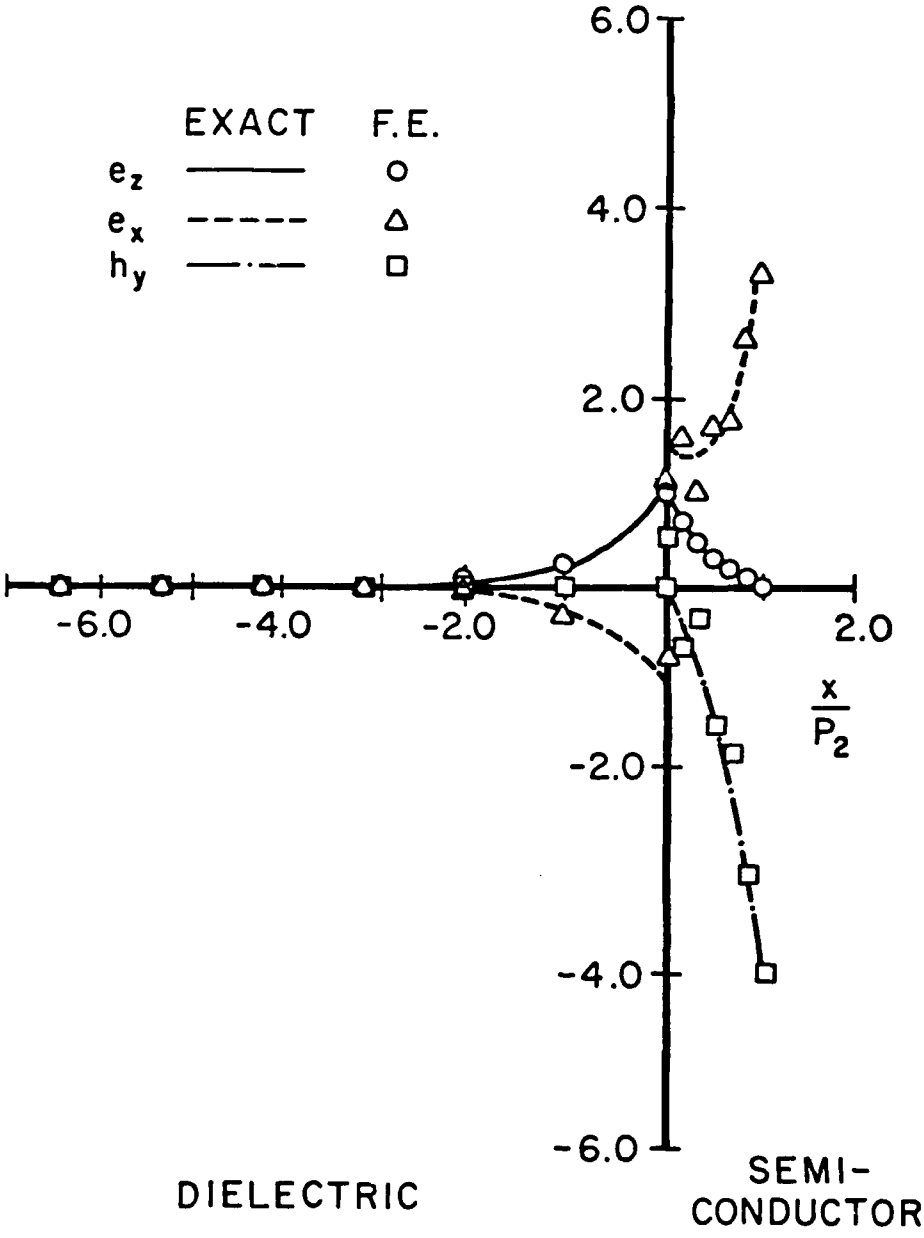

Fig.2(a). Modal field distributions of components (e_z, e_x, h_y) taken from the branches of the exact and finite-element (F.E.) dispersion spectra for case (2): P_1=320μm, P_2=50μm, unidirectional branch, $\bar{\beta}$=-1.4, $\bar{\omega}$=.101.

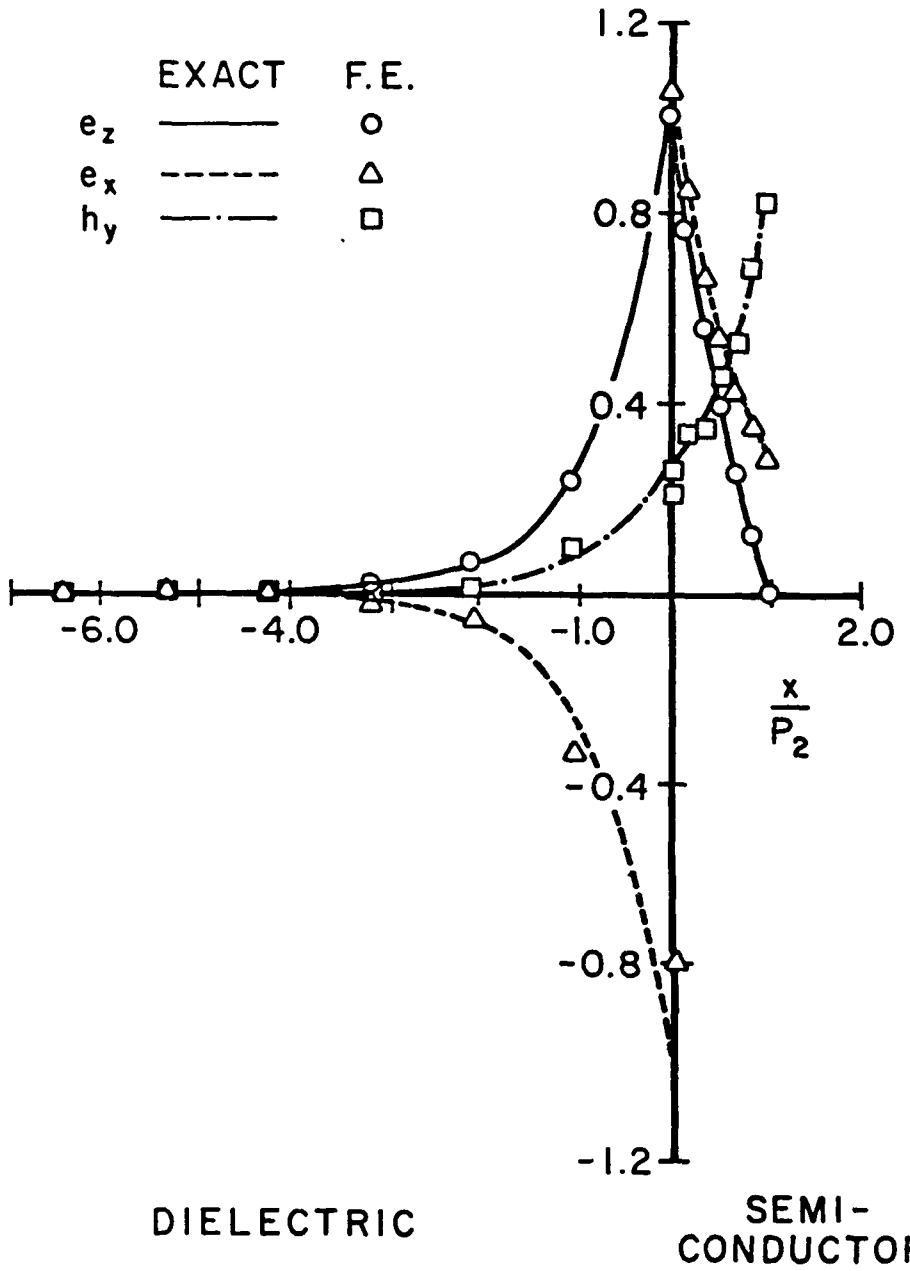

Fig.2(b). Modal field distributions of components (e_z,e_x,h_y) taken from the branches of the exact and finite-element (F.E.) dispersion spectra for case (2): P_1=320μm, P_2=50μm, lower branch, $\bar{\beta}$=-1.4, $\bar{\omega}$=.381.

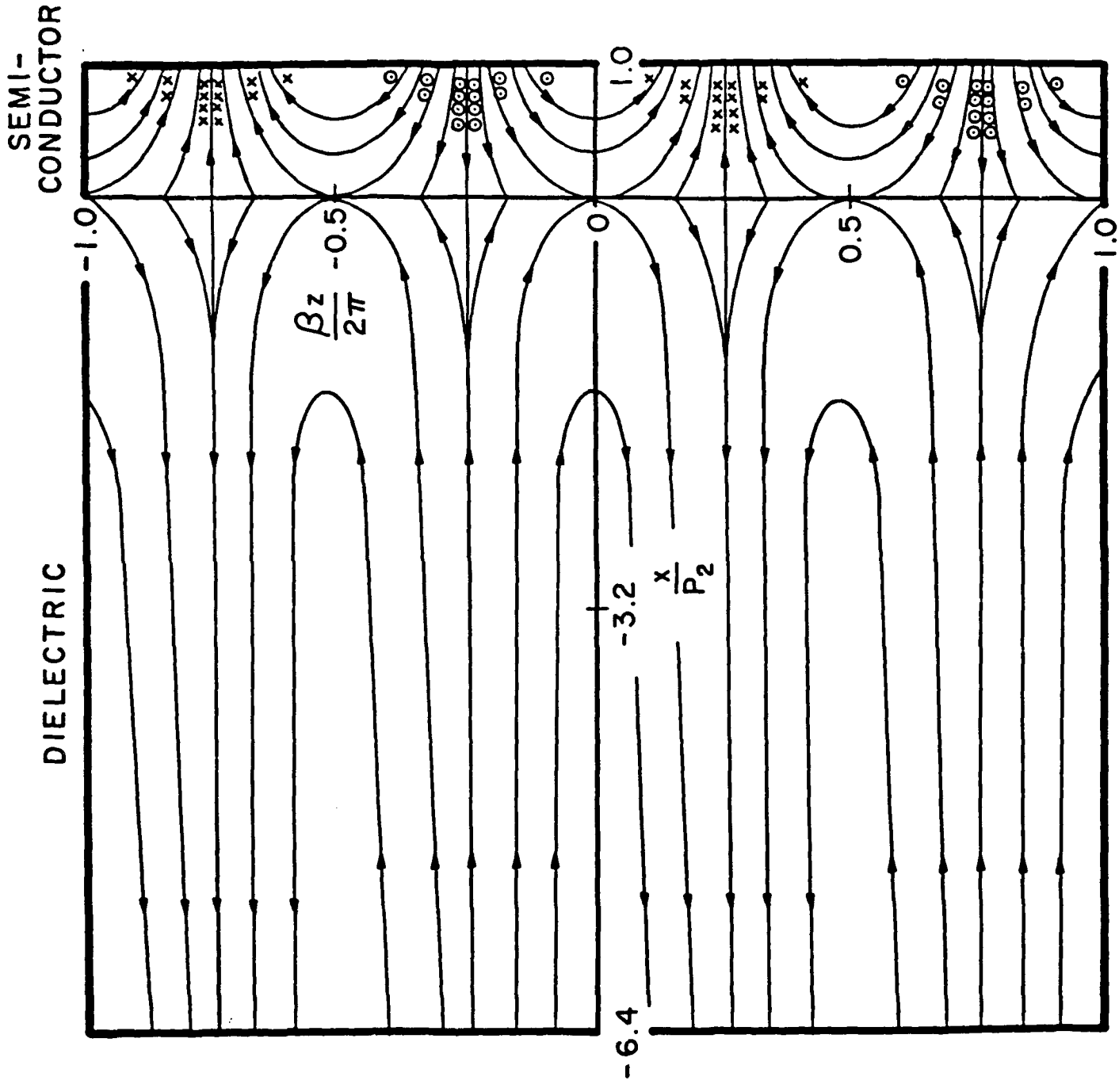

Fig.3(a). Field structure of components E(——) and H(⊙,x) obtained from the finite-element formulation for case (2):P_1=320μm,P_2=50μm, unidirectional branch, $\bar{\beta}$=-1.0, $\bar{\omega}$ =.078.

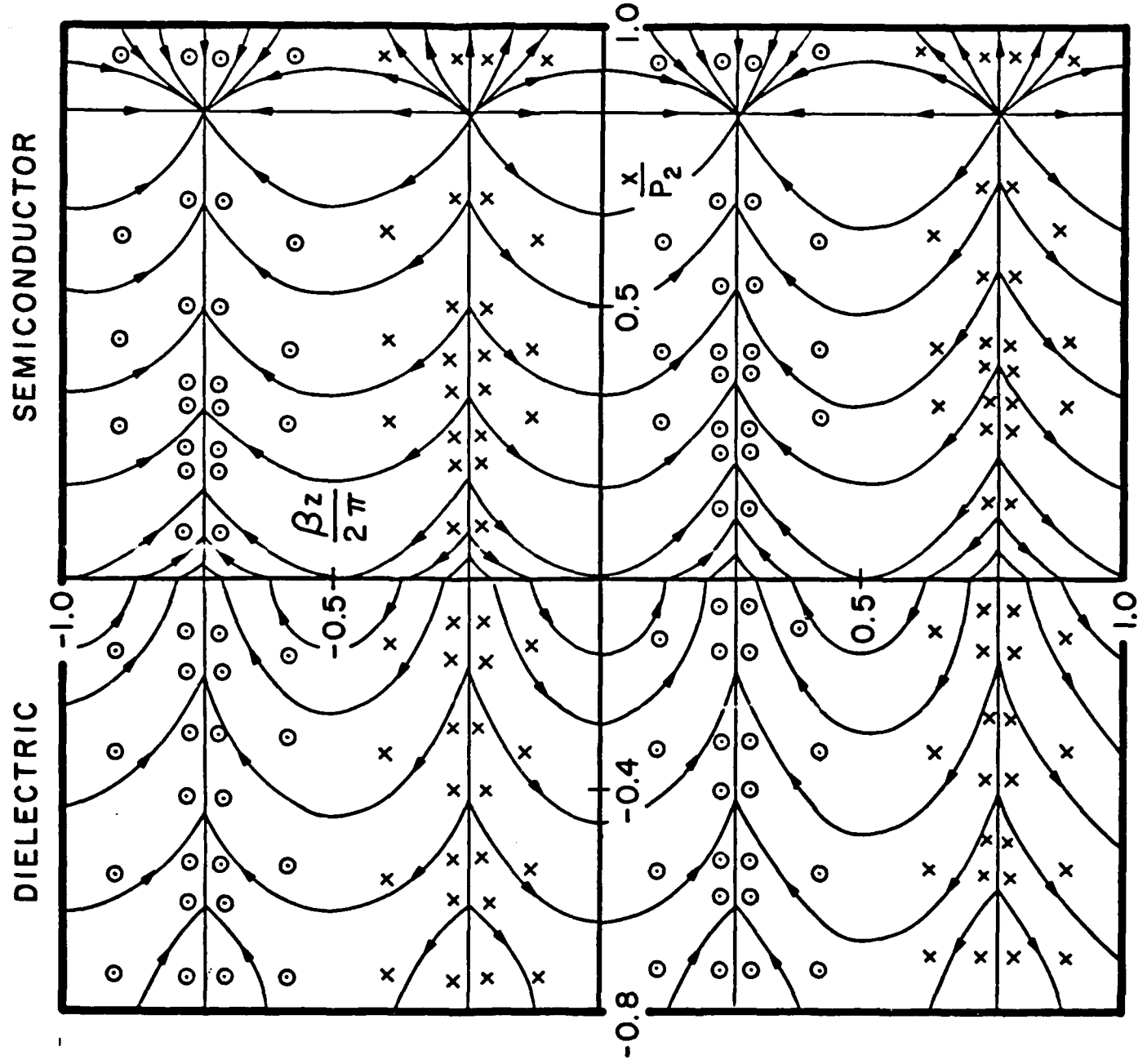

Fig.3(b). Field structure of components E(——) and H(⊙,x) obtained from the finite-element formulation for case (1): P_1=80μm, P_2=100μm, lower branch, $\bar{\beta}$=1.2, $\bar{\omega}$=.847.

APPENDIX C

"TWO-DIMENSIONAL FINITE-ELEMENT ANALYSIS OF RECTANGULAR WAVEGUIDES WITH ISOTROPIC n-TYPE SEMICONDUCTOR MATERIAL"

(To be submitted to IEEE Transactions on Microwave Theory and Techniques)

TWO-DIMENSIONAL FINITE-ELEMENT ANALYSIS OF RECTANGULAR WAVEGUIDES WITH ISOTROPIC n-TYPE SEMICONDUCTOR MATERIAL

N. Mohsenian*, Student Member, IEEE, T. J. Delph†,

and D. M. Bolle‡, Fellow Member, IEEE

This work was supported in part by the Army Research Office under Grant DAAG29-85-K-0081.

---

*Department of Computer Science and Electrical Engineering, Lehigh University, Packard Laboratory #19, Bethlehem, Pa. 18015.

†Department of Mechanical Engineering and Mechanics, Lehigh University, Packard Laboratory #19, Bethlehem, Pa. 18015.

‡D.M.Bolle was with CSEE Department of Lehigh University until August 1,1988. He is presently at New York Polytechnic Institute.

I. INTRODUCTION

Finite-element analysis of dielectric waveguides used in design of millimeter-wave and optical integrated circuits has attracted the attention of many researchers in recent years [1]-[8]. A powerful and versatile technique, the finite-element method can be applied to anisotropic waveguiding structures with arbitrary shaped cross sections to obtain the propagation characteristics and field distributions in the waveguide. However a serious drawback is the appearance of non-physical, spurious modes in the calculated dispersion spectrum of the dielectric waveguides which do not satisfy the divergence-free condition on the magnetic field vector, i.e., $\nabla \bullet H=0$, [2]-[5]. A number of efforts have been made to suppress or eliminate these non-physical solutions by various methods [3],[6]-[8].

In this paper we present a finite-element formulation in terms of the transverse components of the magnetic fields to investigate the propagation characteristics of two-dimensional gyroelectrically loaded waveguides. Spurious modes are eliminated by the direct inclusion of the relation $\nabla \bullet H=0$ proposed by Hayata et al., [7]. These configurations use surface magnetoplasmons on high quality semiconducting substrates, and have applications to the design of quasi-optical integrated non-reciprocal devices in the millimeter (mm) and submillimeter (smm) wavelengths.

Extensive analytical and numerical studies of planar one-dimensional canonical structures employing surface magnetoplasmons have been carried out previously [9],[10]. However, as the geometry of such models becomes more complex, the problem of obtaining the dispersive behavior requires more powerful numerical techniques such as the finite-element method. A finite-element formulation for one-dimensional problems involving surface magnetoplasmons on semiconductors has been presented by the authors in [11]. The purpose of the present work is to extend this to the analysis of two-dimensional structures.

II. FINITE-ELEMENT FORMULATION

We consider an embossed waveguide as depicted in figure 1., with a doped n-type InSb material as the semiconducting substrate overlaid on the dielectric medium. The structure is enclosed by perfectly conducting planes. The permeability is taken to be a constant for all regions. When exposed to a uniform d.c. biasing field in the y-direction, the permittivity remains a scalar constant for the dielectric and vacuum regions, but becomes an asymmetric tensor for the semiconducting medium

$$\epsilon_2(\omega) = \begin{bmatrix} \xi & 0 & -j\eta \\ 0 & \zeta & 0 \\ j\eta & 0 & \xi \end{bmatrix} \qquad (1)$$

where $\xi=\epsilon^{(o)}-\dfrac{\omega_p^2(\omega-j\nu)}{\omega[(\omega-j\nu)^2-\omega_c^2]}$, $\zeta=\epsilon^{(o)}-\dfrac{\omega_p^2}{\omega(\omega-j\nu)}$, $\eta=\dfrac{-\omega_p^2\omega_c}{\omega[(\omega-j\nu)^2-\omega_c^2]}$

Here $\epsilon^{(o)}$ is the static dielectric constant of the semiconducting medium, ω is the frequency of wave propagation, ν is the collision frequency, ω_p is the plasma frequency, and ω_c is the cyclotron frequency. The electromagnetic wave is assumed to travel in the z-direction. For the isotropic case, $\omega_c=0$, resulting in

$$\xi=\zeta=\epsilon^{(o)}-\frac{\omega_p^2}{\omega(\omega-j\nu)} \quad \text{and } \eta=0.$$

Finally, the semiconductor and dielectric are taken to be lossless in this analysis, implying $\nu=0$. Maxwell's equation for the magnetic field components then takes the form

$$\nabla \times \left([\epsilon(\omega)]^{-1} \nabla \times H \right) - \omega^2 \mu_o \epsilon_o H = 0 \qquad (2)$$

Here μ_o and ϵ_o are the vacuum permeability and permittivity and $[\epsilon(\omega)]$ is the permittivity tensor.

For the finite-element formulation, the two-dimensional domains comprising the vacuum, dielectric and semiconductor media are divided into quadrilateral elements, where the unknown quantities, in this case h_x, h_y, and h_z components of the magnetic field intensity in the

structure, are represented by interpolating functions that contain the values of the field intensity at the nodes of each element. The use of all three components of the magnetic field vector as the dependent variables is possible because H is continous across the interfaces in the structure.

A Galerkin formulation was used to generate the finite-element equations from multiplying the equation in (2) by interpolating functions $N_i(x,y)$ and integrating over the different regions of the waveguide denoted by $\mathcal{A}$, [11], where the index i ranges over those nodal points at which no geometric boundary conditions are imposed for components of H field. These components were approximated in the following manner: $h_x(x,y)=[N(x,y)]\{h_x\}$, $h_y(x,y)=[N(x,y)]\{h_y\}$, and $h_z(x,y)=j[N(x,y)]\{h_z\}$. Here $[N(x,y)]$ is the row vector of interpolating functions and $\{h\}$ is the column vector of nodal point values. Divergence theorem was then used to derive the final equations in (3). The complete derivation of this is presented in the appendix. It may be noted that the contour integral associated with the application of divergence theorem vanishes due to the continuity of components of electric field.

$$\begin{bmatrix} [B] & [C] & [D] \\ [C]^T & [E] & [F] \\ [D]^T & [F]^T & [G] \end{bmatrix} \bullet \begin{bmatrix} \{h_x\} \\ \{h_y\} \\ \{h_z\} \end{bmatrix} = 0 \qquad (3)$$

here T stands for transpose and the coefficients of matrices in (3) are given by

$$B_{ij} = \iint_{\mathcal{A}} \left(\Phi_1 \frac{\partial N_i}{\partial \bar{y}} \frac{\partial N_j}{\partial \bar{y}} + [\Phi_2 - (\frac{\bar{\omega}}{\bar{\beta}})^2] N_i N_j \right) d\bar{x}d\bar{y} \qquad (4)$$

$$C_{ij} = \iint_{\mathcal{A}} \left(-\Phi_3 \frac{\partial N_i}{\partial \bar{v}} N_j - \Phi_1 \frac{\partial N_i}{\partial \bar{y}} \frac{\partial N_j}{\partial \bar{x}} \right) d\bar{x}d\bar{y} \qquad (5)$$

$$D_{ij} = \iint_{\mathcal{A}} \left(-\Phi_3 \frac{\partial N_i}{\partial \bar{y}} \frac{\partial N_j}{\partial \bar{y}} + \Phi_2 N_i \frac{\partial N_j}{\partial \bar{x}} \right) d\bar{x}d\bar{y} \qquad (6)$$

$$E_{ij} = \iint_{\mathcal{A}} \left(\Phi_3 [\frac{\partial N_i}{\partial \bar{x}} N_j + N_i \frac{\partial N_j}{\partial \bar{x}}] + \Phi_1 [\frac{\partial N_i}{\partial \bar{x}} \frac{\partial N_j}{\partial \bar{x}} + N_i N_j] - (\frac{\bar{\omega}}{\bar{\beta}})^2 N_i N_j \right) d\bar{x}d\bar{y} \qquad (7)$$

$$F_{ij} = \iint_{\mathcal{A}} \left(\Phi_3 \frac{\partial N_i}{\partial \bar{x}} \frac{\partial N_j}{\partial \bar{y}} + \Phi_1 N_i \frac{\partial N_j}{\partial \bar{y}} \right) d\bar{x}d\bar{y} \qquad (8)$$

$$G_{ij} = \iint_{\mathcal{A}} \left(\Phi_2 \frac{\partial N_i}{\partial \bar{x}} \frac{\partial N_j}{\partial \bar{x}} + \Phi_1 \frac{\partial N_i}{\partial \bar{y}} \frac{\partial N_j}{\partial \bar{y}} - (\frac{\bar{\omega}}{\bar{\beta}})^2 N_i N_j \right) d\bar{x}d\bar{y} \qquad (9)$$

Here $\bar{\omega}$ and $\bar{\beta}$ are the normalized frequency and propagation constant, respectively, given by, $\bar{\omega}=\omega t/c$, $\bar{\beta}=\beta t$, where t is the height of the semiconducting medium and c is the velocity of light. The coordinates x and y were also normalized according to $\bar{x}=\bar{\beta}x/t$ and $\bar{y}=\bar{\beta}y/t$. For the semiconducting medium Φ_1, Φ_2 and Φ_3 take the form

$$\Phi_1 = \frac{\xi}{\xi^2-\eta^2} \quad , \quad \Phi_2 = \frac{1}{\zeta} \quad , \quad \Phi_3 = \frac{\eta}{\xi^2-\eta^2}$$

For the dielectric region, we have $\Phi_1 = \Phi_2 = \frac{1}{\epsilon_1}$ and $\Phi_3=0$, where ϵ_1 is the relative dielectric constant of the dielectric medium.

The finite-element dispersion spectrum obtained from the system in (3) includes spurious solutions. Therefore, we adopted the method employed by Hayata and coworkers [7] to include the finite-element equations derived from the relation $\nabla \bullet H=0$ in our formulation to eliminate the spurious solutions. Upon application of Galerkin technique to the divergence free condition of magnetic field the equations in (10) were obtained [7].

$$\begin{bmatrix} \{h_x\} \\ \{h_y\} \\ \{h_z\} \end{bmatrix} = \begin{bmatrix} [U] \\ [T_z]^{-1} \begin{bmatrix} [T_x] & [T_y] \end{bmatrix} \end{bmatrix} \bullet \begin{bmatrix} \{h_x\} \\ \{h_y\} \end{bmatrix} \qquad (10)$$

Here [U] is the unity matrix and the elements of other matrices are

$$T_{z_{ij}} = \iint_{\mathcal{A}} N_i N_j d\bar{x}d\bar{y} \; , \quad T_{x_{ij}} = - \iint_{\mathcal{A}} N_i \frac{\partial N_j}{\partial \bar{x}} d\bar{x}d\bar{y} \; , \quad T_{y_{ij}} = - \iint_{\mathcal{A}} N_i \frac{\partial N_j}{\partial \bar{y}} d\bar{x}d\bar{y}$$

Substituting the equations in (10) into our previous results, (3), and multiplying by the transpose of the coefficient matrix in (10), the final finite-element equations were generated in terms of the transverse components of the magnetic field for which the dispersion spectrum

does not contain spurious modes.

$$\left[\ S\ \right]\bullet\begin{bmatrix}\{h_x\}\\ \{h_y\}\end{bmatrix}=0 \qquad (11)$$

where

$$\left[\ S\ \right]=\begin{bmatrix}[U]\\ [T_z]^{-1}\left[\ [T_x]\ \ [T_y]\right]\end{bmatrix}^{T}\bullet\begin{bmatrix}[B] & [C] & [D]\\ [C]^{T} & [E] & [F]\\ [D]^{T} & [F]^{T} & [G]\end{bmatrix}\bullet\begin{bmatrix}[U]\\ [T_z]^{-1}\left[\ [T_x]\ \ [T_y]\right]\end{bmatrix} \qquad (12)$$

It should be noted that the matrix [S] is a full symmetric matrix, moreover the system of equations in (11) do not constitute a standard eigenvalue problem. However, nontrivial solutions require that the determinant of [S] must vanish. Given a value of $\overline{\beta}$, one may obtain corresponding values of $\overline{\omega}$ by evaluating this determinant numerically and employing standard numerical root-finding techniques.

APPENDIX

In this section we will demonstrate the derivation of the system of equations given in (3) from the Maxwell's equation in form of (2). Rewriting this vector equation in terms of the magnetic field components and applying the Galerkin technique, the following results are obtained

$$\iint_{\mathcal{A}} \Big(-j\Phi_3\Big(\frac{\partial^2 h_z}{\partial y^2} - \frac{\partial^2 h_y}{\partial z \partial y}\Big)+\Phi_1\Big(\frac{\partial^2 h_y}{\partial y \partial x} - \frac{\partial^2 h_x}{\partial y^2}\Big)-\Phi_2\Big(\frac{\partial^2 h_x}{\partial z^2} - \frac{\partial^2 h_z}{\partial z \partial x}\Big) - \Big(\frac{\omega}{c}\Big)^2 h_x\Big) \cdot N_i(x,y)\, dxdy \tag{A1}$$

$$\iint_{\mathcal{A}} \Big(\Phi_1\Big(\frac{\partial^2 h_z}{\partial z \partial y} - \frac{\partial^2 h_y}{\partial z^2}\Big)+j\Phi_3\Big(\frac{\partial^2 h_y}{\partial z \partial x} - \frac{\partial^2 h_x}{\partial z \partial y}\Big)+j\Phi_3\Big(\frac{\partial^2 h_z}{\partial x \partial y} - \frac{\partial^2 h_y}{\partial x \partial z}\Big) - \Phi_1\Big(\frac{\partial^2 h_y}{\partial x^2} - \frac{\partial^2 h_x}{\partial x \partial y}\Big)-\Big(\frac{\omega}{c}\Big)^2 h_y \Big) \cdot N_i(x,y)\, dxdy \tag{A2}$$

$$\iint_{\mathcal{A}} \Big(\Phi_2\Big(\frac{\partial^2 h_x}{\partial x \partial z} - \frac{\partial^2 h_z}{\partial x^2}\Big)-\Phi_1\Big(\frac{\partial^2 h_z}{\partial y^2} - \frac{\partial^2 h_y}{\partial y \partial z}\Big)-j\Phi_3\Big(\frac{\partial^2 h_y}{\partial y \partial x} - \frac{\partial^2 h_x}{\partial y^2}\Big) - \Big(\frac{\omega}{c}\Big)^2 h_z \Big) \cdot j\, N_i(x,y)\, dxdy \tag{A3}$$

where the $N_i(x,y)$ are the finite-element interpolating functions and the integrals are taken over domain $\mathcal{A}$ of the problem. The components of the magnetic field are approximated in the following manner: $h_x(x,y)=[N(x,y)]\cdot\{h_x\}$, $h_y(x,y)=[N(x,y)]\cdot\{h_y\}$ and $h_z(x,y)=j[N(x,y)]\cdot\{h_z\}$. Then divergence theorem was used to generate the finite-element equations in the form

$$[B]\cdot\{h_x\}+[C]\cdot\{h_y\}+[D]\cdot\{h_z\}+\oint_{\mathcal{B}}\Big(-j\Phi_3\Big(\frac{\partial h_z}{\partial y}-\frac{\partial h_y}{\partial z}\Big)+\Phi_1\Big(\frac{\partial h_y}{\partial x}-\frac{\partial h_x}{\partial y}\Big)\Big)\, n_y\, N_i\, dl \tag{A4}$$

$$[C]^T\cdot\{h_x\}+[E]\cdot\{h_y\}+[F]\cdot\{h_z\}+\oint_{\mathcal{B}}\Big(j\Phi_3\Big(\frac{\partial h_z}{\partial y}-\frac{\partial h_y}{\partial z}\Big)-\Phi_1\Big(\frac{\partial h_y}{\partial x}-\frac{\partial h_x}{\partial y}\Big)\Big)\, n_x\, N_i\, dl \tag{A5}$$

$$[D]^T\cdot\{h_x\}+[F]^T\cdot\{h_y\}+[G]\cdot\{h_z\}+\oint_{\mathcal{B}}\left(\Phi_1\left(\frac{\partial h_z}{\partial y}-\frac{\partial h_y}{\partial z}\right)+j\Phi_3\left(\frac{\partial h_y}{\partial x}-\frac{\partial h_x}{\partial y}\right)\right) n_y\, j\, N_i\, dl$$

$$-\oint_{\mathcal{B}}\Phi_2\left(\frac{\partial h_x}{\partial z}-\frac{\partial h_z}{\partial x}\right) n_x\, j\, N_i\, dl \qquad \text{(A6)}$$

The i, jth element in the matrices [B], [C], [D], [E], [F], [G] were given in section II and the line integrals in equations (A4), (A5), and (A6) are to be evaluated around the boundary $\mathcal{B}$ of the area $\mathcal{A}$ under consideration, with (n_x, n_y) being the components of the unit normal vector to $\mathcal{B}$. From Maxwell's equations it can be easily shown that the terms of the line integrals of (A4) and (A5) represent the e_z component, while the line integrals of (A6) represent the e_x and e_y components of electric field, respectively. Now with the continuity of e_x, e_y, and e_z along the proper interfaces, one can derive the elimination of the line integrals which are to be evaluated around the boundary of each element between two different media. It is also not difficult to show that the line integrals vanish at the enclosed planes according to the boundary conditions. Once assembled, the finite-element equations have the form given in (3).

REFERENCES

[1]-C.Yeh, K.Ha, S.B.Dong, and W.B.Brown," Single mode optical waveguides," Appl. Opt., vol. 18, pp.1490-1504, May 1979.
[2]-M.Ikeuchi, H.Sawami, and H.Niki," Analysis of open-type dielectric waveguides by the finite-element iterative method," IEEE Trans. Microwave Theory Tech., vol. MTT-29, pp.234-239, Mar. 1981.
[3]-N.Mabaya, P.E.Lagasse, and P.Vandenbulcke," Finite element analysis of optical waveguides," IEEE Trans. Microwave Theory Tech., vol. MTT-29, pp.600-605, June 1981.
[4]-B.M.A.Rahman and J.B.Davies," Finite-element solution of integrated optical waveguides," Journal of Lightwave Tech., vol. LT-2, pp.682-688, Oct. 1984.
[5]-M.Koshiba, K.Hayata, and M.Suzuki," Improved finite-element formulation in terms of the magnetic field vector for dielectric waveguides," IEEE Trans. Microwave Theory Tech., vol. MTT-33, pp.227-233, Mar. 1985.
[6]-B.M.A.Rahman and J.B.Davies," Penalty function improvement of waveguide solution by finite elements," IEEE Trans. Microwave Theory Tech., vol. MTT-32, pp. 922-928, Aug. 1984.
[7]-K.Hayata, M.Koshiba, M.Eguchi, and M.Suzuki," Vectorial finite-element method without any spurious solutions for dielectric waveguiding problems using transverse magnetic-field component," IEEE Trans. Microwave Theory Tech., vol. MTT-34, pp. 1120-1124, Nov. 1986.
[8]-T.Angkaew, M.Matsuhara, and N.Kumagai," Finite-element analysis of waveguide modes: a novel approach that eliminates spurious modes," IEEE Trans. Microwave Theory Tech., vol. MTT-35, pp. 117-123, Feb. 1987.
[9]-S.H.Talisa and D.M.Bolle," Fundamental considerations in millimeter and near-millimeter component design employing magnetoplasmons," IEEE Trans. Microwave Theory Tech., vol. MTT-29, pp. 916-923, Sept. 1981.
[10]-S.H.Talisa and D.M.Bolle," Performance predictions for isolators and differential phase shifters for the near-millimeter wave ranges," IEEE Trans. Microwave Theory Tech., vol. MTT-29, pp. 1338-1343, Dec. 1981.
[11]-N.Mohsenian, T.J.Delph, and D.M.Bolle," Analysis of waveguiding structures employing surface magnetoplasmons by the finite-element method," IEEE Trans. Microwave Theory Tech., vol. MTT-35, pp. 464-468, April 1987.

Lehigh University

College of Engineering and Applied Science

Packard Laboratory 19
Bethlehem, Pennsylvania 18015
Telephone (215) 758-4601

October 26, 1989

Jagdish Chandra
Acting Director
Electronics Division
U. S. Army Research Office
P. O. Box 12211
Research Triangle Park
North Carolina 27709-2211

Dear Dr. Chandra:

Attached, per your recent request are 20 copies of the semi-annual report on the ARO grant (DAAG29-85-K-0081).

Should there be any questions, please do not hesitate to get in touch with me at the above address.

Sincerely,

Richard Decker

D. Richard Decker

'm
Attachment
cc: James W. Mink

ARMY RESEARCH OFFICE

The next semi-annual report of progress on your ARO-supported research project, covering the period through 30 June, will be due by the end of the following month. A form is enclosed for your use in the preparation of this report. TWENTY COPIES ARE REQUIRED.

Please include in this report any substantive contact with Army laboratory personnel, such as visits in either direction, letters and phone calls, You may also be aware of potential technological applications of the research results. If so, please indicate them as part of this report.

A copy of the abstract of each manuscript submitted for publication during this reporting period should be attached and made a part of the progress report. The body of the report should not exceed two pages. Brevity and informality should prevail; no distribution of this report is made outside of the Army, and it is simply intended to provide the sponsoring agency with a general awareness of the direction and extent of progress.

Please be sure that a copy of each manuscript submitted for publication is sent to ARO at the same time.

SECOND NOTICE

Jagdish Chandra

JAGDISH CHANDRA
Acting Director
Electronics Division

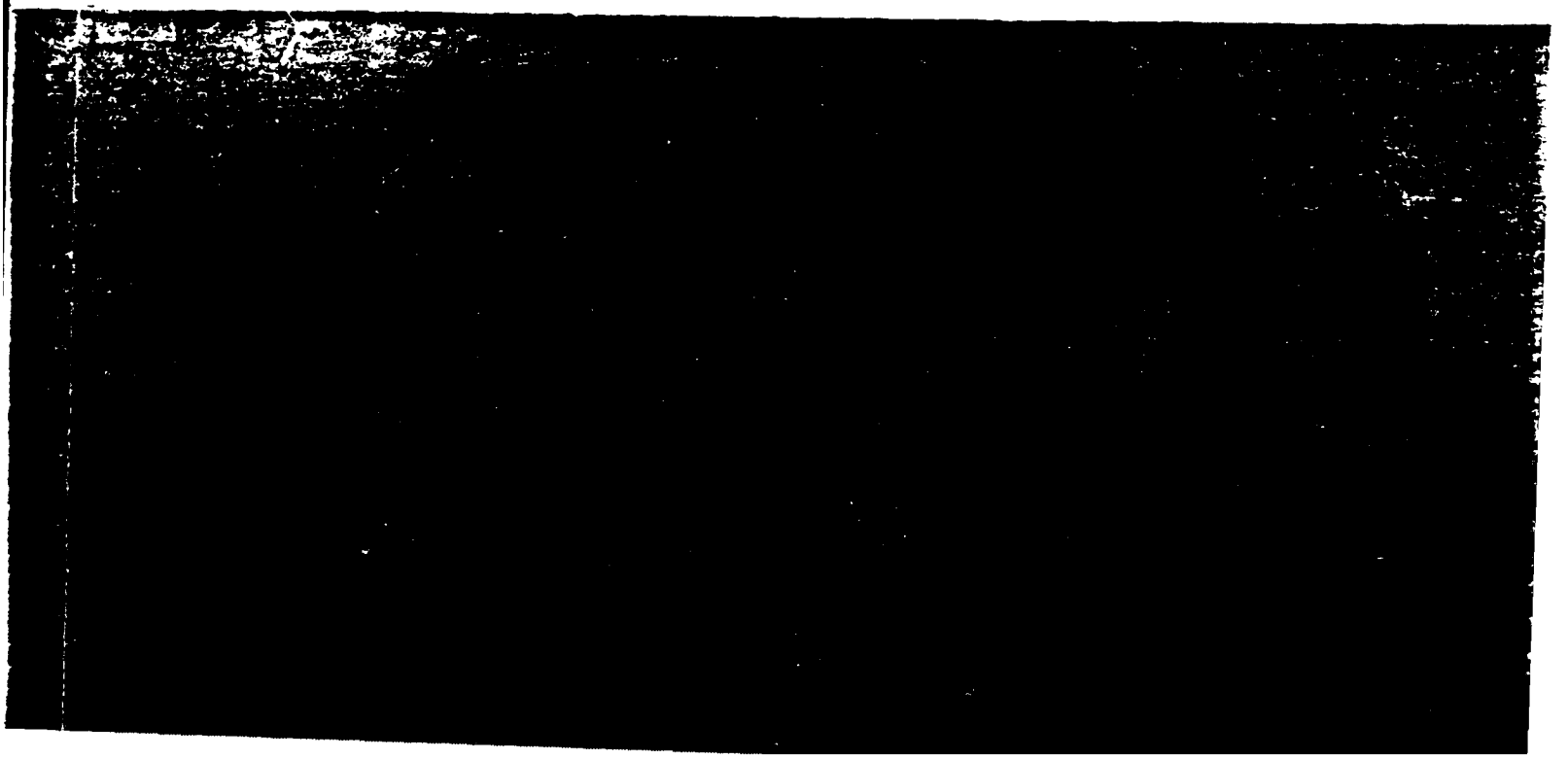

PROGRESS REPORT

TWENTY COPIES REQUIRED

1. ARO PROPOSAL NUMBER: 21125-EL

2. PERIOD COVERED BY REPORT: 1 January 1989 - 30 June 1989

3. TITLE OF PROPOSAL: Non Reciprocal Components in the 140 & 220 GHz Bands Utilizing Magento-Plasmons on Semiconducting Substrates

4. CONTRACT OR GRANT NUMBER: DAAG29-85-K-0081

5. NAME OF INSTITUTION: Lehigh University

6. AUTHORS OF REPORT: D. Richard Decker

7. LIST OF MANUSCRIPTS SUBMITTED OR PUBLISHED UNDER ARO SPONSORSHIP DURING THIS REPORTING PERIOD, INCLUDING JOURNAL REFERENCES:

"Analysis of Waveguiding Structures Employing Surface Magnetoplasmons by the Finite Element Method", submitted to IEEE Trans. Microwave Theory Tech.

8. SCIENTIFIC PERSONNEL SUPPORTED BY THIS PROJECT AND DEGREES AWARDED DURING THIS REPORTING PERIOD:

C. J. Wei
Department of Computer Science and Electrical Engineering
Lehigh University
Bethlehem, PA 18015

D. R. Decker
Department of Computer Science and Electrical Engineering
Lehigh University
Bethlehem, PA 18015

Research Report

For the Period : Jan.10 to Aug.31, 1989

'Magneto-plasma in Semiconductors at 120-170GHz Band'

Theoretical and Experimental studies on Surface Plasmon and Magneto-plasmon Modes in Semiconductors

C.J.Wei, and D.R.Decker

CSEE Dept., Packard Lab.19, Lehigh University,
Bethlehem, PA 18015

Sept.23,1989

THEORETICAL AND EXPERIMENTAL STUDY OF SURFACE PLASMON AND MAGNETOPLASMON MODES IN SEMICONDUCTORS

C.J.Wei, and D.R.Decker,

CSEE Department, Packard Lab.19, Lehigh University, Bethlehem, PA 18015

This report briefly presents the results of investigations on surface plasmons and surface magneto-plasmons on surface of a semi-infinite semiconductor or slab of material, either a uniform bulk medium or a medium with 2-dimentional(2DEG) carrier gas at the surface. The work is a continuation of the project carried out by previous investigators, Prof.Bolle and T. Hwang. The intentions of this report are twofold. First, we extend the theoretical study of surface plasmon modes and magnetoplasmon modes to the case of various magnetic-field-to-surface-direction configurations and the case taking into account the interaction of surface plasmons with a 2D electron gas (2DEG) of a semiconductor near the submillimeter band. It represents our efforts on exploration of novel 2DEG non-reciprocal devices at near-millimeter bands, where the frequency is too low to be useful in a conventional bulk semiconductor in comparison with the carrier relaxation rate even in the case where it is cooled down to 77 K. The mobility of a 2DEG in GaAs-AlGaAs heterostructures with moderate carrier density has been achieved up to $5x10^5$ cm^2/Vsec at 77 K and 4 million cm^2/Vsec at 4.2K in contrast to about $5x10^4$ cm^2/Vsec at 77 K and $2x10^5$ cm^2/Vsec for pure bulk GaAs material. While intensive carrier relaxation in bulk material causes heavy loss of rf power which severely limits the usefulness of the plasma effects in real applications, the superior mobility properties of 2DEG layers, as an alternative, may be promising for this purpose. Secondly, we extend the study of magnetoplasmons for various relative orientations of the field, wavevector and surface to investigations of the field-dependence of dispersion properties. So far, attention has mainly been restricted to the so-called Voigt geometry, in which k is at right angles to H_o, and H_o is in the surface plane. Finally we present a new approach to the excitation of surface plasmons. Surface plasmon is featured with its sensitivity to the variation of surface conditions, since the confinement of electro-magnetic waves at the surface is considerably improved to the conventional bulk or slab modes. Any EM wave devices using 2DEG surface plasmons depend on an intensive interaction of EM wave with surface 2D carriers. We'll examine the requirements on material parameters and xitation conditions in order to realize surface plasmon modes with higher confinment factors. A simple yet effective new approach for excitation of the surface plasmon mode and a method to detect the modes existing in the semiconductor waveguide are proposed.

This paper is divided into four parts. First we give a survey of surface plasmons in semiconductors. Secondly we describe magneto-plasmons for various field orientation configurations and give the conditions for exisistence of surface magneto-plasmons. Thirdly, we propose a new approach for excitation of surface modes. A detection technique using space-harmonic analysis is given. Experimental results are presented. Finally we draw some conclusions.

1. SPACE SURFACE PLASMON MODES IN A SEMICONDUCTOR SLAB WITH OR WITHOUT 2DEG

A detailed study of surface plasmons in a homogeneous semiconductor has been given by Bolle et al and R.F.Wallies [1, 2]. M.Nakayama presented an elementary treatment of surface polaritons and plasmons for the case of surface charge sheet conductance, typically, caused by a 2DEG located at the interface of the semiconductor and surrounding dielectrics. Here we directly quote their results without going into the details.

1.1 Effective conductivity of a bulk semiconductor and surface conductivity of a 2DEG

The Drude expression of effective conductivity of a bulk semiconductor at high frequency reads as

$$\sigma = \frac{q^2 N_d}{m_e} * \frac{1}{(j\omega + \nu_m)} = \sigma_p \qquad (1)$$

where ν_m is the momentum relaxation rate and so ω_p , the plasma frequency is expressed by:

$$\omega_p^2 = (q^2 N_d / \epsilon_o m_e) \qquad (2)$$

The term $j\omega$ accounts for the carrier inertial effect and in derivation of the expression, energy relaxation has been neglected and the semiconductor is assumed to be isotropic and uniform. The effective dielectric consstant is therefore expressed by

$$\epsilon_{eff} = \epsilon_r \epsilon_o + \sigma / j\omega \qquad (3)$$

For a 2D carrier gas there is also a similar expression for the surface conductivity corresponding to the charge sheet conduction in the interface. If we replace the carrier concentration N_d with surface carrier density N_s in cm^{-2}.

1.2 Dispersion equation for a slab of semiconductor with 2DEG on the surface

The dispersion equation for a slab of semiconductor surrounded on both sides by identical dielectrics with surface conductivity σ_s on the upper surfaces is found by solving Maxwell's

equations and matching the boundary conditions on the surface. The dispersion relation for TM Modes can be obtained from the following simultaneous transcedental equations.

$$\frac{(\epsilon_{eff}/\alpha_1+\epsilon_o/\alpha_o)(\epsilon_{eff}/\alpha_1+\epsilon_o/\alpha_o-\sigma_s/j\omega)}{(\epsilon_{eff}/\alpha_1-\epsilon_o/\alpha_o)(\epsilon_{eff}/\alpha_1-\epsilon_o/\alpha_o+\sigma_s/j\omega)}=\exp(-2\alpha_1 L) \tag{4}$$

$$\alpha_1^2= k^2-\epsilon_{eff}\omega^2/C^2 \tag{5}$$

$$\alpha_o^2=k^2-\epsilon_o\omega^2/C^2 \tag{6}$$

where the parameters α_1 and α_o represent the transverse attenuation factor respectively in the slab and the surrounding dielectrics. For a guided slab mode, α_1 is required to be imaginary while α_o is real. To obtain surface mode both α_1 and α_o are required to be real. L is the thickness of the slab. The dispersion equations are also available and will not be given here since they have less utility for nonreciprocal devices.

When $Re(\alpha_1 L)>>1$ the dispersion is reduced to that corresponding to the single inteface case.

$$\epsilon_{eff}/\alpha_1+\epsilon_o/\alpha_o=0 \qquad \text{for the surface mode at the bottom surface} \tag{7}$$

$$\epsilon_{eff}/\alpha_1+\epsilon_o/\alpha_o=\sigma_s/jw \qquad \text{for the surface mode at the upper surface} \tag{8}$$

The first expression gives the normal surface plasmon for a single interface of a bulk semiconductor. The second one is the surface conduction supported plasmon mode also for the case of a single interface.

On the other hand, the expression reduces to that of the conventional slab mode for dielectric waveguide, when the surface conduction vanishes $\sigma_s=0$.

The solution of the dispersion equations can be obtained for various modes, namely slab modes and surface modes for different material parameters. In order to satisfy the requirement of lower loss with a view toward applications, higher mobility 0f 50,000 $cm^2/Vsec$ is assumed throughout the calculations. First the solution for slab modes shows the attenuation of EM waves is practically independent of the surface conduction and decreases with frequency and bulk carrier concentration. These results can be understood since the EM energy is distributed over the slab and the interaction with surface carriers is therefore very weak. The decrease of loss with frequency is expected because of the reduced effect of relaxation. Figure 1(a) and (b) gives the effects of N_d on the dispersion relation-propogation factor β and attenuation factor α versus frequency , from which the loss increase with increasing N_d is apparent. Figures 2 and 3

give the dispersion relations for a conventional surface mode supported by bulk carrier conduction. We are interested particularly in the condition of greater localization of EM waves on the surface, namely a greater confinement factor. From expressions (5) and (6), it is readily seen that the greater localization can be only realized when both α_1 and α_0 are large, or the propogation constant β must much higher than β_0. In the case of vanishing carrier relaxation this condition is readily satisfied at surface plasmon resonance, $\omega_s = \omega_p/(1+\epsilon_r^{-1})$, where β approaches to infinity. However with carrier relaxation taken into account, the condition is only partly satisfied when the bulk carrier concentration is chosen in a marginal range . With higher carrier concentration, the EM energy spreads over the surrounding dielectric and penetrates into the slab a skin depth. In this case, the confinement is poor and the surface plasmon velocity approaches that of light in vacuum, very similar to the surface mode in metal. The material with too low carrier concentration can obviously not support a surface mode. The range of carrier concentrations to give higher confinment is estimated about 2.5--5 $10^{14}/cm^3$ at frequency of 120-170GHz.

On the other hand, the 2DEG supported surface plasmon modes have the feature of greater confinement and stronger interaction with the surface carriers. Figures 4(a) and (b) give the calculated results of a 2DEG supported surface mode verses N_s.. Again mobility of 50,000 $cm^2/Vsec$ is assumed. The propogation constant β is much higher than β_0 and the attenuation increases with N_s. Fig.5 plots the dispersion and attenuation vs. frequency for the same parameters. The higher attenuation represents a stronger interaction of the surface mode with surface carriers. However the loss can be expected to be greatly reduced if mobiiity is taken to be higher than $10^6 cm^2/Vsec$. Moreover, higher gain can be obtained when the 2DEG posesses a gain mechnism, as proposed elswhere by the authors [4].

The critical requirements on the material parameters, namely the carrier concentration and mobility, however, present limitations on the usefulness of surface plasmon modes and experimental difficulties at the near millimeter bands.We will discuss this point later.

2. SPACE MAGNETOPLASMON MODES IN A SEMICONDUCTOR SLAB, SURFACE MODES OF A SEMI-INFINITE MEDIUM

(1). Dielectric susceptibility tensor of a semiconductor

The plasma properties of a bulk semiconductor in the presence of DC magnetic field are characterized by a dielectric susceptibility tensor ϵ_{eff}, and we assume that the bulk susceptibility characterises the entire specimen up to the surface. The ϵ_{eff} tensor is derived from the carrier equations govering the carrier movement which is subject to a Lorentz force

$$F_m = q (v \times B) \qquad (9)$$

and is given by

$$\epsilon_{eff} = \epsilon_r \, I + 1/j\omega \, \sigma \tag{10}$$

where σ is the conductivity tensor of the bulk semiconductor which has a gyroelectric form given by

$$\sigma = \begin{bmatrix} \sigma_t & j\sigma_h & 0 \\ -j\sigma_h & \sigma_t & 0 \\ 0 & 0 & \sigma_p \end{bmatrix} \tag{11}$$

$$\sigma_t = \omega_p^2 (j\omega + \nu_m) / ((j\omega + \nu_m)^2 + \omega_c^2) \tag{12}$$

$$\sigma_h = \omega_p^2 j\omega_c / ((j\omega + \nu_m)^2 + \omega_c^2) \tag{13}$$

$$\sigma_p = \omega_p^2 / (j\omega + \nu_m) \tag{14}$$

where the magnetic field is assumed to be in the z-direction and the specimen is otherwise isotopic. The ω_c is the cyclotron resonance frequency and is given by $\omega_c = q B / m_e^*$.

For the case of a 2DEG system the surface conductivity is characterized by a 2D-tensor in the plane of the interface when the magnetic field is normal to the surface and the normal component of the conductivity vanishes due to confinement of the surface carrier movement. When the magnetic field is parallel to the surface the tensor becomes diagonal one.

The susceptibility tensor is diagonized in the rotating-wave coordinate system, $e_+ = e_x + j\, e_y$ and $e_- = e_x - j\, e_y$ with the diagonal components of $\sigma_+ = \sigma_t + \sigma_h$ and $\sigma_- = \sigma_t - \sigma_h$. In this case an incident, linearly polarized EM wave undergoes a rotation of polarization with distance, which is called the Faraday effect and the corresponding modes are called Helicon modes.

(2). Dispersion equation in an infinite and homogeneous medium

The discussion of magneto-plasmon modes in bulk or layered media is a matter of solving Maxwell's equations with boundary conditions when the medium is specified by the susceptibility tensor. Interest is not restricted to geometries in which surfaces are present; even the solutions in a bulk medium are of some complexity [5].

Maxiwell's equations, when the susceptibility tensor is incoorporated , are written as

$$\text{curl } (E) = - j\omega \, B \tag{15}$$

$$\text{curl } (H) = j\omega \, \epsilon_{eff} E \tag{16}$$

$$\text{div } (D) = \rho \qquad D = \epsilon_r \epsilon_o E \tag{17}$$

$$\text{div } (B) = 0 \qquad B = \mu_o H \tag{18}$$

Combining the equations we have:

$$\text{curl}\ (\ \text{curl}\ E) - \beta_o^2 \epsilon_{eff} E = 0 \qquad (19)$$

where $\beta_o^2 = \omega^2 / c^2$. Note that $\epsilon_{eff} E$ is tensor product. Substitution of $H \infty \exp(j\omega t - j\ kr)$ leads, eventually, to the dispersion equation ω versus k.

$$\det |\ (k_i k_j - \delta_{ij} k^2) + \beta_o^2 \epsilon_{eff}| = 0 \qquad (20)$$

For various orientation of the DC magnetic field with respect to the wavevector the solutions differ from each other. For the case that the magnetic field is perpendicular to the wavevector we have

$$k^2 - \beta_o^2 \epsilon_e = 0 \qquad (21)$$

and $\epsilon_e = \epsilon_t - \sigma_h^2 / \epsilon_t$ is the effective dielectric constant, where $\epsilon_t = \epsilon_r \epsilon_o + \sigma_t / j\omega$.

For a real device design, layered structures on a semiconductor substrates are both more practical and preferable. The loss in the bulk semiconductor is reduced due to the smaller volume of bulk material in layered structures. In this way, it is necessary to acquire strong interaction between the EM wave and the layered structure or a wave guided along the interface is required. In what follows we discuss the magneto-plasmon modes in the simplest layered structures: magneto-plasmon in a slab and semiinfinite semiconductors.

(3). Magnetoplasmons in Voigt Configuration

In the Voigt configuration, H_o is at right angles to the wavevector k and is in the plane of the interface of layered structures. This is the most useful geometry for design of non-reciprocal devices. We discuss the simplest layered structure: a slab of thickness d surrounded - by air dielectric as shown in fig.6. We are only interested in TH modes and the TE modes are of no concern since nonreciprocity occurs only if the electric field is partially circular-polarized with respect to the DC magnetic field. The solution of Maxwell's equations is obtained by setting the boundary conditions at the interface and at infinity. The fields vanish at infinity and the boundary conditions at the interface are continuity of the tangential componets of E and discontinuity tangential H set by the surface conduction as follows:

$$E_{1x} = E_{2x} \quad \text{and} \quad H_{1z} - H_{2z} = -\ i_x = \sigma^s_t E_x \qquad (22)$$

where TH modes are under consideration and propogation is in the x direction and y is the normal direction to the surfaces and $\sigma^s{}_t$ is the surface transverse conductivity of the 2DEG. For TH modes we have only the field components: H_z, E_x and E_y. Note that the E_x component is related to H_z by

$$\epsilon_t E_x + j\sigma_h E_y = \frac{\partial H_z}{\partial y} \tag{23}$$

Assuming that the wave in the medium has the form of $\exp(j\omega t - j\beta x + \alpha_1 y)$, we have, eventually, the solution of the dispertion relation:

$$\frac{(-\alpha_1/\epsilon_e + \beta\sigma_h/(\epsilon_t{}^2-\sigma_h{}^2) - \alpha_o/(\epsilon_o*\delta))(\alpha_1/\epsilon_e + \beta\sigma_h/(\epsilon_t{}^2-\sigma_h{}^2) + \alpha_o/\epsilon_o)}{(-\alpha_1/\epsilon_e + \beta\sigma_h/(\epsilon_t{}^2-\sigma_h{}^2) + \alpha_o/\epsilon_o)(\alpha_1/\epsilon_e + \beta\sigma_h/(\epsilon_t{}^2-\sigma_h{}^2) - \alpha_o/(\epsilon_o*\delta))}$$

$$= \exp(-2\alpha_1 d) \tag{24}$$

where

$$\delta = (1 - \sigma^s{}_t * \alpha_o/\epsilon_o) \tag{25}$$

The dispersion relation can be obtained by simultaneously solving the dispertion equations in the bulk medium and surrounding region:

$$\alpha_1{}^2 = \beta^2 - \beta_o{}^2(\epsilon_t - \sigma_h{}^2/\epsilon_t) \tag{26}$$

$$\alpha_o{}^2 = \beta^2 - \beta_o{}^2 \tag{27}$$

The algebraic problems involved in a theoretical discussion of various magnetoplasmon modes on a slab are fairly severe. Even for a semi-infinite medium, for which the thickness $d \to \infty$ and the exponetial term is zero, the solution requires considerable numerical effort. Note that when the surface conduction is zero, there is no non-reciprocity in expr.(16) which can be verified by reversing the sign of β, resulting in no change of the expression. This is because a slab structure is actually a symmetric configuration and the waves propogating in the reverse direction see no difference from the forward direction. However, when we discuss the surface magneto-plasmon mode in a semi-infinite medium we do have nonreciprocity, since it is no longer a symmetric structure. Moreover, the properties of the surface magneto-plasmons in a slab of semiconductor can be approximately described by those on the surface of a semi-infinite medium. It is expected that the drawbacks of a conventional surface plasmon mode, namely the higher loss and shallow penetration of energy into the semiconductor, can be partially

removed, since the effects of carrier relaxation are overshadowed by the cyclotron resonance effects of the carriers provided that the magnetic field is sufficient high so that $\omega_c >> \nu_m$.

Fig.7(a) and (b) show the calculated results of propogation constant Re(β) and loss Im(β) as a function of external magnetc field for a surface magneto-plasmon mode on the surface of an infinite medium. The two curves correspond to different propogation directions. The difference of the curves shows the nonreprocity of the wave propogation. The frequency is fixed at f_o=150GHz and the material is GaAs with doping level of $10^{15}cm^{-3}$ and mobility of 5,000 cm^2/Vsec. It is seen that the propagation phase velocity is almost constant, but the loss is reduced considerably in one direction for H_o>6 kG. In the reverse direction, the loss varies to a lesser extent and there is a maximum loss at H_o=1.35 Tesla. When the mobility of the material becomes higher, to 50,000 cm^2/Vsec, namely, the carrier relaxation has less effect. and cyclotron resonance can be expected. The calculation results are plotted in fig.8(a) and (b). There exists very strong narrow resonance in one direction around H_o=9kG, which is considered the cyclotron resonance. However other broader resonances in both directions appear as well. These peaks are not identified and they may be the collision induced loss peaks. The great difference of propagation properties, either in loss or in phase velocity, can be utilized to the best for design of non-reprocical devices. However, cooling is necessary in order to acquire the high mobility or the lower relaxation effects. Fig.9(a) and (b) show the dispersion relations of surface magneto-plasmons for H_o=0.5Tesla, and material parameters as above in fig.7(a) and (b). Again cyclotron resonance at f=220 GHz in one direction is clearly seen, where the loss in the other direction is minimum. There are other peaks at lower frequency, which are assumed to be induced by carrier relaxation. The cyclotron resonance occurs in the direction whereby the rotation of the ellipsoidly rotated electric field is synchronously resonant with the Lorentz force. This is only possible for one particular direction.

Approximate explicit expressions can be obtained for the parameters in the regiem of high carrier density , $\omega_p^2/\omega\nu_m >> 1$ so that the following term is approximately equal to

$$\sigma_h\beta/(\epsilon_t^2 - \sigma_h^2) \; -\beta\omega\omega_c/\omega_p^2 \qquad (28)$$

The choice of the plasma frequency should be appropriately low on the other hand so that the confinement of EM energy is not greatly reduced to maintain adequate interaction with the carriers in the medium. We discuss two extreme cases, i.e., the case of complete confinement at the surface, and the case of the low frequency limit. For the complete confinement of EM waves at the surface, the propagation constant β approaches infinity and so do the transverse constants α_o and α_1, so that we have $\alpha_o=\alpha_1=\beta$. In this case, the surface magneto-plasmon

frequency is given by:

$$\omega_{sh} = \left(\frac{\omega_c + j\nu_m}{2}\right) + \left[\left(\frac{\omega_c + j\nu_m}{2}\right)^2 - \epsilon_r \omega_p^2\right]^{1/2} \qquad (29)$$

where the upper sign and the lower sign coorespond to different propogation directions. The imaginary part of ω_{sh} represents the attenuation of the surface mode with time. For exiistance of a surface magneto-plasmon mode in a relatively long time scale, the necessary condition is $\nu_m << \omega_c$.

For the low frequency regime, the propagation velocities for both directions are close to that in vacuum to the first order of approximation. The second order of modification gives the propagation constants as:

$$\beta = \beta_o + \frac{\beta_o \omega}{4\omega_p^2}\left[\left(\omega_c/\omega_p\right)^2 \omega + \left(2\nu_m \omega\right)^{1/2} \frac{\omega_c}{\omega_p}\right) + j\left(\nu_m + \left(2\nu_m \omega\right)^{1/2} \omega_c/\omega_p\right] \qquad (30)$$

where the upper sign and the lower sign again represent the results for two different propagation direction. It is shown that the non-reciprocity lies primarily in the direction-dependence of the loss. The physical origin of the nonreprocal loss behavior is that the partially circularly-polarized electric field in one direction is an active Helicon-like mode, whereas in the other direction it is a passive anti-helicon-like mode. It is worthwhile to point out that a greater nonreciprocal property can be achieved only for a material such as GaAs with moderate doping level and higher magnetic field so that the surface EM waves can penetrate a considerably larger portion of the volume of the slab specimen and under the conditions that the cyclotron frequency exceeds the carrier relaxation rate. For higher carrier density, the field energy of surface EM waves is further from the semiconductor in the vacuum, rendering a vanishingly small non-reciprocal effect.

Now we briefly discuss the surface magneto-plasmon modes supported by surface conduction. For the sake of simplicity, we assume that the semiconductor has very high resistivity and the dielectric constant is ϵ_r. In this case the volume loss of the modes is practically zero. The surface conductivity may originate from 2DEG sheet conduction and is in the form of a 2-dimensinal diagonal tensor. The dispersion equations for the surface modes in a semiinfinite specimen are given by

$$\epsilon_o/\alpha_o + \epsilon_r/\alpha_1 - \sigma^s{}_t/\, j\omega = 0 \qquad (31)$$

$$\alpha_o{}^2 = \beta^2 - \beta_o{}^2 \qquad (32)$$

$$\alpha_1{}^2 = \beta^2 - \beta_o{}^2 \epsilon_r \qquad (33)$$

and $\sigma^s{}_t = \omega_{ps}{}^2(j\omega+\nu^s)/[c\, j\omega((j\omega+\nu^s)^2+\omega^s{}_c)]$ (34)

is the transverse sheet conductivity of the 2DEG, where $\omega_{ps} = q^2N_s/(\epsilon_o m^{*s})$ and $\omega^s{}_c = qB/m^{*s}$ is the surface cyclotron frequency. The super index 's' indicates the parameter of the 2DEG. In comparison with eq.(8) we conclude that the dispersion relations of a magneto plasmon mode are similar to those of a normal surface mode without magnetic field. However, the effective relaxation rate and the effective frequency are modified as:

$$\nu^s{}_{eff} = \nu^s - \omega_p{}^2\nu^s/(\omega^2+\nu^s)^2 \quad (35)$$

$$\omega_{eff} = \omega + \omega_p{}^2\omega/(\omega^2+\nu^s)^2 \quad (36)$$

respectively. Therefore it is expected that the loss is a decreasing function of the magnetic field.

(4) Magneto-plasmon modes for the case of magnetic field normal to the surface

Other orientations of magnetic field with respeect to the propogation and surface than Voigt's are also of interest. Unfortunately, little attention has been paid to a general solution taking into full account the arbitrary orientation of the magnetic field probably because of the formidable algebraic work. We are not going to do this job either but, instead, analyze a special case, namely the case that the magnetic field is normal to the surface.

The magneto-plasmon modes in the configuration with normal magnetic field may be separated into TH and TE modes. However, for a mixed TE and TH mode the field components are related to each other through the antidiagonal tensor elements to an extent depending on the relative value of their field components. For the TH modes, the electric field is in the plane with DC magnetic field and the current componets are diagonalized with respect to the electric field. Therefore, the boundary conditions give rise to the same dispersion equation as eq.(4), in which the ϵ_{eff} is replaced with ϵ_t. However, the dispersion equation related to the α_1 and β in the semiconductor must be derived from epr.(20) whereby the k vector is $\mathbf{k} = \beta x + j\alpha_1 z$:

$$(\alpha_1{}^2 - \beta^2+\beta_o{}^2\epsilon_t)(\alpha_1{}^2\epsilon_p - \beta^2\epsilon_t + \beta_o{}^2\epsilon_p\epsilon_t) + (\beta^2 - \beta_o{}^2\epsilon_p)\beta_o{}^2\sigma_h{}^2 = 0 \quad (37)$$

The dispersion relation can be obtained by simultaneously solving (37). (32) and modified (4) .

Again, the surface modes are of concern and their behavior can be described by the solution in the limit of thickness approaching to infinity, namely the case of a semi-infinite medium.

Figures 10 and 11 collect the calculated results of propagation constant and loss as a function of cyclotron frequency or magnetic field. The parameters are taken as before, i.e., $N_d = 10^{15}cm^{-3}$ and mobility μ=5000 cm^2/Vs. It is shown that the phase velocity does not change with magnetic field and is practically constant. There are two modes which have different loss characteristics. One mode shows a decreasing loss behavior with magnetic field, while the loss of the other mode has a maximum at a certain field. There is no non-reciprocity effect for this configuration since the magnetic field normal to the surface has the same symmetry geometries for both directions. The field- dependence of the loss is stronger than in the case of the Voigt configuration (compare these figures to fig. 7).

The intrinsic frequency of surface magneto-plasmons for this configuration is defined when the propogation constant $\beta \rightarrow \infty$, leading to the condition of:

$$\epsilon_p(\omega)\, \epsilon_t(\omega) = 1 \tag{38}$$

For the high frequency and high field limit, the intrinsic magneto-plasmon frequency is given by:

$$\omega_{mp}^2 = \omega_p \frac{\epsilon_r + (\omega_p/\omega_c)^2}{\epsilon_r - 1 + \epsilon_r(\omega_p/\omega_c)^2} \tag{40}$$

The dispertion relations for this configuration with a 2DEG on the sample surface are more tedious and the modes can no longer be separated into TH and TE modes. We will not go into the details here. M.Nakayama has given a formular for the surface modes existing on the interface and for the semiconductor treated as a simple dielectric with ϵ_r [3].

3. EXPERIMENTS AND RESULTS

(1) Excitation Methods of Surface Plasmon Modes

The excitation of surface plasmon modes has been well-studied on metal surface at optical or infrared bands. No progresses has been reported, however, on surface plasmons in a semiconductor at millimeter or near-millimeter bands. This is probably since the relaxation rate at these bands in semiconductors is comparable or even much higher than the frequency so that the surface modes are either damped very fast and they can only exist in a very short spatial range (for moderate carrier density), or approach a conventional surface EM wave mode with small energy penetration into the sample up to a skin depth (for high carrier density). It appears that the surface mode at the intrinsic frequency, the most interesting situation, can hardly exist due to the heavy loss. Moreover, the very short wavelength near

this frequency presents a difficult task of excitation.

The previous investigators utilized quasi-optical excitation methods--prism coupling and grating coupling and the results were not encouraging. Actually, the band of 110-170 GHz is well above the submillimeter bands where the EM waves have little optical ray attributes. The lower end of the EM spectrum features strong diffraction effects, especially when one uses a horn antenna as an excitation source. The diffraction causes large stray coupling to the detector, so that the signal of the surface mode, in most cases, is immersed in it and can hardly be identified. While the excitation by grating is intrinsicly narrow-banded, the prism coupling would require a prohibitively large volume of semiconductor specimen and becomes unpractical. We, therefore, envisaged experiments using conventional microwave excitation methods, namely, edge excitation and grating waveguide excitation.

The experimental schemes for the exitation are shown in figures 12 and 13. For edge excitation, the signal is coupled at the edge end of a dielectric waveguide to the slab of sample. Quartz is used to construct a slab waveguide which is coupled to a horn antenna. The quatz waveguide is placed in the horn normal to the E plane so that only TH modes are excited and so are appropriate for the semiconductor waveguide. The features of edge excitation are simplicity and broad-band response. However, other radiation modes can also be excited via the air. For our configurations, three kinds of modes may be generated, i.e., two are waveguide modes, slab modes and surface modes, the others are radiation modes. To identify the modes, special interference techniques are necessary.

The second excitation method is to use a grating waveguide. This method can eliminate the stray modes and preserve the desired mode by appropriately choosing the grating space and letting it be equal to a half-wavelength of the desired mode. However, this has the drawback of narrow band performance. The narrow band performance requires precise fabrication of the waveguide to reduce the insertion loss. Fig.14 shows the insertion loss of a grating waveguide versus frequency. The waveguide consists of a slab semiconductor in the middle that is surrounded by two symmetric gratings at a short distance from the surfaces. Parallel metal plates are placed beyond the grating with a tapered end in contact with the semiconductor to reduce the stray radiation to the detection horn. The spacing of the grating is 1.4mm, which cooresponds to a half-wavelength of the slab mode of 0.35mm thick semiconductor at f=150 GHz. It is shown that there are two peaks of transmission close to each other. The specular transmission behavior may be caused by misalignment of the grating waveguide, since the waveguide was hand-made. At any rate, narrow transmission behavior is clearly demonstrated.

(2) Space harmonics technique for detection plasmon modes in semiconductors

A Space harmonic technique is envisaged for detection and analysis of the modes existing on

the surface of the slab sample. Assume that there are several modes at the signal frequency with different wavelengths propagating along the slab as an incident signal:

$$V_{in} = a_1 e^{-i\beta_1 x+\theta_1} + a_2 e^{-i\beta_2 x+\theta_2} + \ldots\ldots \quad (41)$$

where x is the distance from the end, a total reflection occurs when a short circuit is placed on the end of the slab waveguide and the reflectedsignal is:

$$V_{ref} = a_1 e^{i\beta_1 x+\theta_1+\pi/2} + a_2 e^{i\beta_2 x+\theta_2+\pi/2} + \ldots\ldots \quad (42)$$

The mixing of the incident waves and reflected waves produces a standing waveform and a Fourier transform calculation of the waveform yields a modal space-spectrum. The produced mixed space harmonics include $2\beta_1$, $2\beta_2$ which are conventional standing waves and, in addition, the mixture of $\beta_1+\beta_2$, $\beta_1-\beta_2$. The beat mixture signal can be identified since it can be produced even when there is no reflection. However, a clear identification requires careful study to separate the basic space harmonics from others. Fortunately, in most case the mixture of different modes is sufficiently weak and the basic space harmonic can be easily recognized. This proposed technique has the features of simplicity in measurement and analysis and does not require more complex set-up as in interference methods.

Fig. 15 thorgh 17 show typical measured standing-wave patterns along the surface of the semiconductor slabs for different carrier densities. The measurement scheme is shown in fig.18. The plasmon modes in the semiconductor slab were excited either with the edge method or with the grating waveguide method. The field strength near the surface was detected by another screened quartz dielectric waveguide and through a horn the signal was fed to the crystal detector. An EH tuner was placed between the source and the feeding quartz waveguide to achieve maximum transmission or matching. As the coupling of the detection head to the different modes are not the same, the measured patterns can only serve as an overall view of the possible modes and hardly can be said to indicate the relative intensities of the modes. To be specific, the coupling to the slab mode is much weaker than to the surface mode since the fied of surface mode is extended further into the air while its wavelength is close to that in air in this frequency range (110-170GHz). Having measured the standing-wave pattern, the Fourier analysis was readily made to produce the space harmonic pattern as shown in fig.19 to 20 respectively transformed from fig.15 to 17. Many other curves have been measured and analyzed for different cases and we add some of the results shown in fig.21 though 24.

Our measurements have revealed several modes along the slab waveguides, as shown in

fig.15 though 24. In fig.15 is shown the detected field distribution along a slab of a lower doped semiconductor. In its Fourier transform spectrum shown in fig.19, the dominant mode has approximately an air wavelength and is less attenuated with distance. This mode is supposed to be the surface mode. We have measured the breakdown voltage of a Schottky contact using a tungsten-probe contact to estimate the doping concentration of the specimen. The approximate doping level is $3x10^{15}cm^{-3}$ and this level is sufficient to support the surface plasmon mode. The calculation shows that the surface plasmon mode at 120 to 170 GHz band has a wavelength almost equal to that in vacuum. On the other hand, the measurements on a slab semiconductor of higher doping (see fig.16 and 17) reveal two or three modes, one being the surface mode of about vacuum wavelength, the others having shorter wavelengths as shown in fig.18. The shorter waves appear near to the short end of the slab and attenuate quickly with distance. To identify these modes we again measured the field distribution with an absorber placed on the other side of the slab. Then, the standing waves of shorter wavelength disappeared and only the surface mode remains, as shown in fig.17 and its space-harmonic diagram, fig.21. Since only the slab bulk modes have fields that penetrate onto the other side and the surface mode has very shallow penetration depth into the sample, it is believed that the space-harmonics of shorter wavelength are slab modes. However, it is not yet understood why the slab modes can survive over such a long distance since our theoretical calculations indicate that the slab modes for such a high doping material should suffer heavy loss. Probably, the slab modes are excited just at the short end. Care must be taken on eliminating the interference of radiation modes, especially because those with wavelength are close to that of the surface mode. In our experiments, we used screening for the excitation edge and also for the detection edge of the dielectric-waveguide and only a small slit was exposed for receiving the rf-energy.

In order to investigate the modes excited in the grating waveguide, we made an extension of the semiconductor slab into the air for about 1.5" and the extended part of the slab was used for measurements. If a slab mode was excited by the grating, its propagation along the slab could be detected. Fig.25 shows the detected field distribution at this extended slab and again two modes are revealed, one mode having an air wavelength and the other having a wavelength approximately equal to the grating spacing. However, the mode of shorter wavelength appears at the beginning of the extension part and decays with distance, while the mode of longer wavelength seems to be growing with distance. One reasonable explanation could be that the test frequency is not correct for the wavelength of the slab mode to coincide with the grating spacing and therefore the slab mode changes into a surface mode with distance.

Although these results are still preliminary, the proposed space harmonic technique has

demostrated great potential in detection and identification of multimodes and investigation of their interaction in an open waveguide system.

(3) Experiments on Magnetic-Field-Dependence of the Transmission for Slab Waveguide

We have carried out experiments of the magnetic field effects on transmission for a variety of configurations using semiconductor slab waveguide or conventional waveguide containing semiconductor slab. The magnetic field was varied, with current ranging in 0 to 24A, from 0 to 6kG for the magnet-spacing of 25mm and from 0 to 12kG when the spacing was reduced to 10mm. The experiments were performed at room temperature and in the 120-170 GHz band. The non-reciprocity was tested by reversing the magnetic field, since this is equivalent to the reversal of propagation direction.

For a slab waveguide, the experiments indicate that there is practically no direction-dependence of transmission, either for the magnetic field normal to the surface or for the Voigt configuration. The results are within our expectations, since the slab mode is symmetric with respect to the magnetic field and a reversal of propagation direction sees no change in the relation of the field to the geometry and the propagation. The field dependence of transmision is shown in fig.27 and 28 respectively for the Voigt configuration and the geometry in which the magnetic field is normal to the surface. For the Voigt configuration, the transmission is reduced by about 5% for H up to 6kG. For the magnetic field normal to the surface, the field-dependence is stronger than the Voigt configuration. In fig.28, the parameter is frequency and it is shown that the transmission may increase or decrease at different frequencies. It is difficult to make comparison with theoretical calculations, since the slab mode is not well-matched. For a mismatched circuit there are waves propagating in both direction. Besides the propagation loss is a function of the field, and a change of matching can result in variation of the total transmission.

In order to realize non-reciprocity of the slab mode in the Voigt configuration, we can use either non-symmetric excitation, in which a one-sided mode, such as a surface mode would be launched, or intentionally place some absorber near one side of the surface. In the latter case, the absorption of the waves will obviously be dependent on the direction, since the magnetic field , in one direction, pulls the EM field away from the slab, resulting in more absorption, while it doesn't in the another direction. Non-reciprocity of the transmission is shown in fig.29. The sample under test has a doping concentration of $3 \times 10^{15} cm^{-3}$ and is 0.35mm thick and $15 \times 20 mm^2$ width by length.

For real non-reciprocal devices it is not a good idea to utilize open slab waveguide since it presents problems of radiation loss and matching difficulty. Instead, conventional waveguide structures containing semiconductor sample are more preferable. To develop such waveguide

nonreciprocal devices requires more theoretical calculations in the framework of two dimensional waveguide and more precise mechnical work to realize them. This is beyond the scope of the present work. However, we have made some primitive experiments to observe the transmission performance for a specific waveguide structure. The semiconductor wafer was first grinded down to 150μm in thickness and was cleaved into dimensions of about 0.7mm by 8mm or 1mm by 8mm. The specimen was placed in a square waveguide off the center axis either in the E plane or with a tilted angle about 70^{o} to the E plane against the narrow wall. The magnetic field is applied in the H plane. The transmission vs. magnetic field for a given frequency (f=145GHz) is shown respectively in figs.30 and 31. For the geometry of the sample in the E-plane, a dramatic increase of the transmission in one direction at H=4.3 kG and when the magnetic is reversed is shown to have pronounced non-reciprocity. Geometric resonance at a particular magnetic field may be responsible for the abrupt increase. The magnetic-field-dependence of transmission for the sample with geometry tilted off the E plane also shows the non-reciprocity characteristics but with no abrupt change with H. Other configurations of sample-waveguide relative placement were tested as well. In particular, no nonreprocity was found when the sample, which was of the dimension 1.5X8 mm^2, was placed on the H plane and against the broad wall of the waveguide.

4. CONCLUSIONS

We have presented theoretical calculations of behavior of surface plasmon modes and magnetic-plasmon modes in semiconductors. The calculation was extended to the case where the semiconductor had a heterolayer of 2DEG on the surface. Carrier relaxation was taken into account in the calculations. It is shown that the surface mode for a conventional semiconductor slab has no intrinsic surface resonance frequency when the carrier relaxation is taken into account and the phase velocity is close to the c_o for the low frequency limit. On the other hand the surface mode supported by surface conduction, such as in the case of 2DEG, has more surface wave properties, i.e., lower phase velocity and more field concentration on the surface. however, heavier loss is anticipated. Theoretical studies of magnetic-plasmon in semiconductors were done for the Voigt geometry and for the case of the magnetic field perpendicular to the surface. It is indicated that there are non-reciprocal properties of transmission for the Voigt configuration and stronger magnetic-field dependence of the transmission, no non-reciprocity though, occuring in the latter configuration. Experiments were performed to qualitatively compare the results to the theoretical calculation. Finally, we proposed several experimental methods. First we proposed an edge excitation method and a grating waveguide excitation method. The first one provides broad-band excitation and different modes may be simultaneously excited. The grating waveguide method.

on the other hand, is capable of excitation of a single mode, surface mode or slab mode, depending on the grating spacing. However it is narrow banded. Secondly, we proposed a novel mode detection technique, namely the space harmonic technique. The proposed method has the feature of simplicity in experimentation, and is easy to understand and analyze.

During this period of time, a new proposal for future research work was prepared which is not included in this report[4]. The future work is proposed to explore the active wave supported by a semiconductor plasma, in addition to further work to develop non-reciprocal devices. For the latter it is suggested to use a material of higher mobility, including heterostructure semiconductors and InSb , etc.

Acknowledgment

The authors wish to thank Prof.N.E.Eberhardt for his valuable discussion, assistance and sugestion in making the measurements.

Reference

1. D.M.Bolle, S.H.Talisa, IEEE Trans. on Microwave Theory and Technique, "Foundamental Considerations in Millimeter and Near-millimeter Component Design Employing Magneto-Plasmons", MTT-29, (1981), 916-

2. R.F.Wallis, "Introduction to Electromagnetic Surface Waves", Electromagnetic Surface Excitation", Springer-Verlag, Berlin, 1986, pp. 2-7

3. M.Nakayama, "Theory of Surface Waves Coupled to Surface Carriers", J. Phys. Soc. Japan, 36-2 (1974), 393-397

4. C.J.Wei and D.R.Decker, "Near- and Sub-millimeter Wave Control and Generation by Using Plasma Effects in Semiconductors", A proposal and project, Internal report for future project (1989), Lehigh University, Bethlehem

Fig.1. Calculated transmission characteristics of a slab semiconductor. $N_d=10^{14}$, 10^{15}, $10^{16}cm^{-3}$form upper to lower respectively. Mobility is taken to be 50,000 cm^2/Vs. (a).dispersion relation, (b) attenuation vs. frequency.

Fig.2. Surface palsmon mode supported by bulk carrier conduction. The mobility $\mu=50.000cm^2/Vs$. $N_d=10^{15}/cm^3$. (a) dispersion, (b) attenuation.

Fig.3. Surface palsmon mode supported by bulk carrier conduction. The mobility $\mu=50.000cm^2/Vs$. $N_d=10^{18}/cm^3$. (a) dispersion, (b) attenuation.

Fig.4. Calculated surface plasmon mode supported by surface cxonductance. The paramieters are taken: $N_s=10^{12}cm^{-2}$, $\mu=50,000cm^2/Vs$ d=0.4mm. (a) dispersion relations, (b) attenuation vs.frequency.

Fig.5. The calculated transmision at f=150GHz vs. surface carrier density. Mobility $\mu=50.000$ cm^2/Vs. (a) wavenumber, (b) attenuation.

Fig.6. Voiglt configuration

Fig.7. The calculated transmission characteristics vurses magnetic field Ho for a Voigt configuration. $N_d=10^{15}/ cm^3$and $\mu=5,000$ cm^2/Vs. f=150GHz. (a) wavenumber, (b) attenuation. The two curves coorespond to different H_o directions.

Fig.8. The calculated transmission characteristics vurses magnetic field Ho for a Voigt configuration. $N_d=10^{15}/ cm^3$ and $\mu=50.000$ cm^2/Vs. f=150GHz. (a) wavenumber, (b) attenuation. The two curves coorespond to different H_o directions.

Fig.9. The calculated transmission characteristics vurses frequency at $H_o=0.5$ Tesla for a Voigt configuration. $N_d=10^{15}/ cm^3$and $\mu=50,000$ cm^2/Vs. (a) wavenumber, (b) attenuation. The two curves coorespond to different propogation directions.

Fig.10. The calculated transmission characteristics of model 1 vurses cyclotron frequency or magnetic field Ho for a configuration of normal H_o to surface. $N_d=10^{15}/ cm^3$ and $\mu=5,000$ cm^2/Vs. f=150GHz. (a) wavenumber, (b) attenuation. $f_c=q H_o/ (2\pi m^*)$.

Fig.11. The calculated transmission characteristics of model 2 vurses cyclotron frequency or magnetic field Ho for a configuration of normal H_c to surface. $N_d=10^{15}/ cm^3$ and $\mu=5,000$ cm^2/Vs f=150GHz. (a) wavenumber, (b) attenuation. $f_c=q H_o/ (2\pi m^*)$.

Fig.12. Edge excitation of TH slab modes or surfact TH modes and edge detection by the use of dielectric waveguide of quatz.

Fig.13. Schematic structure of grating waveguide which is coupled to a horn anttena and in which a slab semiconductor is placed in the middle and the slab has an extension out of the grating waveguide for testing.

Fig.14. Measured transmission coefficient vs. frequency of the grating waveguide coupled with slab semiconductor. The semiconductor has thickness of 0.35mm and doping level of $3x10^{15}/cm^3$.

Fig.15. The detected field distribution close to the surface of the semiconductor at edge excitation

condition. $N_d=3x10^{15}/cm^3$.

Fig.16. The detected field distribution close to the surface of the semiconductor at edge excitation condition. $N_d=3x10^{17}/cm^3$.

Fig.17. The detected field distribution close to the surface of the semiconductor at edge excitation condition. $N_d=3x10^{17}/cm^3$. An absorber is placed on the other side of the slab.

Fig.18. Fourier transform of the diagram of fig15. and its space harmonic is shown.

Fig.19. Fourier transform of the diagram of fig16. and its space harmonic is shown.

Fig.20. Fourier transform of the diagram of fig17. and its space harmonic is shown.

Fig.21. The detected field distribution close to the surface of the semiconductor at edge excitation condition. $N_d=1x10^{17}/cm^3$.

Fig.22. The detected field distribution close to the surface of the semiconductor at edge excitation condition. $N_d=1x10^{17}/cm^3$. An absorber is placed on the other side of the slab.

Fig.23. Fourier transform of the diagram of fig21. and its space harmonic is shown.

Fig.24. Fourier transform of the diagram of fig22. and its space harmonic is shown.

Fig.25. The detected field distribution close to the surface of the extended part of the semiconductor at grating waveguide excitation condition. $N_d=3x10^{15}/cm^3$. An absorber is placed on the other side of the slab. It is shown that the higher wavnumber mode excited by grating decays with distance,while the amplitude of lower wavenumber grows, showing the higher mode's transfering into surface mode.

Fig.26. Fourier transform of the diagram of fig25. and its space harmonic is shown.

Fig.27. Transmission as a function of magnetic field for a Voigt configuration of the slab. $N_d=3x10^{15}/cm^3$. d=0.4mm.

Fig.28. Transmission as a function of magnetic field for normal H_o configuration of the slab. $N_d=3x10^{15}/cm^3$. d=0.4mm. The curves cooresponde to different test frequency.

Fig.29. Transmission as a function of magnetic field for a Voigt configuration of the slab. $N_d=3x10^{15}/cm^3$. d=0.4mm. An absorber is placed near the slab, which gives rise to non-reciprocity in transmission.

Fig.30. Transmission as a function of magnetic field for the configuration of waveguide containing semiconductor slab in the E-plane displaced from the center of the waveguide. $N_d=3x10^{15}/cm^3$. d=0.15mm. H_o is normal to the slab.

Fig.31. Transmission as a function of magnetic field for the configuration of waveguide containing semiconductor slab 70^0-tilted off the E-plane against the narrower wall of the waveguide. $N_d=3x10^{15}/cm^3$. d=0.15mm. H_o is normal to the slab.

Fig 1 dispersion a) and attennuation b) relations of slab GaAs

Mobility=50000, thickness=0.35mm, Nd=10^14, 15, 16 respec.

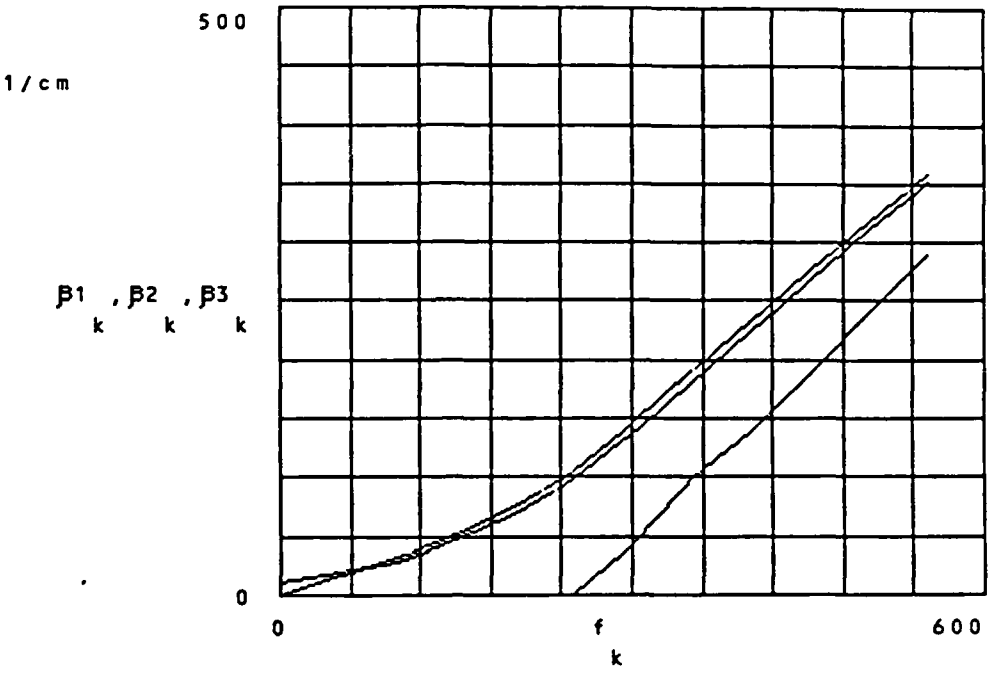

(a)

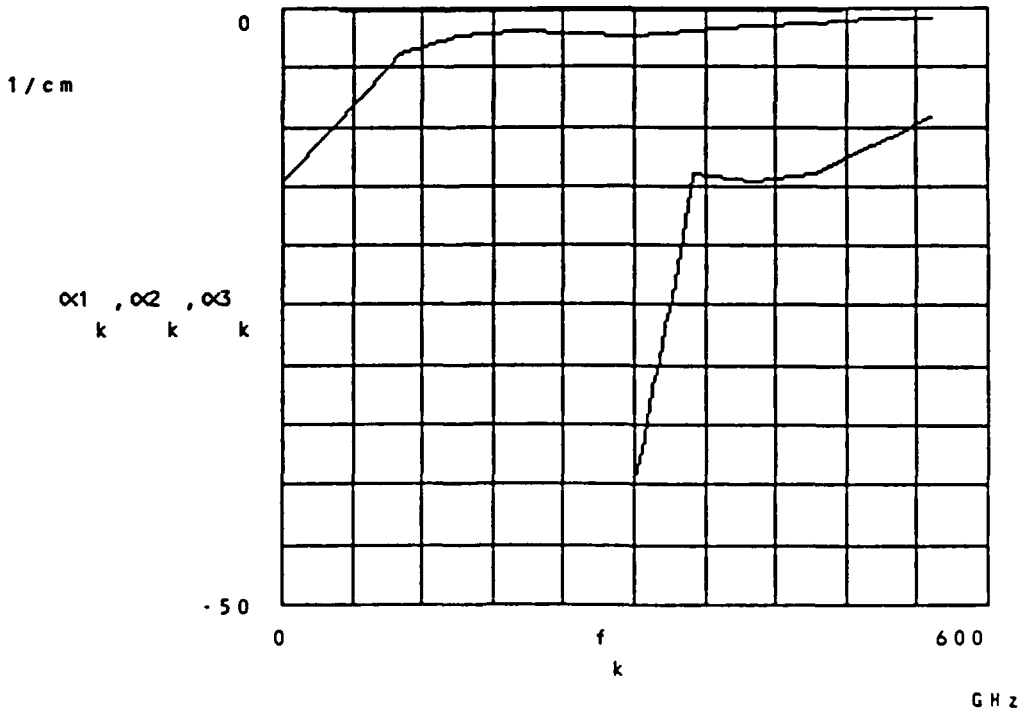

(b)

Fig.2 GaAs slab of 0.35mm,without mobility 50000 and Nd=10^15 cm-3 surfae mode by surface equation

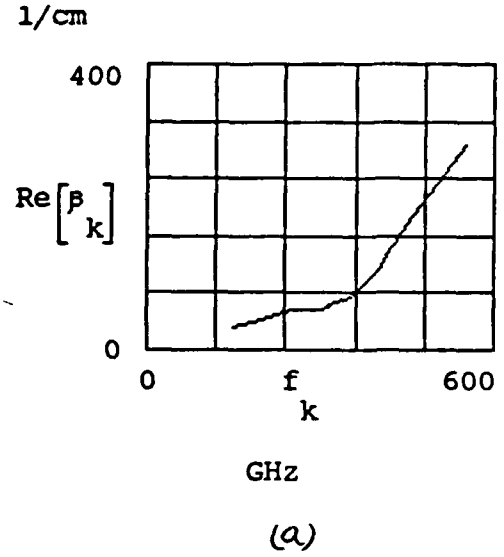

(a)

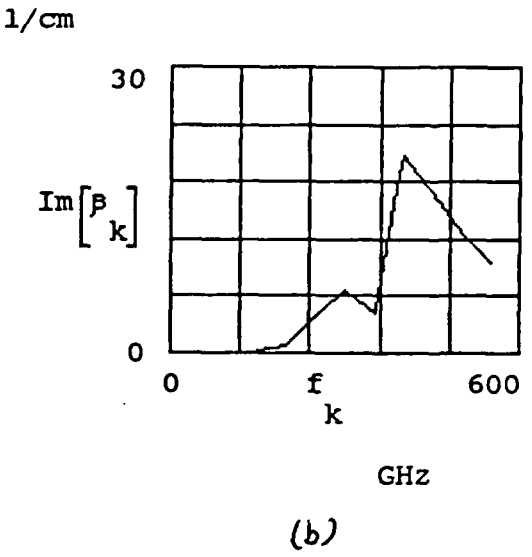

(b)

Fig.3 GaAs slab of 0.35mm,without mobility 25000 and Nd=10^18 cm-3 surfae mode by surface equation

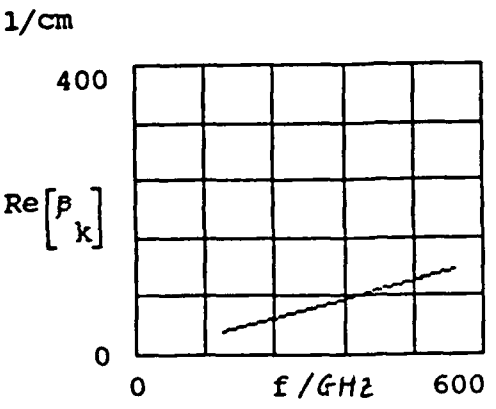

(a)

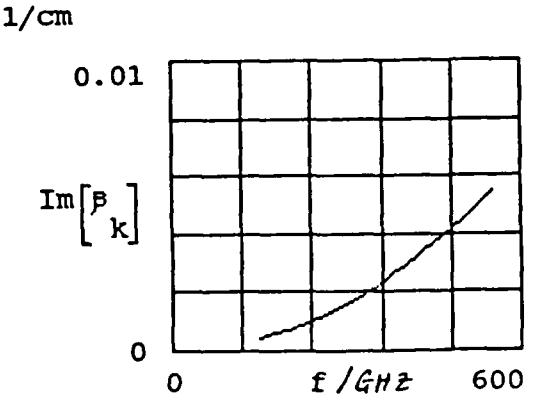

(b)

Fig.4 pure surface plasmon mode, $Ns=10^{12}/cm^3$

slab GaAs with mobility 50000, d=0.4mm, β, ∝ versus frequency

$$f_k := \frac{\omega_k}{6.28} \cdot 300$$

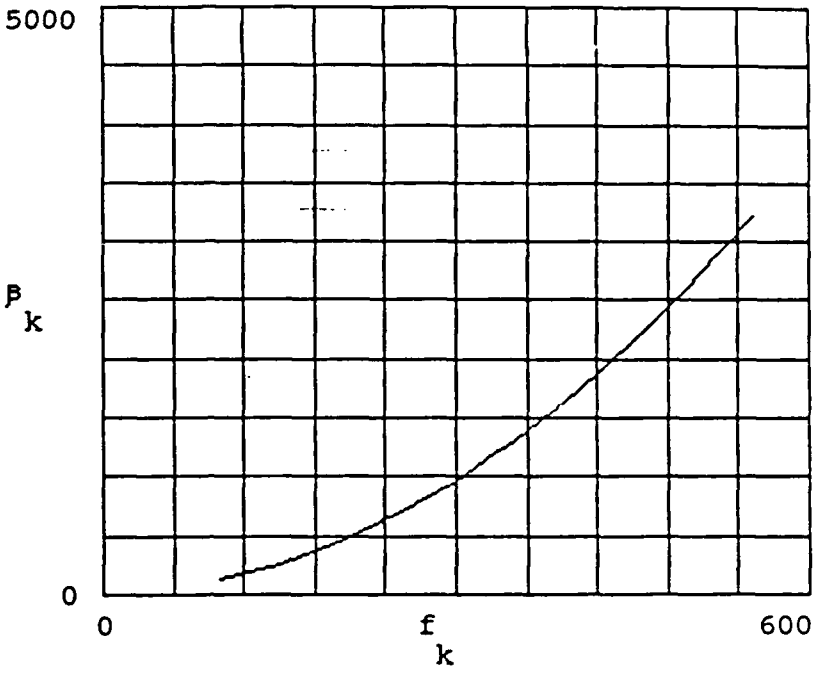

(a)

GHz

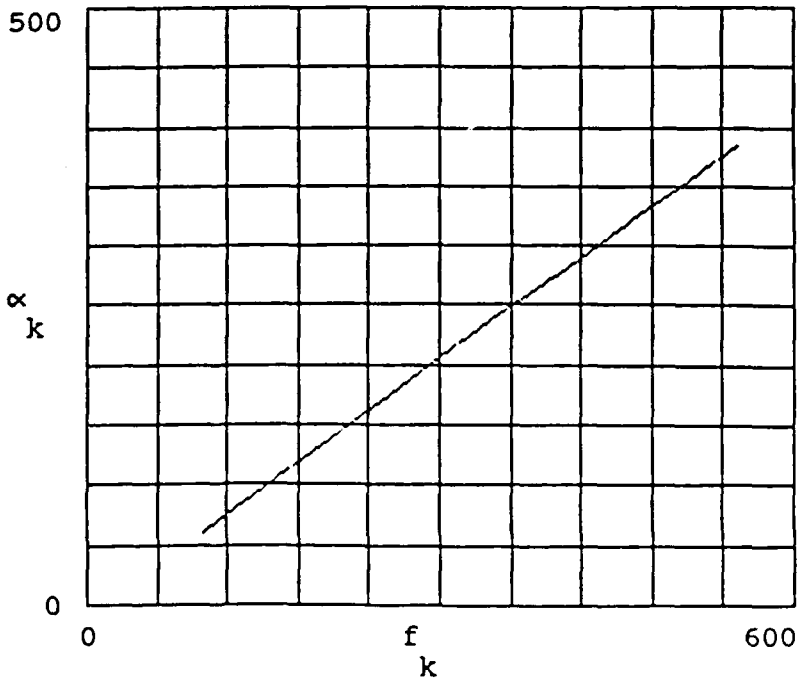

(b)

Fig5. slab GaAs with mobility 150000, d=0.4mm, β, α versus surface carrier density

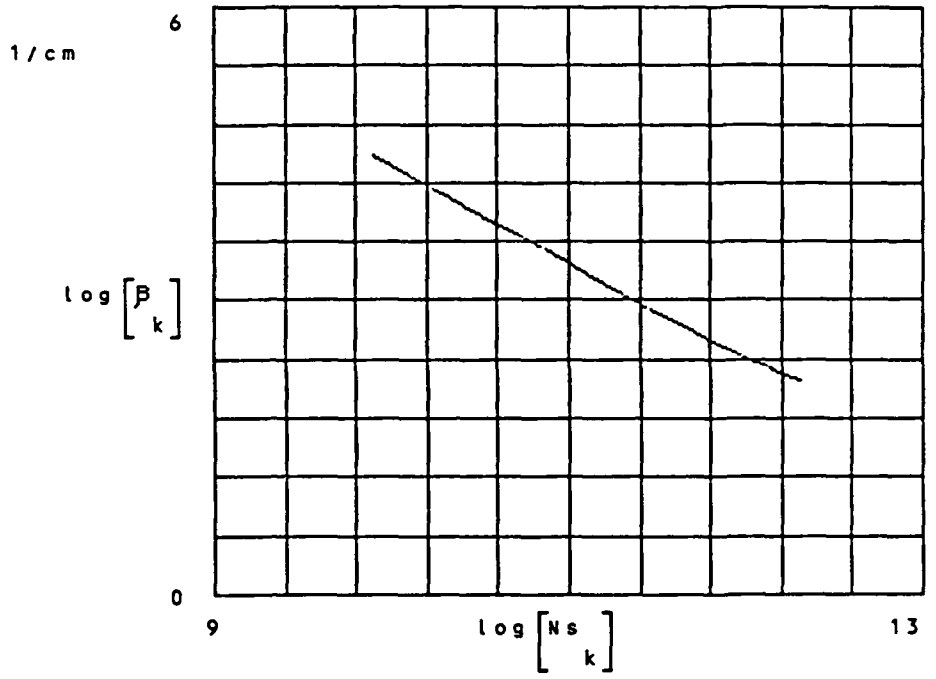

f=150GHz 1/cm3 in log plot

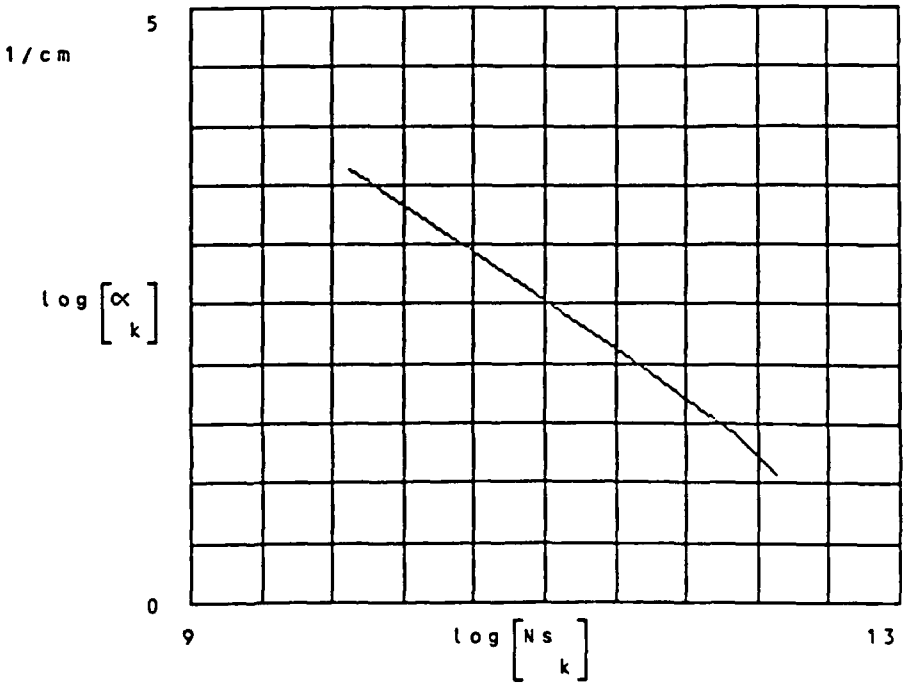

f=150GHz 1/cm3 in log plot

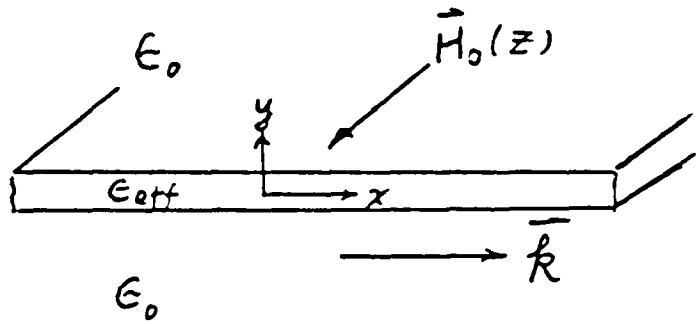

Fig.6. Scheme of a Voiglt configuration

Fig.7. The calculated transmission characteristics vurses magnetic field Ho for a Voigt configuration. $N_d=10^{15}/\ cm^3$. μ=5,000 cm^2/Vs. (a) wavenumber, (b) attenuation. The two curves coorespond to different H_o directions.
$f = 150\ GHz$

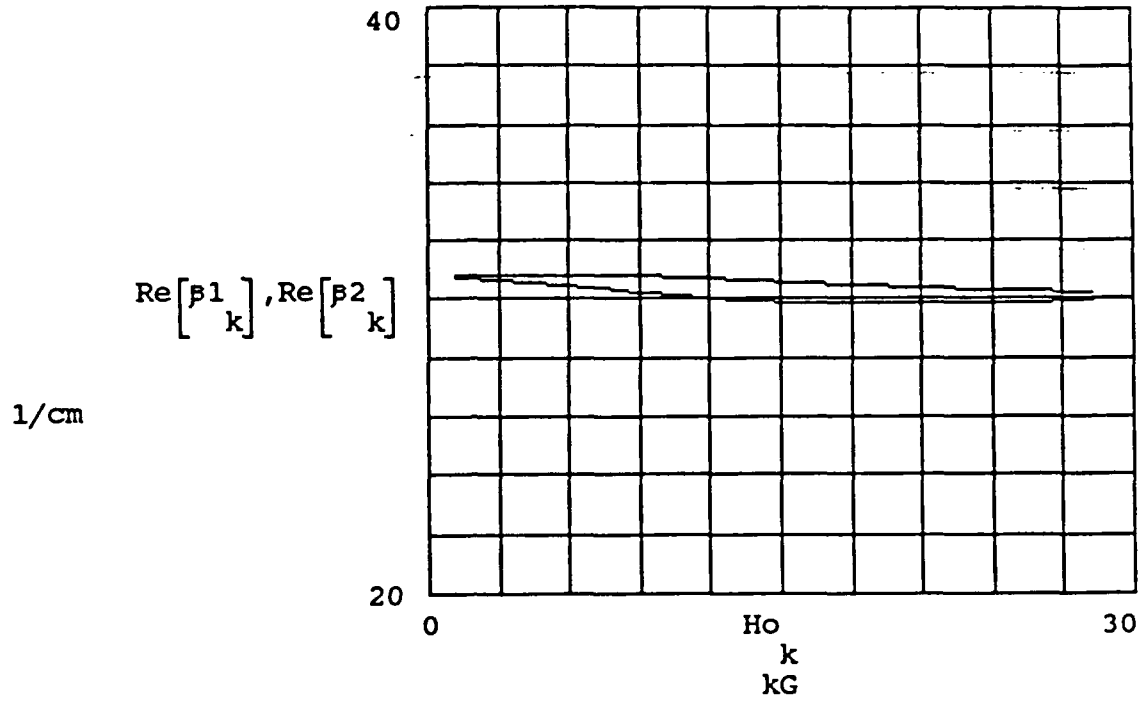

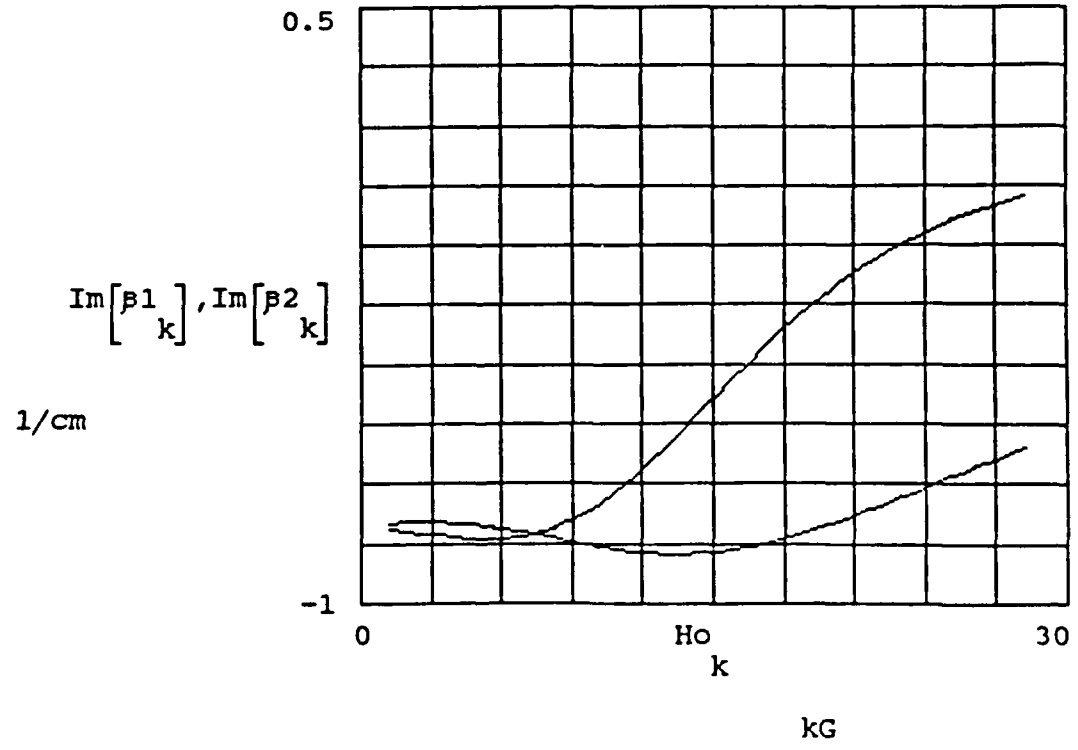

Fig.8. The calculated transmission characteristics vurses magnetic field H_o for a Voigt configuration. $N_d=10^{15}/\ cm^3$. $\mu=50{,}000\ cm^2/Vs$. (a) wavenumber, (b) attenuation. The two curves coorespond to different H_o directions. $f=150GHz$.

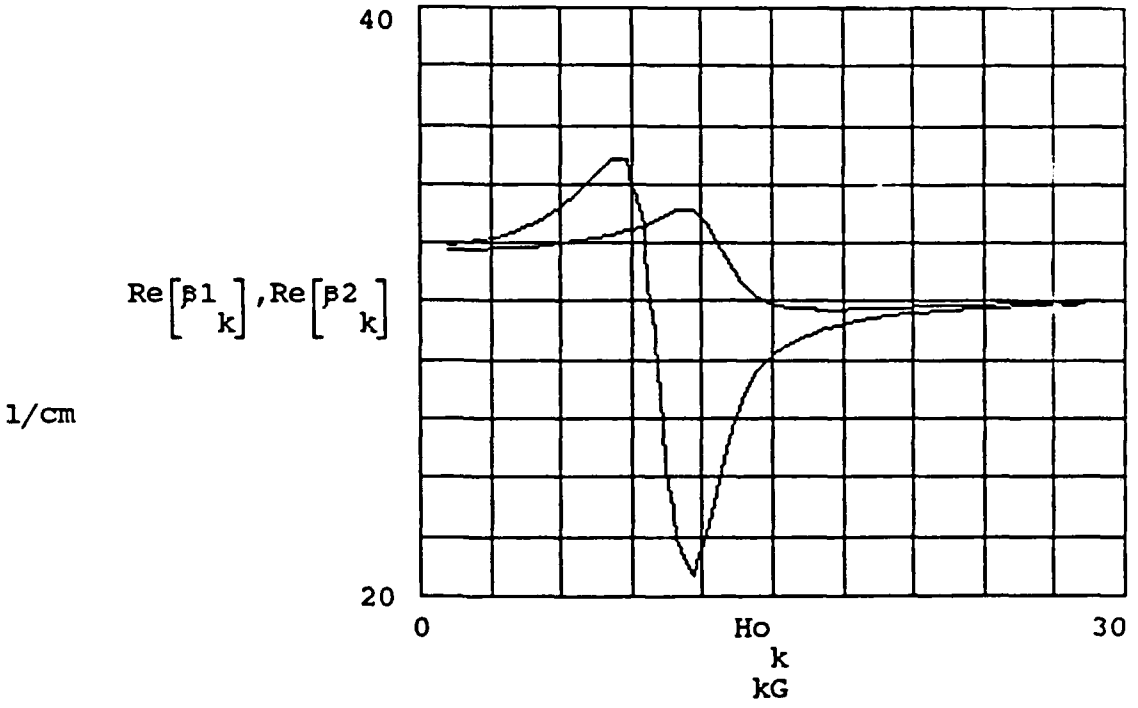

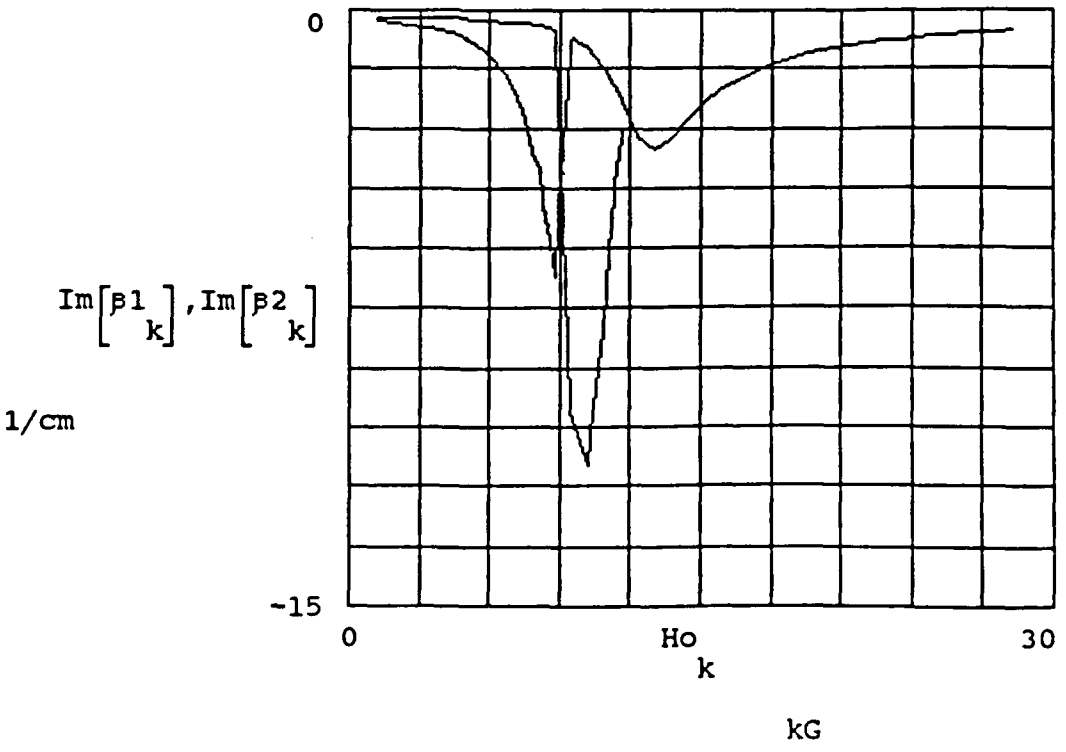

Fig.9. The calculated transmission characteristics vurses frequency at H_o=0.5 Tesla for a Voigt configuration. N_d=10^{15}/ cm^3. μ=50,000 cm^2/Vs. (a) wavenumber. (b) attenuation. The two curves coorespond to different propogation directions.

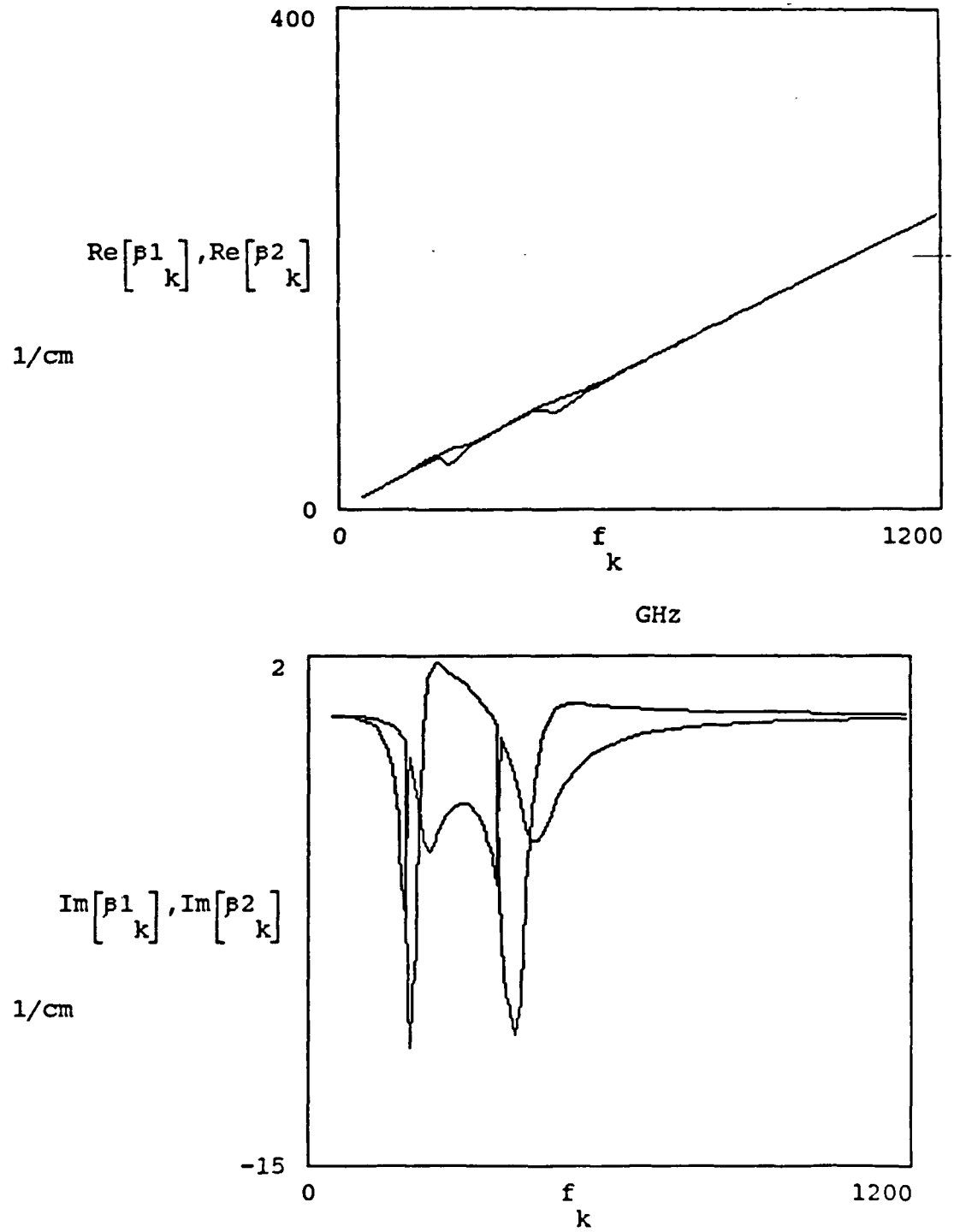

Fig.10. The calculated transmission characteristics of model 1 vurses magnetic field Ho for a configuration of normal H_o to surface. $N_d=10^{15}/\ cm^3$. μ=5,000 cm^2/Vs. (a) wavenumber, (b) attenuation. $f=150GHz$, $\frac{1}{f_c}=\frac{2\pi\varepsilon_0}{\sigma_H}$

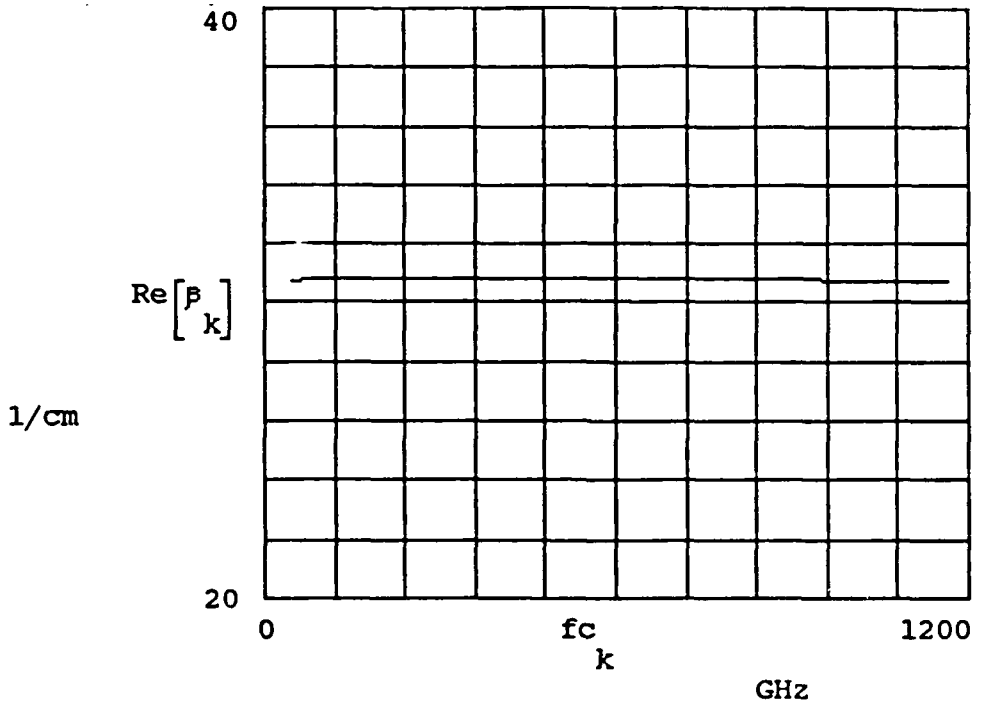

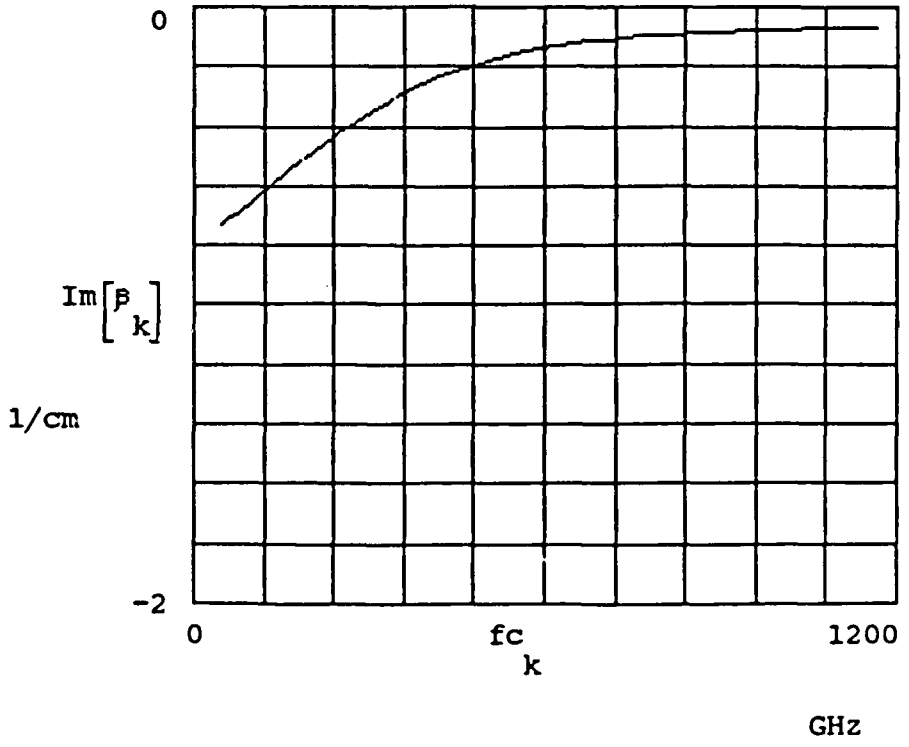

Fig.11. The calculated transmission characteristics of model 2 vurses magnetic field Ho for a configuration of normal H_o to surface. $N_d=10^{15}$/ cm^3. μ=5,000 cm^2/Vs. (a) wavenumber, (b) attenuation. $f = 150\,GHz$, $f_c = \frac{2\mu}{2\pi\sqrt{\mu\varepsilon}}$

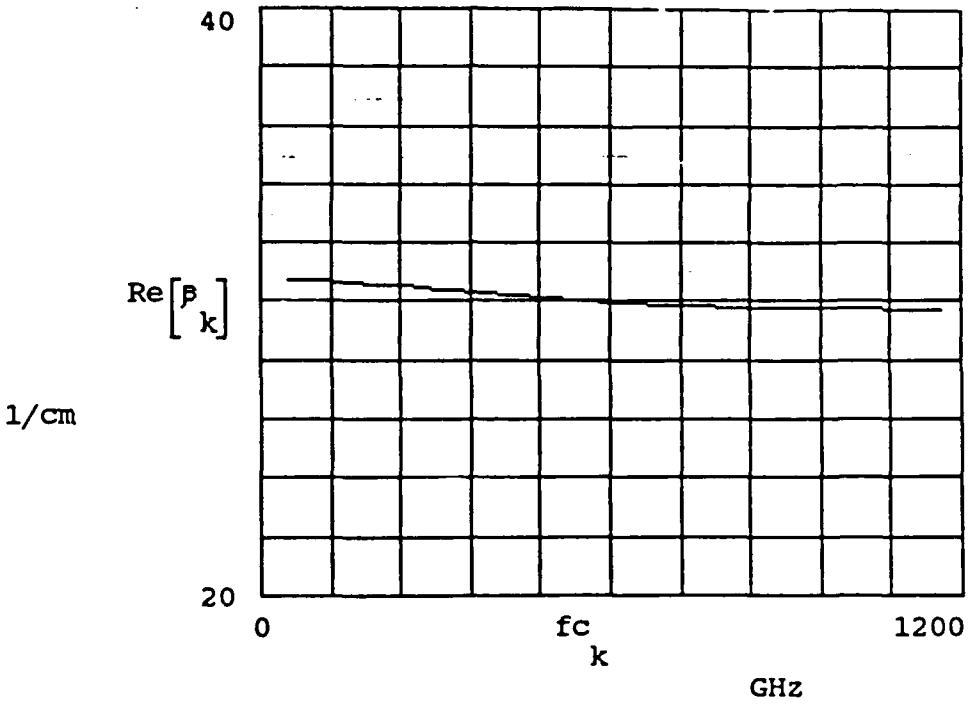

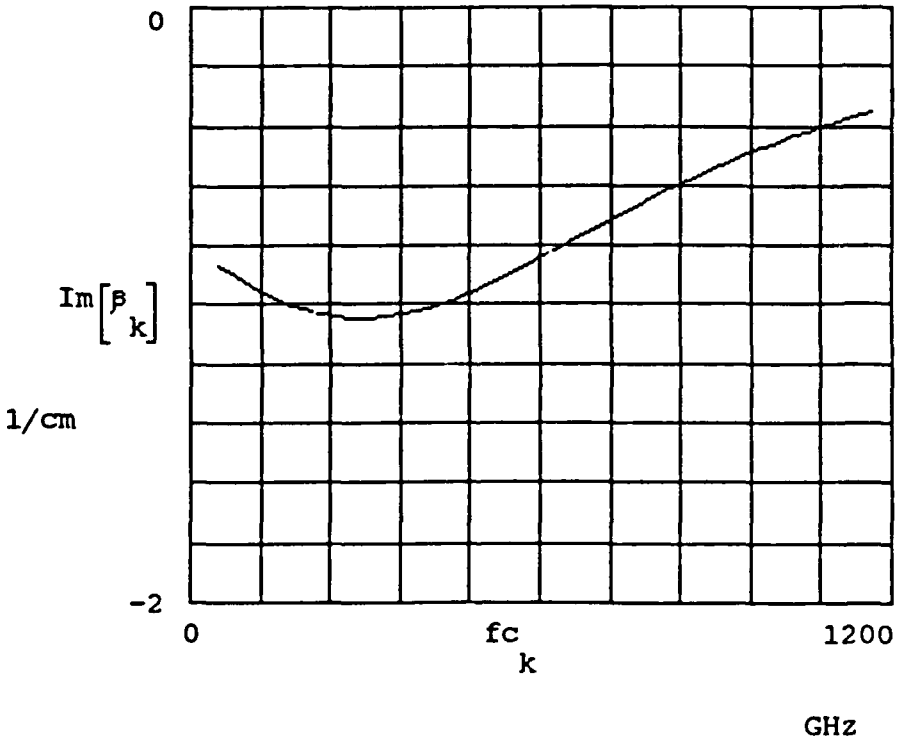

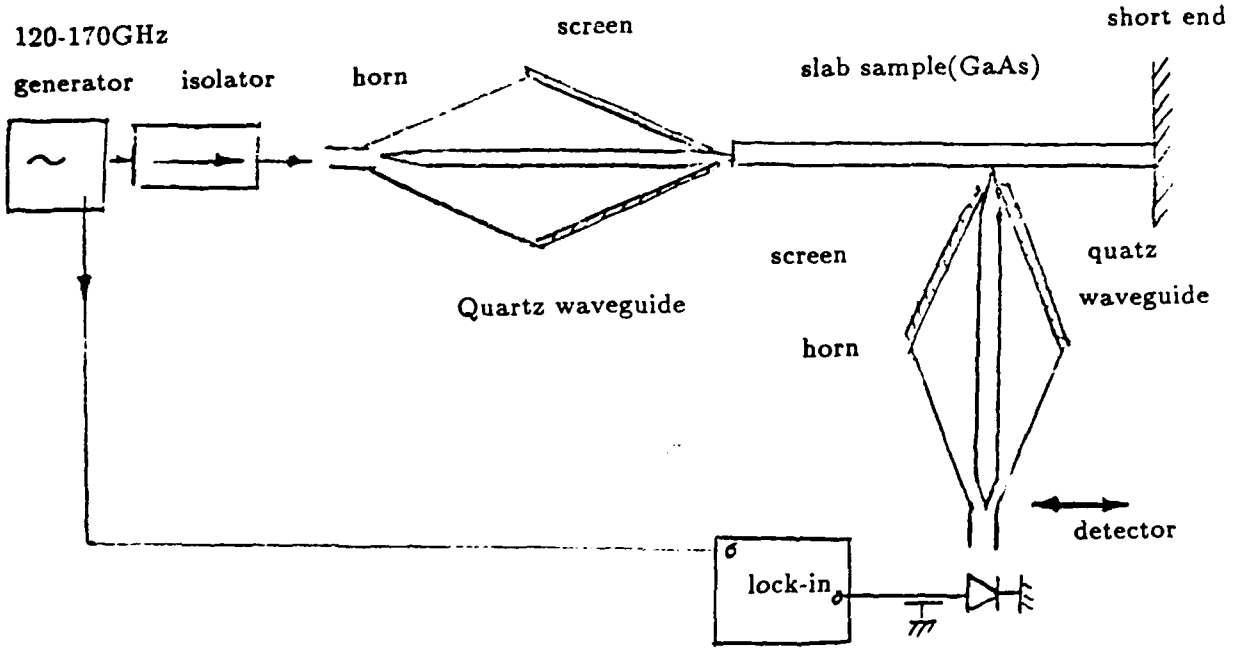

Fig.12 The test configuration for detection of the propogation modes in a slab of semiconductor using standing wave method

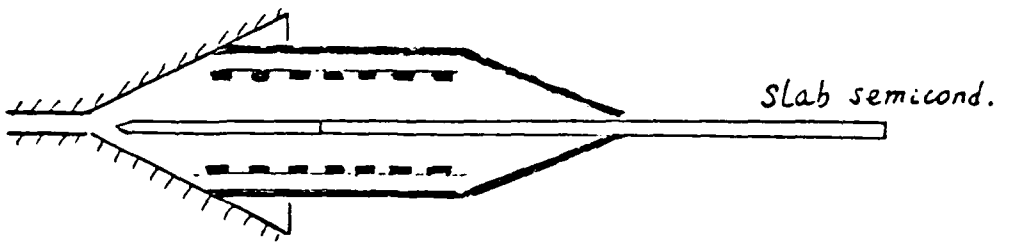

Fig.13. Schematic structure of grating waveguide which is coupled to a horn anttena and in which a slab semiconductor is placed in the middle and the slab has an extension out of the grating waveguide for testing.

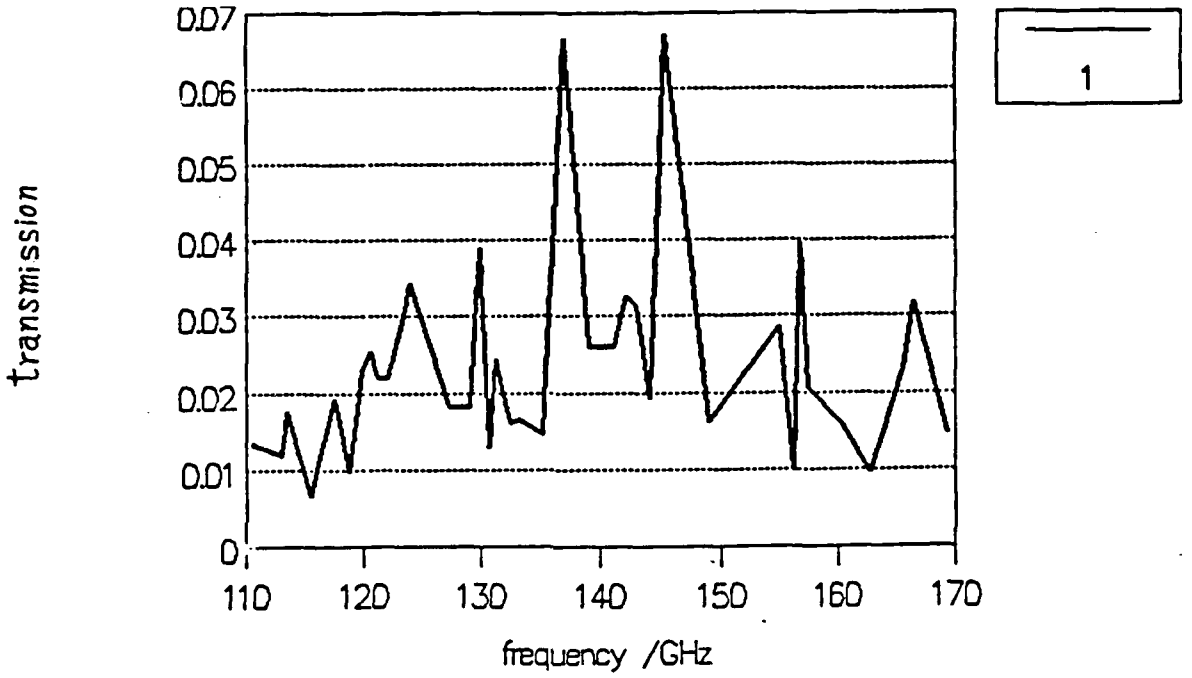

Fig.14. Measured transmision coefficient vs. frequency of the grating waveguide coupled with slab semiconductor. The semiconductor has thickness of 0.35mm and doping level of $3x10^{15}/cm^3$.

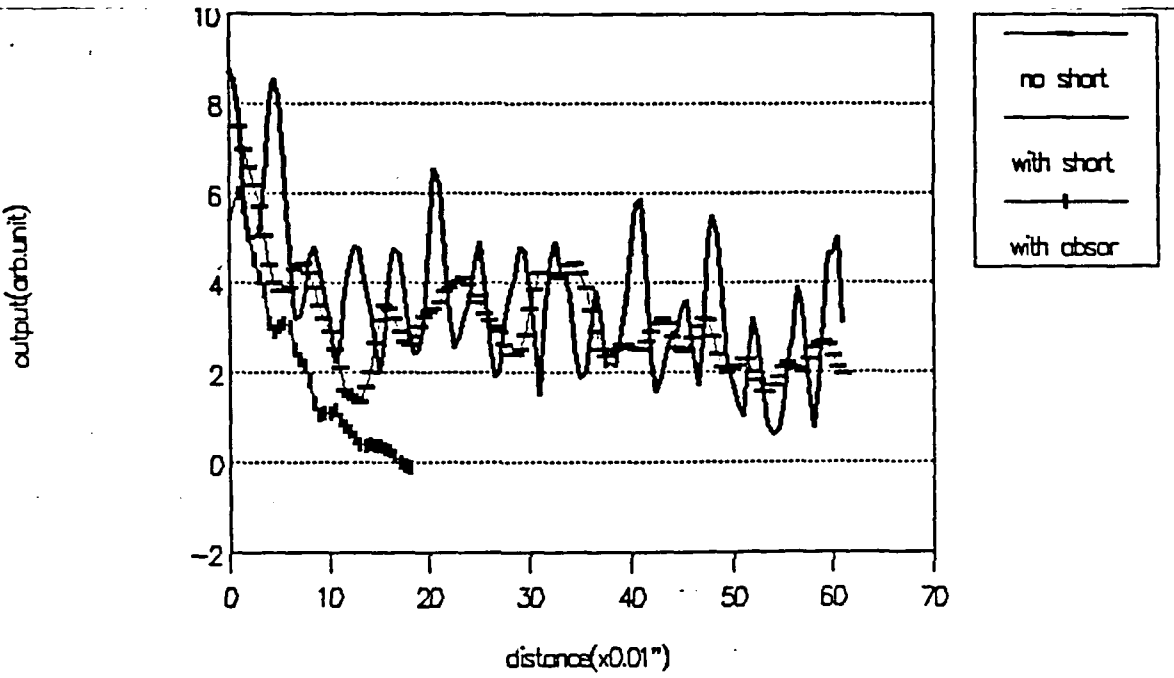

Fig.15. The detected field distribution close to the surface of the semiconductor at edge excitation condition. $N_d=3x10^{15}/cm^3$.

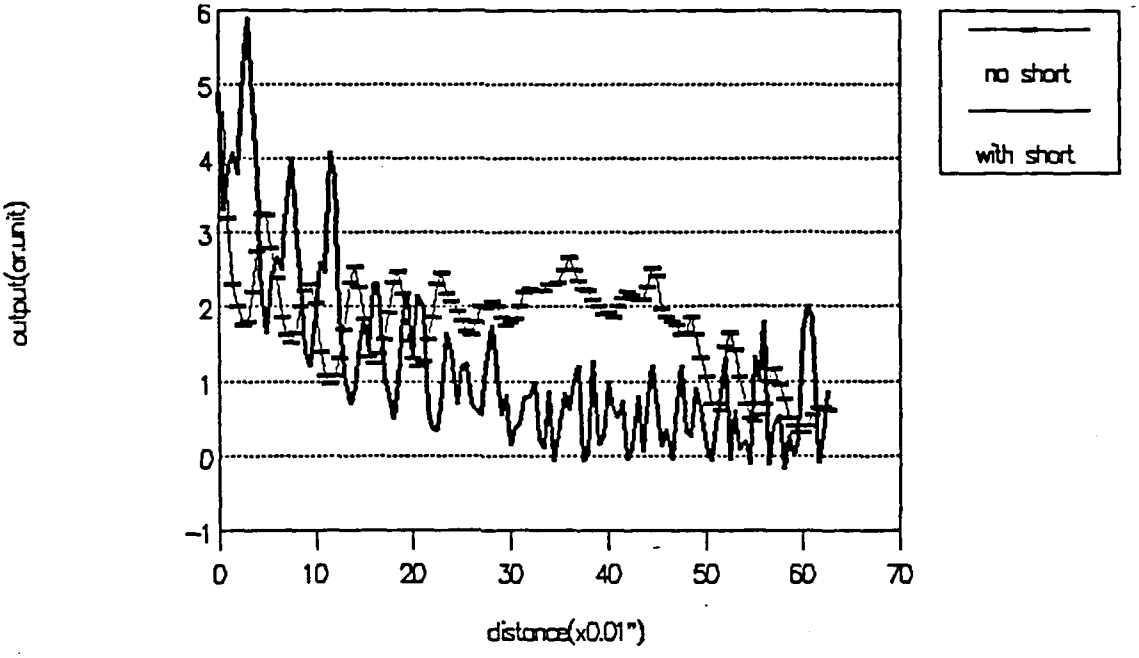

Fig.16. The detected field distribution close to the surface of the semiconductor at edge excitation condition. $N_d=3x10^{17}/cm^3$.

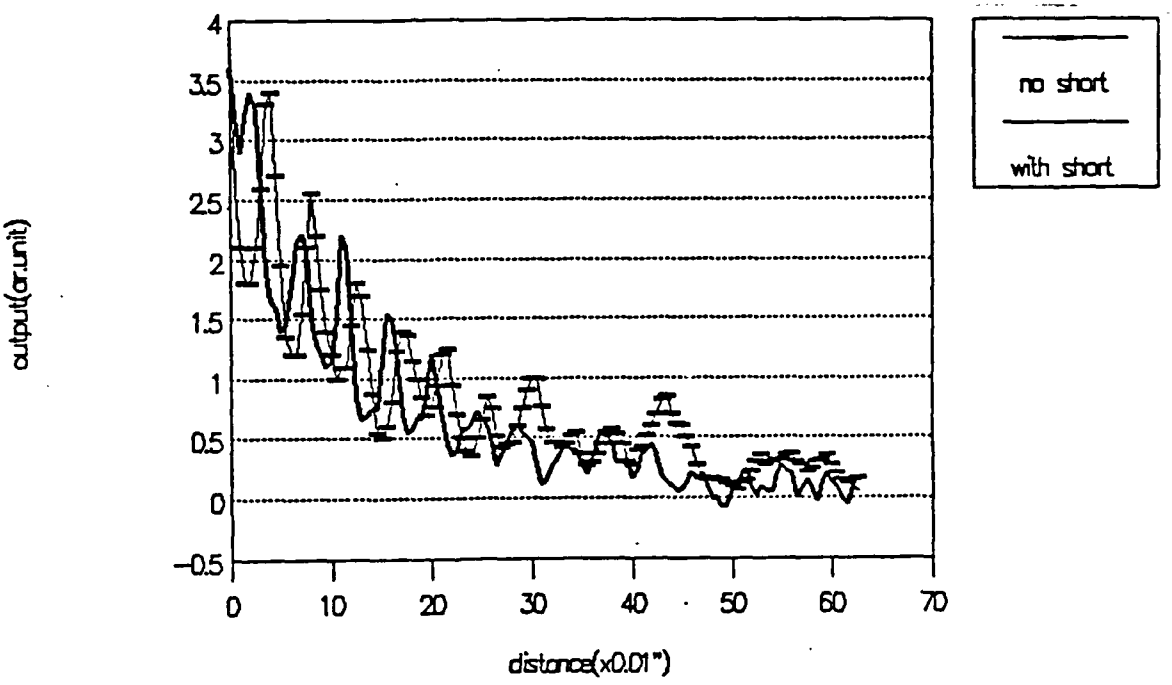

Fig.17. The detected field distribution close to the surface of the semiconductor at edge excitation condition. $N_d=3x10^{17}/cm^3$. An absorber is placed on the other side of the slab.

$k := 0 \ldots 126$

$g_k := READ(LNASCV)$

$g_{127} := g_{126}$

$u := fft(g)$

$k := 0 \ldots 63$

$N_k := \frac{5}{64} \cdot \frac{k}{0.256}$

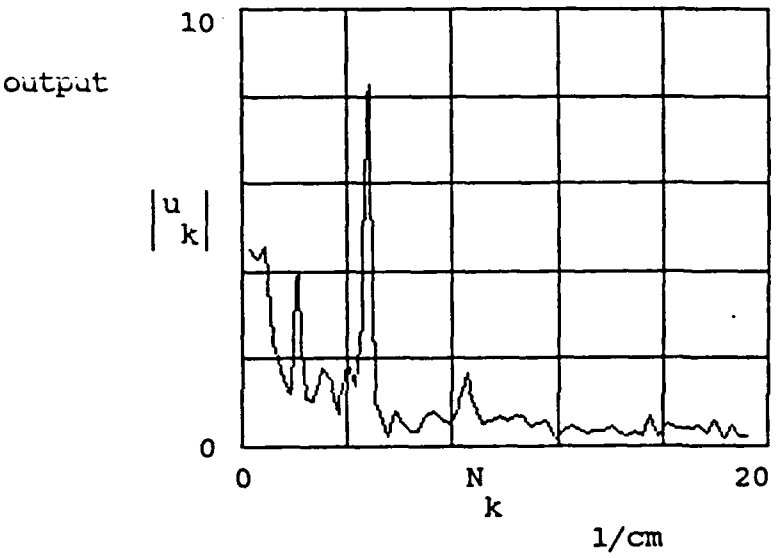

Fig.18 The space-spectrum vs.wavenumber
for a high-resistivity sample
Edge excitation with short end
without attaching absorber

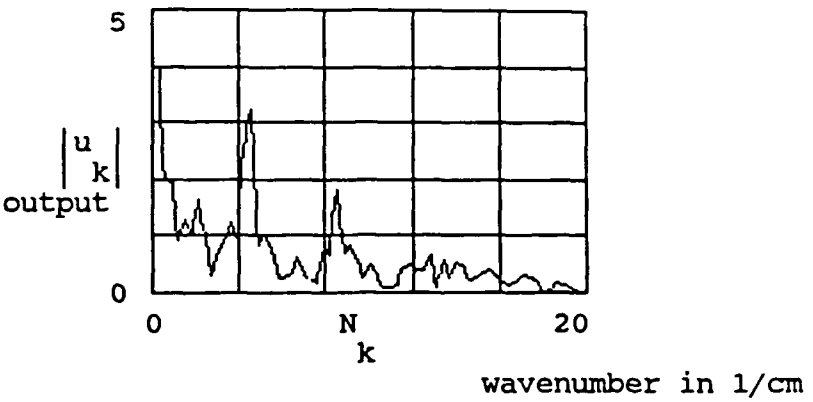

Fig.19 The plot of output spectrum for a sample with higher conductivity and short end

output

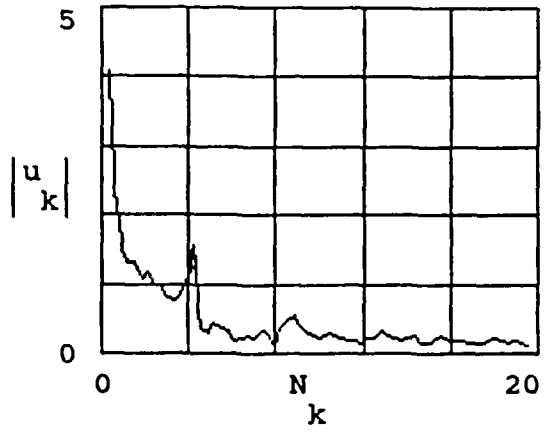

wavenumber in 1/cm

Fig.20 The plot of output spectrum for a sample with higher conductivity and with short end A side magneic is applied,absorber on back side of the sample,from the figure it is seen the mode with short wavelength is disapeared

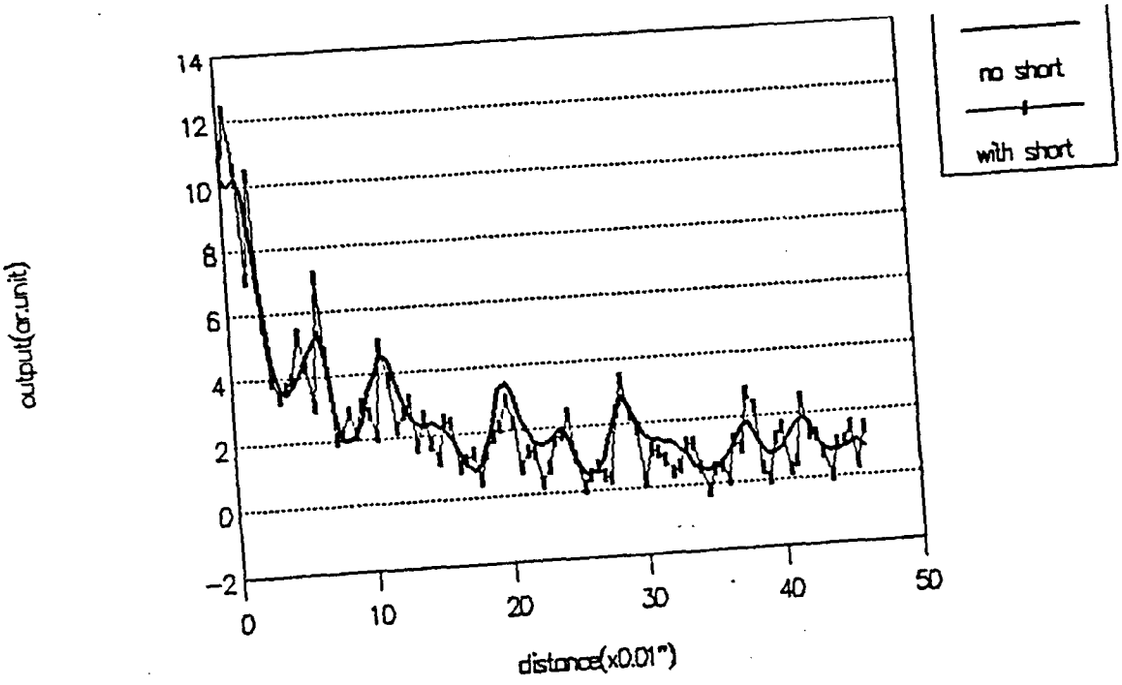

Fig.21. The detected field distribution close to the surface of the semiconductor at edge excitation condition. $N_d \doteq 1 \times 10^{17}/cm^3$.

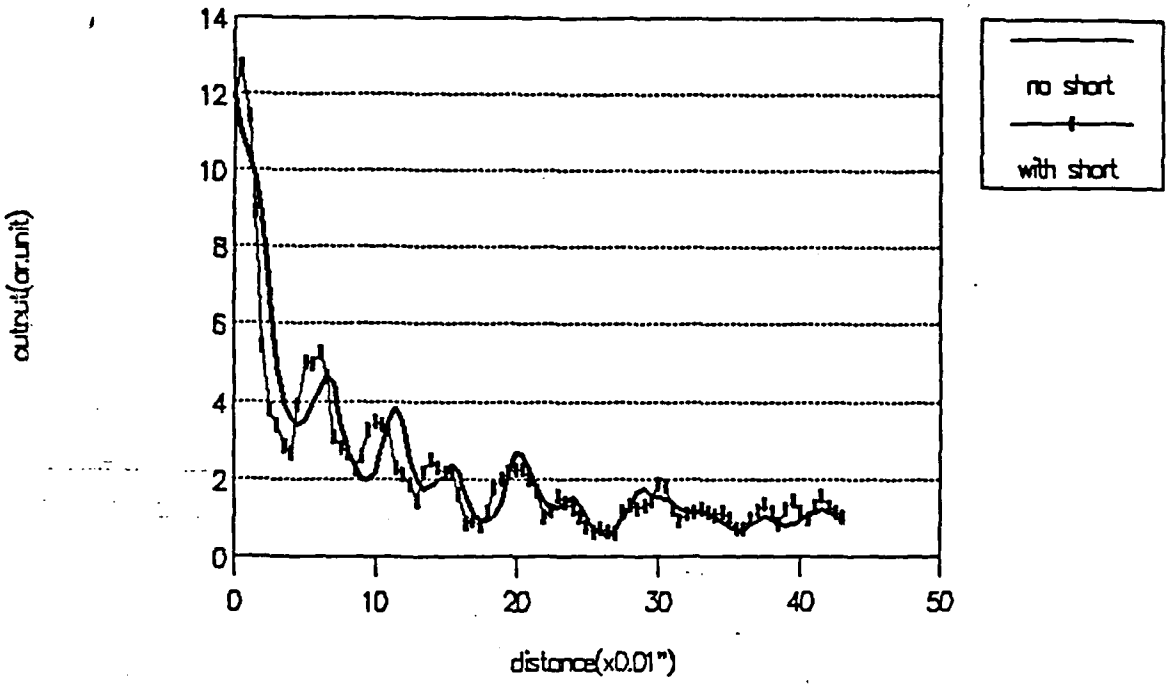

Fig.22. The detected field distribution close to the surface of the semiconductor at edge excitation condition. $N_d \doteq 1 \times 10^{17}/cm^3$. An absorber is placed on the other side of the slab.

$k := 0 \ldots 63$

$g_k := READ(MNASCV)$

$u := fft(g)$

$k := 0 \ldots 31$

$N_k := \frac{5}{32} \cdot \frac{k}{0.256}$

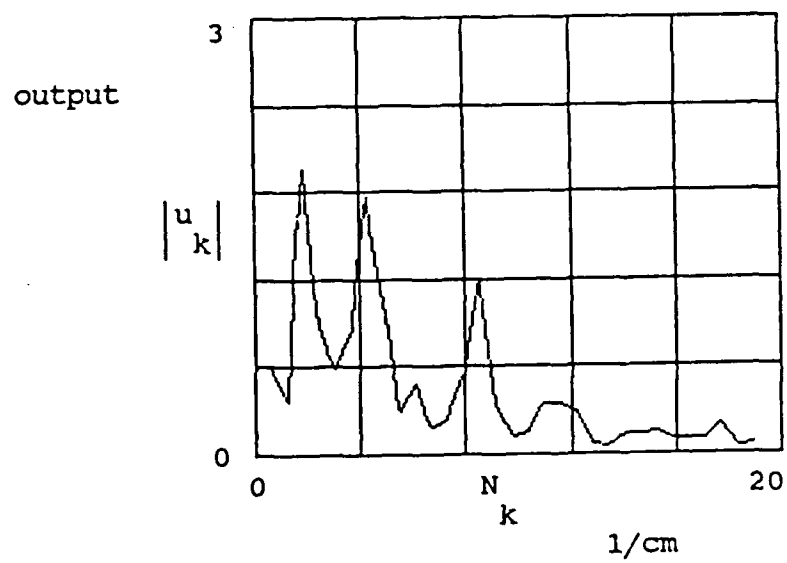

Fig.23 The space-spectrum vs.wavenumber
for a moderate-resistivity sample
Edge excitation with short end
without absorber

without attaching absorber

$k := 0 \ldots 63$

$g_k := READ(MASCV)$

$u := fft(g)$

$k := 0 \ldots 31$

$$N_k := \frac{5}{32} \cdot \frac{k}{0.256}$$

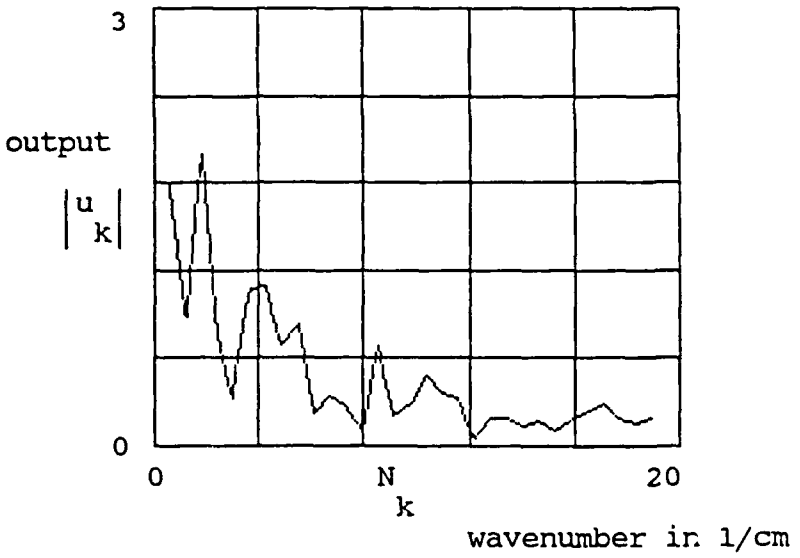

Fig.24 The space spectrum vs.wavenumber for a slb of sample with moderate resistivity,edge excitation,with short end and absorber on back side

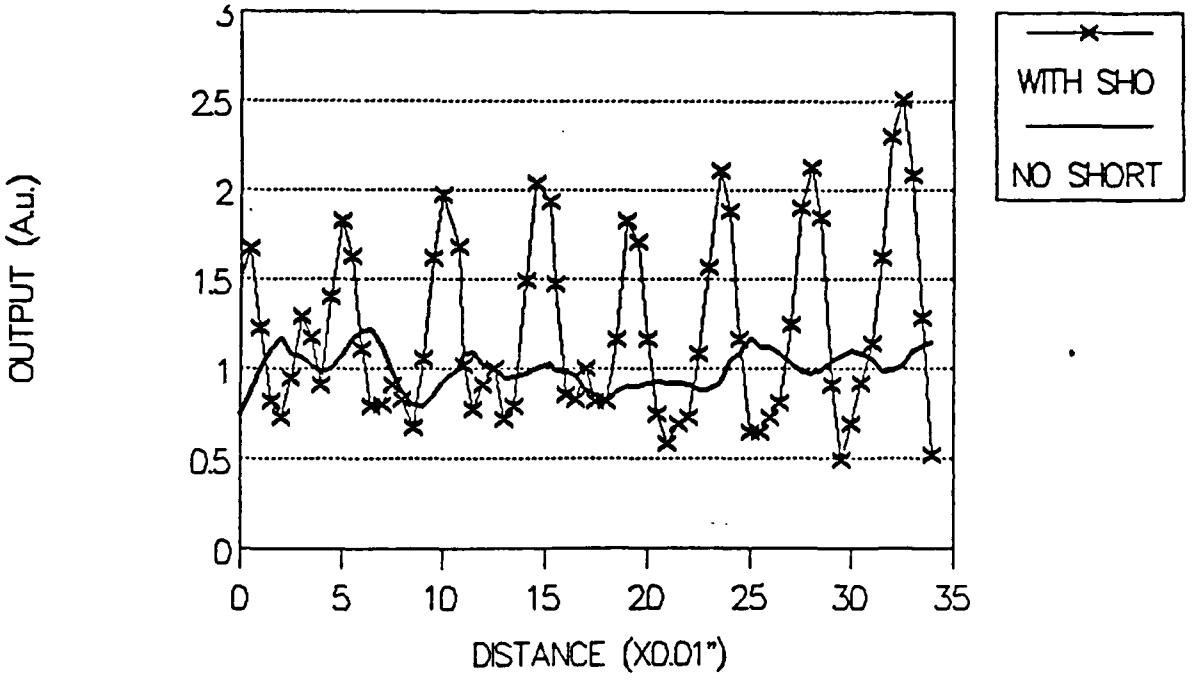

Fig.25. The detected field distribution close to the surface of the extended part of the semiconductor at grating waveguide excitation condition. $N_d=3x10^{15}/cm^3$. An absorber is placed on the other side of the slab. It is shown that the higher wavnumber mode excited by grating decays with distance,while the amplitude of lower wavenumber grows, showing the higher mode's transfering into surface mode.

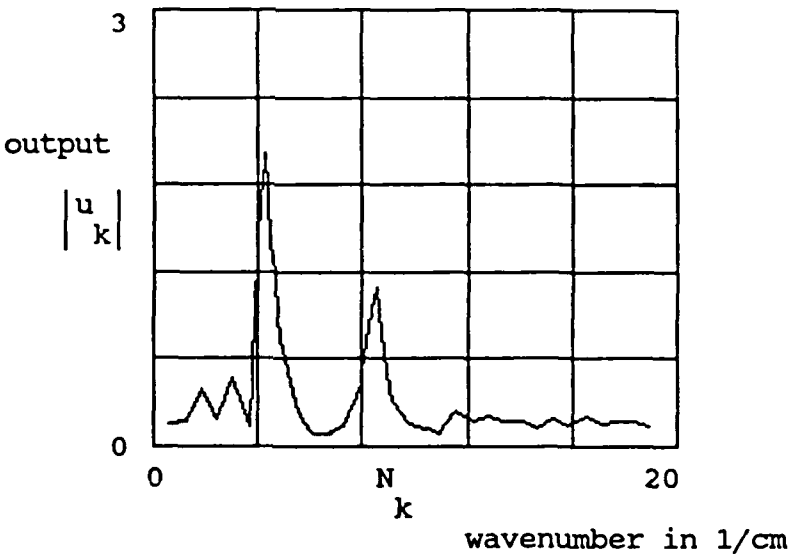

Fig.2ℓ The space spectrum vs.wavenumber for the the extension of a grating waveguide with low resistivity,with short end and. The first peak cooresponds to the surface mode, which grows with distance and the second peak is slab mode excited by grating and attenuates with distance.

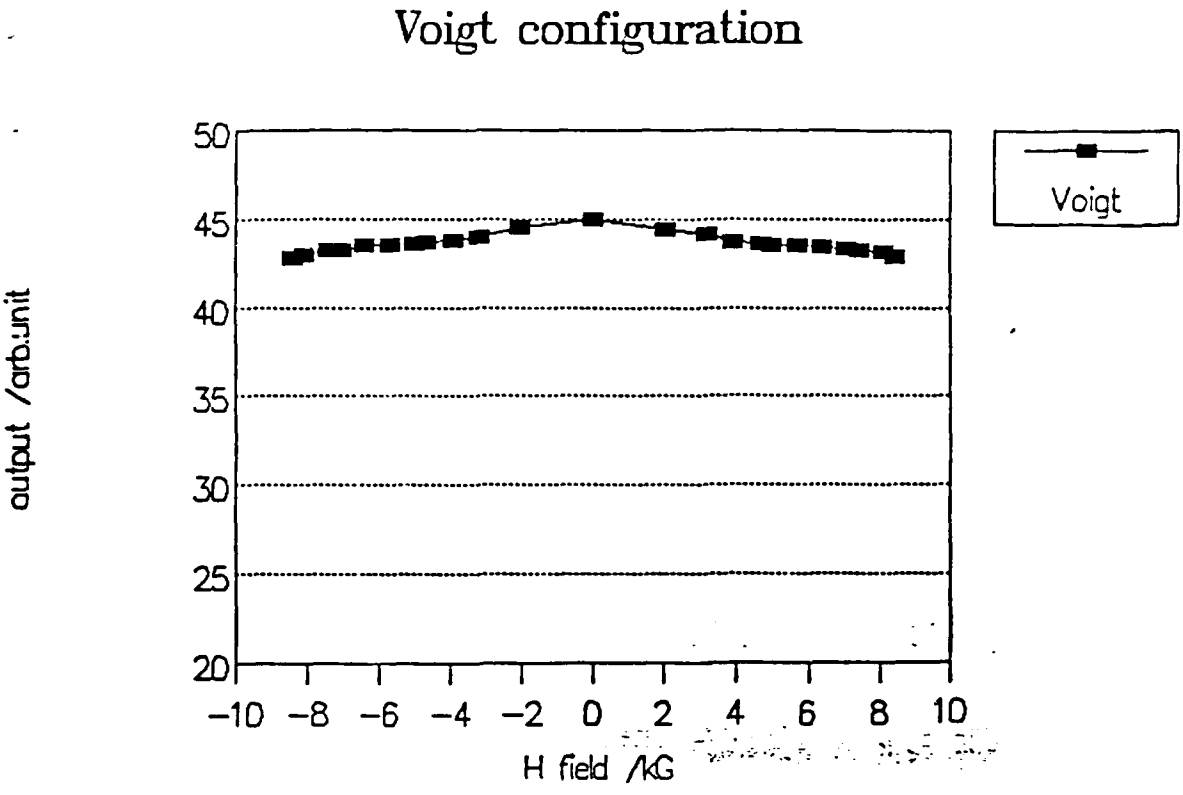

Fig.27. Transmission as a function of magnetic field for a Voigt configuration of the slab. $N_d=3x10^{15}/cm^3$. d=0.4mm.

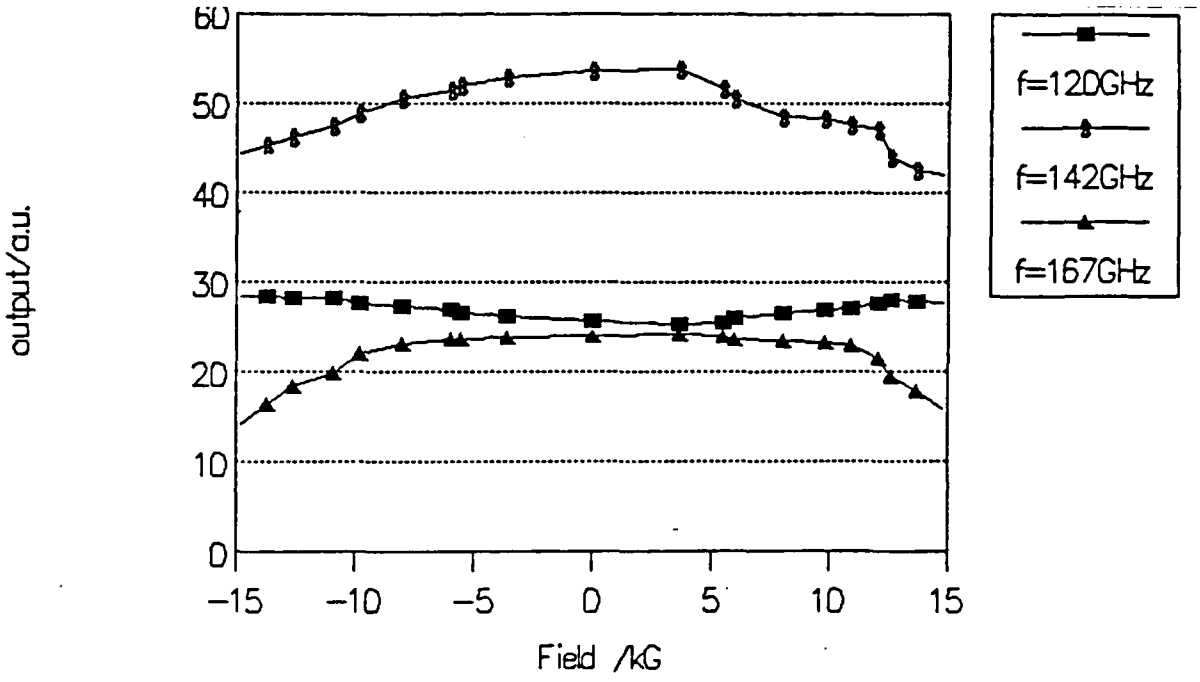

Fig.28. Transmission as a function of magnetic field for normal H_o configuration of the slab. $N_d=3x10^{15}/cm^3$. d=0.4mm. The curves cooresponde to different test frequency.

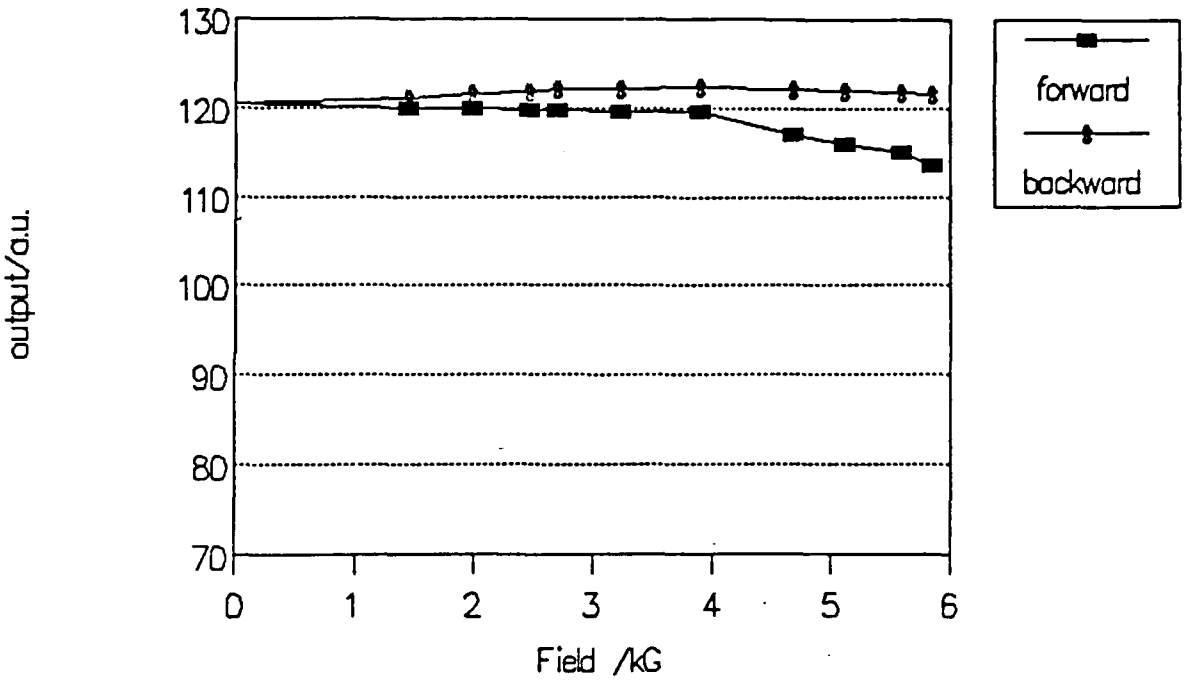

Fig.29. Transmission as a function of magnetic field for a Voigt configuration of the slab. $N_d=3x10^{15}/cm^3$. d=0.4mm. An absorber is placed near the slab, which gives rise to non-reciprocity in transmission.

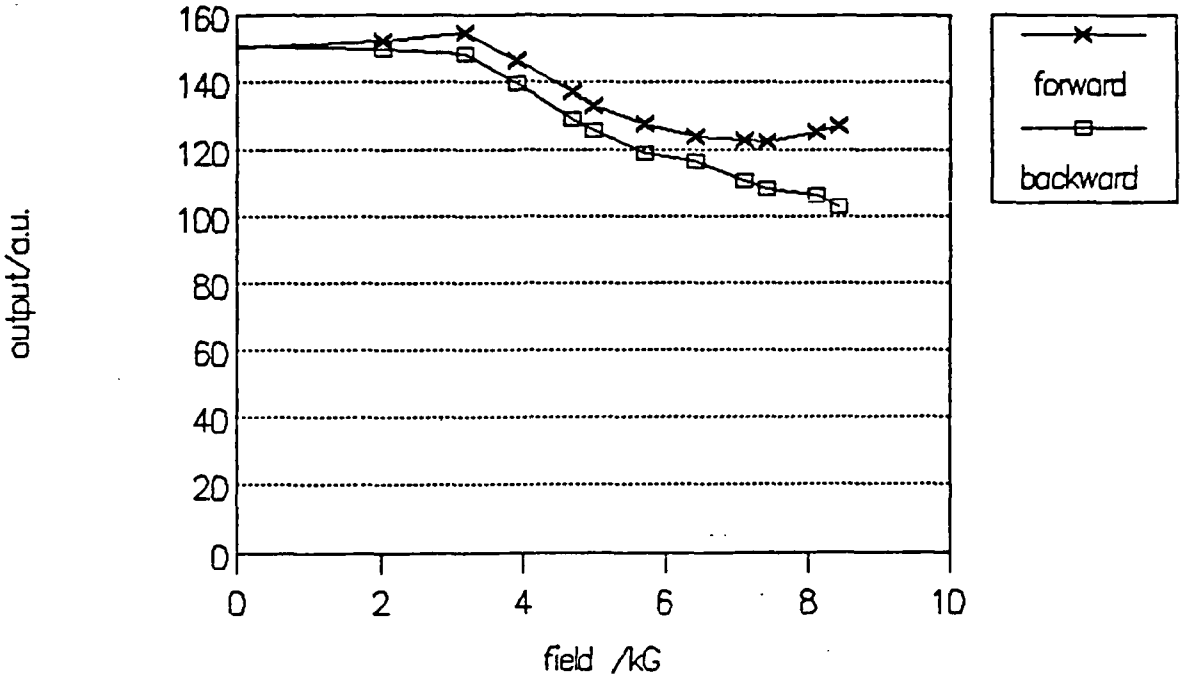

Fig.30. Transmission as a function of magnetic field for the configuration of waveguide containing semiconductor slab in the E-plane displaced from the center of the waveguide. $N_d=3x10^{15}/cm^3$. d=0.15mm. H_o is normal to the slab.

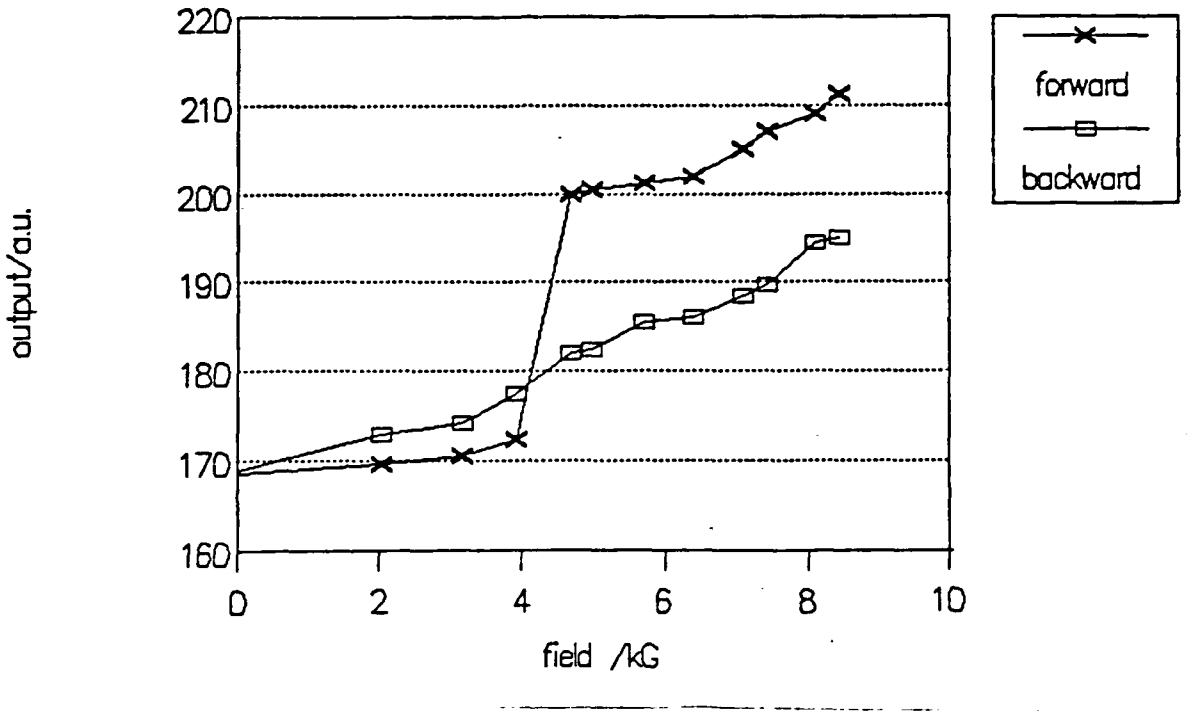

Fig.31. Transmission as a function of magnetic field for the configuration of waveguide containing semiconductor slab 70^0-tilted off the E-plane against the narrower wall of the waveguide. $N_d=3x10^{15}/cm^3$. d=0.15mm. H_o is normal to the slab.